

**NASA TECHNICAL NOTE**



**NASA TN D-7691**

**NASA TN D-7691**

(NASA-TN-D-7691) DESCRIPTION OF THE  
METEOROID DETECTION EXPERIMENT FLOWN ON  
THE PIONEER 10 AND 11 JUPITER FLYBY  
MISSIONS (NASA) 120 p HC \$4.50 CSCL 22C

N74-35282

H1/31      Unclass  
51190

# DESCRIPTION OF THE METEOROID DETECTION EXPERIMENT FLOWN ON THE PIONEER 10 AND 11 JUPITER FLYBY MISSIONS

*Compiled by Robert L. O'Neal*

*Langley Research Center*

*Hampton, Va. 23665*



NATIONAL AERONAUTICS AND SPACE ADMINISTRATION • WASHINGTON, D. C. • AUGUST 1974

1. Report No. NASA TN D-7691	2. Government Accession No.	3. Recipient's Catalog No.	
4. Title and Subtitle DESCRIPTION OF THE METEOROID DETECTION EXPERIMENT FLOWN ON THE PIONEER 10 AND 11 JUPITER FLYBY MISSIONS		5. Report Date August 1974	6. Performing Organization Code
		8. Performing Organization Report No. L-9517	10. Work Unit No. 755-42-01-01
7. Author(s) Robert L. O'Neal		11. Contract or Grant No.	13. Type of Report and Period Covered Technical Note
9. Performing Organization Name and Address NASA Langley Research Center Hampton, Va. 23665		14. Sponsoring Agency Code	
		12. Sponsoring Agency Name and Address National Aeronautics and Space Administration Washington, D.C. 20546	
15. Supplementary Notes			
16. Abstract  A Meteoroid Detection Experiment is being conducted on the Pioneer 10 and 11 Jupiter flyby missions. This experiment has the objective of measuring the population of $10^{-9}$ and $10^{-8}$ grams mass particles in interplanetary space with emphasis on making these measurements in the Asteroid Belt. The instrument design, which uses the pressurized-cell-penetration detection technique, and the tests involved in obtaining a flight-qualified instrument are described. The successful demonstration of flight-quality penetration detectors to function properly under long-term simulated space environments is also described.			
17. Key Words (Suggested by Author(s)) Meteoroid detection Asteroid Asteroid Belt Jupiter Pioneer 10 and 11		18. Distribution Statement Unclassified - Unlimited  STAR Category 31	
19. Security Classif. (of this report) Unclassified	20. Security Classif. (of this page) Unclassified	21. No. of Pages 125	22. Price* \$4.50



## CONTENTS

	Page
SUMMARY . . . . .	1
I. INTRODUCTION . . . . .	3
By Robert L. O'Neal, Langley Research Center	
II. TECHNICAL APPROACH . . . . .	7
By Robert L. O'Neal, Langley Research Center	
III. PRESSURE CELL DETECTOR PANELS . . . . .	13
By B. B. Brown, Jr., Langley Research Center	
IV. PRESSURE MONITORING SYSTEM . . . . .	37
By Leonard R. McMaster, Langley Research Center and Carl D. Parker, Research Triangle Institute	
V. ELECTRONIC SYSTEM . . . . .	53
By John Thomson, Langley Research Center	
VI. PRESSURIZED PANEL LIFE TESTS . . . . .	79
By Carl D. Parker, Research Triangle Institute	
VII. SIMULATION OF HEAVY ION AND PROTON IRRADIATION EFFECTS ON PRESSURE SWITCH OPERATION . . . . .	93
By Larry K. Monteith, North Carolina State University	
VIII. CALCULATION OF THE LEAK-DOWN TIMES FOR PRESSURIZED CELL METEOROID PENETRATION DETECTORS . . . . .	103
By Donald H. Humes, Langley Research Center	
IX. CONCLUDING REMARKS . . . . .	123
By Robert L. O'Neal, Langley Research Center	

PRECEDING PAGE BLANK NOT FILMED

DESCRIPTION OF THE METEOROID DETECTION EXPERIMENT FLOWN  
ON THE PIONEER 10 AND 11 JUPITER FLYBY MISSIONS

Compiled by Robert L. O'Neal  
Langley Research Center

SUMMARY

A Meteoroid Detection Experiment instrument system has been developed and qualified for flight on the Pioneer 10 and 11 Jupiter flyby missions. The instrument consists of 0.5 m<sup>2</sup> of penetration-sensitive sensors subdivided into 234 individual stainless-steel pressurized cells and an electronics system for detecting, counting, and storing the occurrence of meteoroid penetration events. The Pioneer 10 instrument exposed 25- $\mu$ m-thick stainless-steel pressurized cells and the Pioneer 11 instrument exposed 50- $\mu$ m-thick stainless-steel pressurized cells to the meteoroid environment. The instrument system weighed 1662 grams and consumed less than 750 mW of electrical power. This system was within the 1770 g and 1 W specified for the instrument.

A simulated life test program was conducted to verify the ability of the penetration sensor system to operate satisfactorily over a period of 1 year in a simulated space environment with no degradation in performance.



## I. INTRODUCTION

By Robert L. O'Neal  
Langley Research Center

In the past decade, the National Aeronautics and Space Administration has been active in planning and conducting missions which utilize instrumented spacecraft to study planets of the solar system. Pioneer 10 and 11 are part of this continuing exploration program. The Pioneer 10 and 11 program, being managed by NASA Ames Research Center at Moffett Field, California, has the main objective of studying the planet Jupiter. Other mission objectives are the study of the interplanetary medium between Earth and Jupiter, the study of the nature of the Asteroid Belt, and the development of technology required for missions to planets beyond Jupiter.

The first of these two Jupiter flyby missions began in March 1972 with the launch of the Pioneer 10 spacecraft from Cape Kennedy, Florida. The mission trajectory is such that the spacecraft passed near the planet Jupiter early in December 1973. Pioneer 11 was launched in April 1973 for a similar Jupiter flyby early in December 1974.

The Pioneer 10 and 11 spacecraft carry several scientific instruments (see fig. I-1) to make measurements related to the mission objectives. A group of investigators at NASA Langley Research Center is responsible for conducting one of the experiments on each of these two missions. This experiment, designated as the Meteoroid Detection Experiment, has the objective of measuring the spatial density of very small meteoroids as the spacecraft travels through interplanetary space, special emphasis being placed on making these measurements in the Asteroid Belt. The Pioneer 10 experiment will detect particles capable of penetrating 25- $\mu$ m stainless-steel sheet, and the Pioneer 11 experiment will detect particles capable of penetrating 50- $\mu$ m stainless-steel sheet. If an average meteoroid normal impact velocity of 18 km/sec, a meteoroid density of 0.5 g/cm<sup>3</sup>, and the use of the penetration equation recommended in reference I-1 are assumed the Pioneer 10 experiment will detect 10<sup>-9</sup> gram and larger particles and the Pioneer 11 experiment will detect 10<sup>-8</sup> gram and larger particles.

These data are used in the continuing effort to better define the meteoroid environment of the solar system and thus give insight and understanding of the dynamics and source of particulate matter in the universe. In addition, they will give an indication of the impact damage hazard presented to spacecraft operating in interplanetary space.

The purpose of this paper is to describe in detail the Meteoroid Detection Experiment instrument design, fabrication, testing, and operation. A number of individuals and specialists were responsible for significant contributions in the development of this instrument and have contributed the subsequent sections of the paper relating to their particular areas.

## REFERENCE

- 1-1. Anon.: Meteoroid Damage Assessment. NASA Space Vehicle Design Criteria (Structures). NASA SP-8042, 1970.

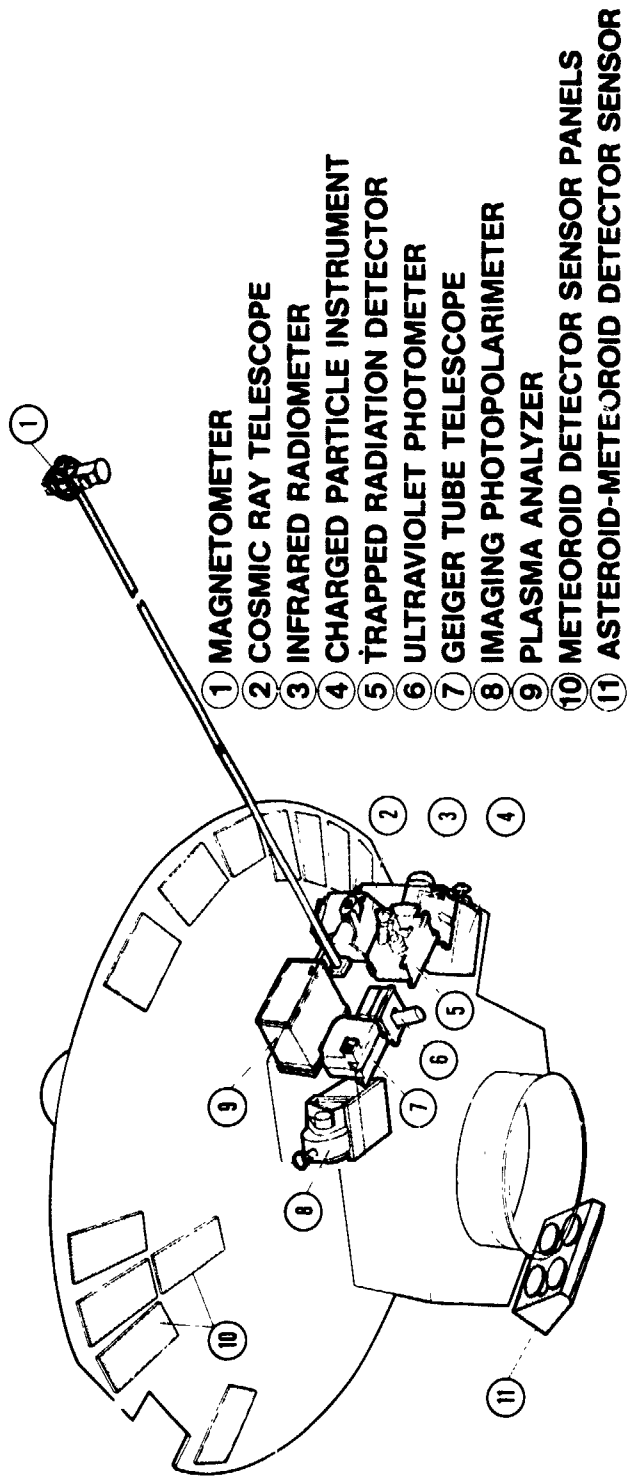


Figure I-1.- Pioneer 10 and 11 scientific experiments.



## II. TECHNICAL APPROACH

By Robert L. O'Neal  
Langley Research Center

### DESIGN APPROACH

The objectives of the Meteoroid Detection Experiment are accomplished by measuring the time, and thus the rate, of meteoroid penetrations in pressurized-cell-type penetration detectors along the spacecraft trajectory. The pressurized cell type of meteoroid detection system has been used extensively in Earth orbit (Explorers XIII, XVI, and XXIII) and in lunar orbit (on all Lunar Orbiter Spacecraft). A description of those applications can be found in references II-1 to II-3. Each of these previous meteoroid penetration experiments measured flux levels in a particular region of space, and in so doing measured a time-averaged meteoroid flux. In these previous experiments, the decrease in sensor-sensitive area as cells were penetrated was of minor concern since the experiments were conducted over a time period sufficient to obtain statistically good data samples of the meteoroid environment. The Pioneer 10 and 11 experiment are different since their objectives are to measure an environment level which may vary throughout the regions of space through which they fly. This requirement dictated that the experiment sensors have sufficient area and have sufficient cells remaining at any point between Earth and Jupiter to be able to detect variations in the environment. To define the minimum size and thus the lightest weight experiment capable of detecting such environment variations, a parametric study was made where sensor thickness, total sensor area, and the number of cells were systematically varied and the penetration history calculated for an estimated interplanetary meteoroid environment model. These calculations showed that if the meteoroid environment model presented in reference II-4 was used, a meaningful experiment could be accomplished with a sensor area of  $0.5 \text{ m}^2$  subdivided into at least 200 individual pressurized cell sensors for both 25- and 50- $\mu\text{m}$ -thick stainless-steel sensors. Based on these results, a decision was made to fly  $0.5 \text{ m}^2$  of 25- $\mu\text{m}$ -thick sensors on Pioneer 10 and  $0.5 \text{ m}^2$  of 50- $\mu\text{m}$ -thick sensors on Pioneer 11, each being subdivided into at least 200 pressurized cells. Stainless steel was selected as the test material for sensing meteoroid penetrations since it had been used to obtain extensive data in Earth and Lunar orbit, and the interplanetary data could, therefore, be correlated with that data with minimum uncertainty. This extensive use had demonstrated stainless steel could be used to fabricate very reliable penetration detectors.

In principle, the pressurized cell detector consists of a cavity which is pressurized with gas and equipped with a pressure-monitoring device. The test material constitutes that part of the pressure-carrying detector structure exposed to the space environment. If and when a meteoroid penetrates the test material, the gas in the cavity will leak out

PRECEDING PAGE BLANK NOT FILMED

and the loss in pressure will be detected as a penetration. The number of cells which have been penetrated is determined at each interrogation of the spacecraft.

The Pioneer 10 and 11 instrument systems were subjected to a very stringent weight and electrical power budget to maximize the number of experiments and the scientific return from the unique scientific opportunities. The weight and power budgets allocated to the Meteoroid Detection Experiment were 1770 g and 1 W. It was necessary to develop a new pressurized cell and sensing technique in order to achieve the required number of pressurized cells and remain within the weight and power limits. The pressurized cell detectors developed were in multi-cell panel form and were mounted to the back of the spacecraft high-gain antenna dish at the points noted in figure II-1 and II-2. The original concept was to fly 12 of these detector panels on each spacecraft. After the panel locations on the spacecraft had been finalized, a spacecraft system sunshade (see fig. II-2) had to be enlarged and, as a result, one of the panels was partially shielded from the meteoroid environment. A 13th detector panel was allocated to the experiment to compensate for this loss in effective sensor area.

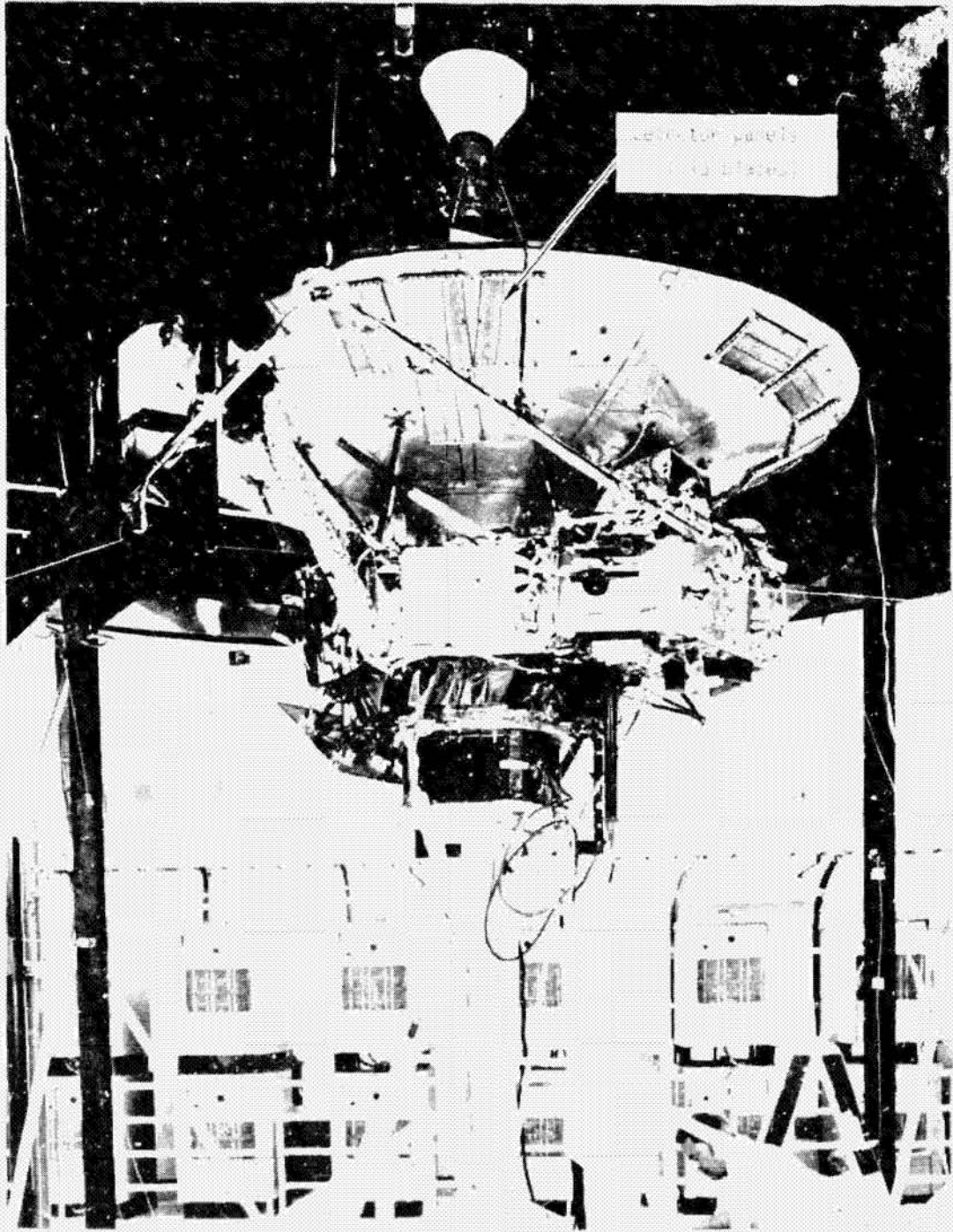
During the mission the spacecraft spins about the axis through the center of the high-gain antenna dish and, with the exception of the first few hours after launch, the dish points toward Earth. The spacecraft trajectory and spacecraft attitude are such that the velocity vector of impacting meteoroids is generally within  $30^{\circ}$  of the spacecraft spin axis. Variations in these parameters which affect the angle at which meteoroids impact the detector panels are considered in the reduction of the meteoroid penetration data.

#### DESIGN VERIFICATION

The Meteoroid Detection Experiment system design evolved through a comprehensive development program. The system design was verified by a series of mechanical and electrical functional tests made at the unit level and also made with the instrument mechanically and electrically integrated with the Pioneer spacecraft system. The instrument flight units were flight qualified through a series of tests conducted both at the unit level and spacecraft level. In addition to meeting the mechanical and electrical functional specifications imposed by the Pioneer Project, an extensive program was conducted to verify that the instrument would be capable of reliably detecting meteoroid penetration events under the severe thermal, vacuum, and radiation environments of space. Special thermal-vacuum tests were conducted where flight-type detector panels were subjected to a continuous functional test under vacuum for a period of 1 year. One group of panels was maintained at room temperature and a second group at liquid nitrogen temperature. A series of radiation tests were also conducted where flight-type pressure switches were functionally tested while being irradiated at levels exceeding those expected in flight. The results of these experiment functional tests are discussed in separate sections of this paper.

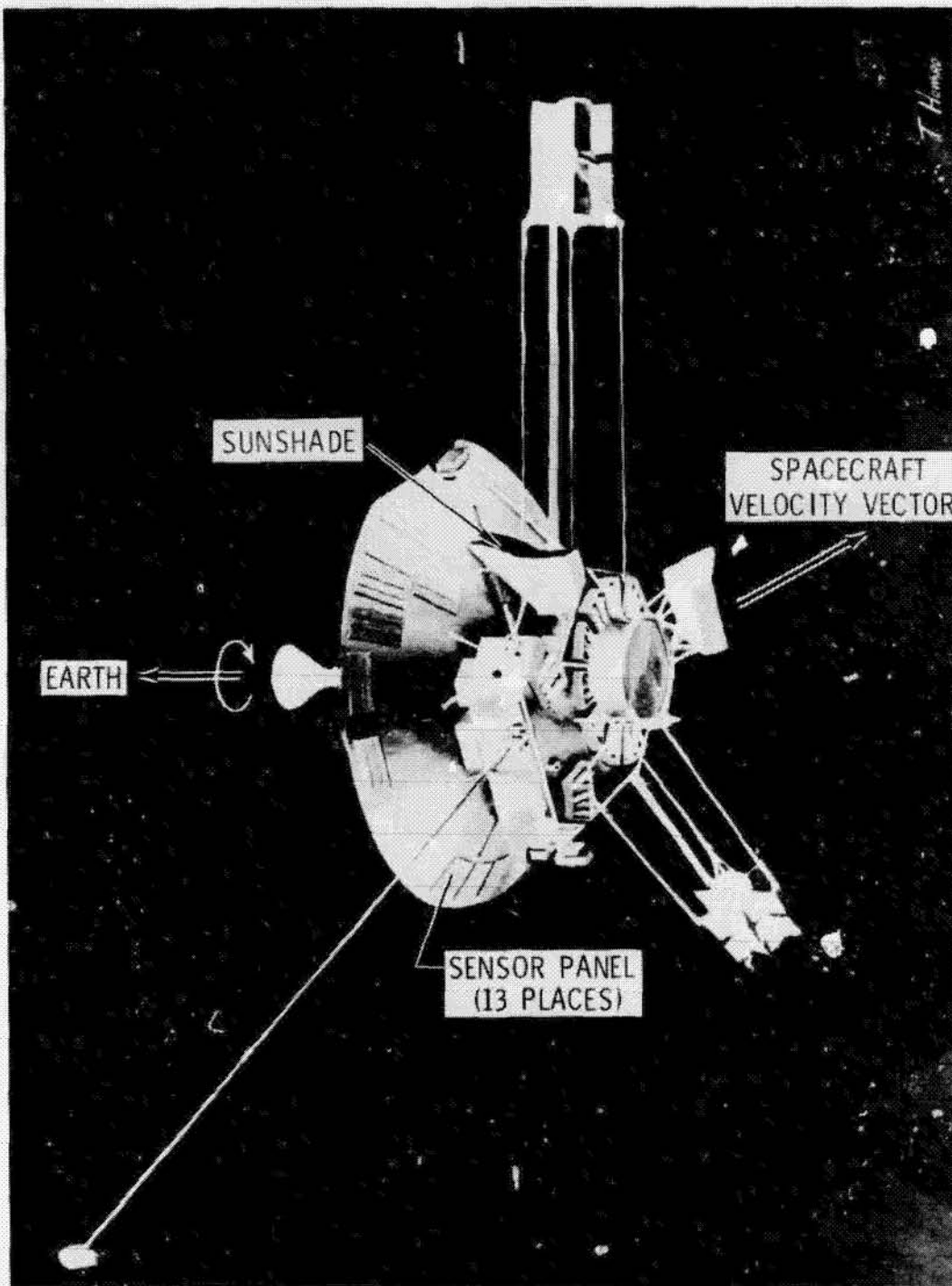
## REFERENCES

- II-1. D'Aiutolo, Charles T., coordinator: The Micrometeoroid Satellite Explorer XIII (1961 Chi) – Collected Papers on Design and Performance. NASA TN D-2468, 1964.
- II-2. O'Neal, Robert L., compiler: The Explorer XXIII Micrometeoroid Satellite – Description and Results for the Period November 6, 1964, through November 5, 1965. NASA TN D-4284, 1968.
- II-3. Grew, Gary W.; and Gurtler, Charles A.: The Lunar Orbiter Meteoroid Experiments – Description and Results From Five Spacecraft. NASA TN D-6266, 1971.
- II-4. Anon.: Meteoroid Environment Model – 1970 Interplanetary and Planetary . NASA Space Vehicle Design Criteria (Environment). NASA SP-8038, 1970.



Keck-ton panels  
in place

Figure 1. The Keck-ton panels are shown in place on the antenna structure.



L-74-1119

Figure II-2.- Sketch showing orientation of spacecraft.



### III. PRESSURE CELL DETECTOR PANELS

By B. B. Brown, Jr.  
Langley Research Center

#### INTRODUCTION

Although considerable experience existed in the fabrication and use of pressurized cells for meteoroid detection in space, it was necessary to devise and develop new design concepts in order to accomplish the experiment objectives with the small weight (1770 grams) allotted to the instrument. Early trade-off studies resulted in a weight breakdown for instrument design as follows:

Item	Weight, grams
Pressurized panels . . . . .	680
Pressure switches . . . . .	455
Electronic system . . . . .	455
Contingency . . . . .	180
Total . . . . .	1770

The pressurized cells flown on Explorer XXIII (ref. III-1), each exposing 90 cm<sup>2</sup> of sensitive area and weighing 78 grams, were too large and too heavy to meet these design criteria. To accomplish the Pioneer experiment design objective of 0.5 m<sup>2</sup> of sensitive area subdivided into 200 pressurized cells, it was necessary to maximize sensitive area with respect to cell internal volume. This condition dictated essentially flat detectors and led to the "air mattress" configuration used in the experiment.

Initial efforts to fabricate air-mattress-type detector units indicated the rejection rate in order to obtain acceptable flight detector arrays would be significant. To reduce the impact of rejected panels on cost and schedule, a decision was made to subdivide the 0.5 m<sup>2</sup> into 12 individual panels. This configuration would, in addition, be more adaptable to mounting to the back of the spacecraft high-gain antenna dish than would large arrays. Development fabrication and tests led to the definition of 0.04 m<sup>2</sup> panels with each subdivided into 18 individually pressurized cells.

A detailed set of written manufacturing, test, and inspection procedures were formulated in the instrument design and construction verification phase. These procedures were followed in all fabrication, inspection, and test activities involving prototype and flight hardware. Written records of the history of each detector panel were maintained and showed the results of all tests and inspections.

## FABRICATION

Some details of the panels, dimensions, and construction are noted in figures III-1 and III-2. The individual cells were fabricated by resistance-welding two sheets, one 25  $\mu\text{m}$  thick and the other 50  $\mu\text{m}$  thick, of annealed 21-6-9 type stainless steel together in a manner to form cavities between the two sheets for later pressurization. The weld pattern for forming the cavities is visible in the photograph (fig. III-3) of a panel structure being welded. A small hole was made in one end of each of the cavities and a copper pressurization tube inserted and silver soldered in place. The preparation of the holes for placement of the pressurization tubes is shown in figure III-4. The installation and silver soldering operations are shown in figures III-5 and III-6. Adjacent cells had the tube installed in opposite ends so that the panel distortion resulting from the tubes would be symmetrical.

After the pressurization tubes were silver soldered in place, the panel was cleaned internally of any solder flux residue by circulating 100° C deionized distilled water through each cell for 2 hours. The apparatus used for this operation is shown in figure III-7. After the flushing was complete, each panel was heated to 100° C in a vacuum oven for a period of 1 hour to remove all water from the cavities. The integrity of each silver solder joint was checked by connecting a helium-sensitive leak detector to each cell and flooding the exterior of the joint with gaseous helium. Only those panels with no leaks were carried further in the fabrication process.

A pressure switch assembly was soft soldered to each of the pressurization tubes. The switch assemblies were installed so that the switch terminals face the same direction as the stainless steel being exposed to the space environment; that is, the switch terminals were on the 25- $\mu\text{m}$  side for Pioneer 10 panels and on the 50- $\mu\text{m}$  side for Pioneer 11 panels. A photograph of the switch installation is shown in figure III-8. A panel with pressure switches installed is shown being leak checked in figure III-9. Again, only those panels displaying no leaks were carried further in the manufacturing process. At this point, the panels were ready for pressurization and final sealing.

The gas used as the pressurizing medium for the cell is a mixture of 75-percent argon and 25-percent nitrogen. The panels were pressurized by using a manifold arrangement as shown in figure III-10. The cells were pressurized to 1175 mm Hg at 22° C and the fill tubes crimped and sealed with soft solder. The sealing operation is shown in figure III-11. The pressurized panels were then leak checked to determine the integrity of the complete panel. Figure III-12 is a photograph of a panel being placed in the leak-check facility. The allowable leak rate used for an acceptable panel was  $1 \times 10^{-9}$  std  $\text{cm}^3/\text{sec}$  or less. This leak rate of  $1 \times 10^{-9}$  std  $\text{cm}^3/\text{sec}$  would require over 5 years for a cell to leak to a pressure sufficient to activate the pressure switch.

Expansion joints to allow the panels to flex with changes in temperature and load were put in all panels passing the leak test. A photograph of this process is shown in figure III-12

The pressure switches were wired by connecting the 18 switches in parallel. The wiring terminated at a terminal block located at one corner of the panel. The spacecraft wiring harness connects the terminal block of each panel to the instrument electronics unit located in the spacecraft instrument compartment. After the electrical leads were soldered to each switch and to the terminal block, the end of each panel including switches and wiring was ultrasonically cleaned. Each electrical connection was then primed with RTV primer, encapsulated with General Electric silicone rubber RTV-511, and cured. The application of silicone rubber to the switches is shown in figure III-14. The impedance between the two terminals at the terminal block was measured to ascertain that the impedance was at least  $1\text{ T}\Omega$  at 500 volts.

The rear surface of each panel was cleaned, primed, and painted with a flat black paint to provide thermal control during the flight mission. Stiffening brackets were attached to each end and to the middle of each panel. These brackets provided rigidity to the panel to enable it to withstand spacecraft launch loads. The brackets were potted to the panel with RTV-511 and RTV-102 silicone rubber. The process is shown in figure III-15.

A shield was placed over each bank of pressure switches to minimize electromagnetic interference to other instruments and spacecraft systems when a pressure switch fires. The shield material is a  $75\text{-}\mu\text{m}$ -thick three-ply laminate of aluminum-Mylar-aluminum. The shield material was folded around the switches and interconnecting wiring and glued in place. The shield is noted in the photograph of a completed panel. (See fig. III-16.)

Each completed panel was then checked to insure that no argon leaks greater than  $1 \times 10^{-9}$  std  $\text{cm}^3/\text{sec}$  were present. After a panel successfully passed the leak check, it was then ready for either qualification-level or flight-acceptance-level thermal-vacuum and vibration tests.

The average weight of each detector panel produced for flight was 96 grams.

#### PANEL TEST PROGRAM

The pressurized cell detector panel design was achieved and verified with the aid of a very thorough test program. Qualification tests were conducted on pressurized cell panels, manufactured as previously described, to determine the capability of the panels to function normally after exposure to higher than expected handling, system tests, launch and space flight environments. Flight acceptance tests were conducted on all panels

fabricated as flight and flight backup units to verify the ability of the panels to function after normally anticipated conditions of launch and space flight environments. In addition to the qualification and acceptance test programs, a life test program was conducted to verify the operation of prototype pressurized cell panels over an extended period under simulated conditions of space flight.

The qualification and flight acceptance test programs are treated in the following paragraphs whereas the life tests are treated in a separate section of this paper.

### Qualification Test Program

Qualification tests were conducted on 12 prototype pressurized cell panels as follows:

Humidity test.- The test panels were installed in a temperature and humidity chamber with conditions as follows:

Temperature . . . . .  $30^{\circ} \text{C} \pm 3^{\circ}$   
 Humidity . . . . .  $95\% \pm 3\%$

The duration of the humidity test was 24 hours. After completion of the test, each panel was given a visual inspection, impedance check, and leak check.

Steady-state acceleration.- Each of the test panels was attached to a spin table and subjected to an acceleration of 48 g for a period of 3 minutes. Each panel was given a visual inspection, impedance check, and leak check after the test.

Shock test.- The test panels were subjected to a half sinusoidal shock test at levels and duration as specified below three times per axis.

Axis	Level, g	Duration, ms
All	$50 \pm 5$	$6 \pm 1$

Each panel was inspected and impedance and leak checked after the test.

Vibration and acoustic tests.- Vibration and acoustic qualification was initially attempted by tests with panels mounted to a rigid base on a shaker table. The vibration levels specified by the Pioneer office were intended to represent vibration and acoustic environments. Results from initial tests indicated, however, that the panel environment achieved on the shaker was much more severe than the environment which panels would experience on the spacecraft during spacecraft level qualification tests. It was apparent that the rigid shaker base was not representative of the flight configuration mounting on the relatively flexible antenna structure. It was also apparent that the acoustic environment could not be adequately simulated by vibration tests on a shaker table. Since time did not permit the design of a realistic unit level vibration test, spacecraft level tests

were used for panel qualification. Prototype panels were mounted on the prototype spacecraft for spacecraft level vibration and acoustic tests. After these tests, the panels and their mounting hardware were visually inspected and the panels were impedance checked and leak checked.

Thermal and thermal-vacuum tests.- The set of 13 detector panels was subjected to the conditions of temperature and vacuum described in figure III-17. The pressure switches in each panel were monitored continuously during the tests to verify that there were no panel leaks or no inadvertent switch firings. All panels were leak checked and impedance checked after completion of the test.

#### Flight Acceptance Test Program

Unit level-flight acceptance tests were limited to vibration and thermal and thermal-vacuum. These tests are described as follows:

Vibration.- The Pioneer 10 panels flight-acceptance vibration tests were accomplished by successful operation of panels on the Pioneer 10 spacecraft during flight-acceptance-level tests. Accelerometer data were obtained on panel vibration levels during these tests and were used to design an acceptance test by using a shaker table for Pioneer 11 flight panels and for Pioneer 10 and 11 backup panels. These tests are described in tables III-1 and III-2.

Thermal-vacuum environment.- All flight and backup panels were subjected to the temperature and vacuum environment shown in figure III-17. Each panel had electrical leads attached and the pressure switches were monitored continuously for panel leaks or inadvertent switch firings. After completion of the tests, all panels were impedance checked and leak checked.

#### TEST RESULTS

Some panel failures were encountered during the qualification and acceptance tests. Six panels developed leaks in the early phase of the qualification-level thermal and thermal-vacuum test. Examination of test data and test setup revealed inadequate shielding between the quartz heaters and the panels which resulted in panels reaching temperatures sufficient to melt the soft solder used in the pressure switches. This temperature was far in excess of the specified 94° C. The test fixture was modified to eliminate the possibility of hot spots in the panels and the test repeated with six new panels. The test was completed with no failures.

During the attempts to qualify prototype panels using panels rigidly mounted to a shaker table for vibration and acoustic environment simulation, numerous panel leaks developed. These leaks were caused by switch and panel structural fatigue. It was con-

cluded that the test levels specified and the test technique were not compatible. Subsequent panel qualification was accomplished by qualification tests on the spacecraft. Qualification tests were accomplished with panels mounted on the spacecraft by using both rigid mounts and soft mounts. Failures from panel and switch structural fatigue were found in hard-mounted panels whereas panels with soft mounts that functioned as vibration dampers suffered no active or incipient failures as verified by visual inspection, impedance tests, and leak tests. The vibration dampers were incorporated into the panel mounting design by the spacecraft contractor and no failures were encountered in subsequent flight-acceptance testing.

One pressurized cell developed a leak during the cold-soak part of the flight-acceptance thermal-vacuum tests for Pioneer 10 panels. This panel was inspected visually, but the area of the leak could not be found. Since this panel was the only case of a leak developing after a panel was accepted and designated as a flight item, no changes in manufacturing or test procedures were made. Spare panels had been included in the test and one was substituted in place of the one with the leaking cell.

No other failures were encountered in the test program. It is believed that all failures resulting during qualification and acceptance testing were adequately analyzed, appropriate corrective action was taken, and the pressurized panels were proven to be flight worthy.

#### REFERENCE

- III-1. Creal, Robert L., compiler: The Explorer XXIII Micrometeoroid Satellite - Description and Results for the Period November 6, 1964, Through November 5, 1965. NASA TN D-4284, 1968.

**TABLE III-1.- Z-AXIS RANDOM VIBRATION FLIGHT ACCEPTANCE TESTS  
FOR PIONEER 11 FLIGHT PANELS**

Frequency, Hz	Power spectral level, $g^2/Hz$
20 to 40 . . . . .	0.1 (at 40 Hz with 12 dB per octave rollup from 20 Hz)
40 to 400 . . . . .	0.1
400 to 2000 . . . . .	0.1 (at 400 Hz with 12 dB per octave rolldown from 400 to 2000 Hz)

**TABLE III-2.- Z-AXIS RANDOM VIBRATION FLIGHT ACCEPTANCE TESTS  
FOR PIONEER 10 AND 11 BACKUP PANELS**

Frequency, Hz	Power spectral level, $g^2/Hz$
20 to 40 . . . . .	0.2 (at 40 Hz with 12 dB per octave rollup from 20 Hz)
40 to 400 . . . . .	0.2
400 to 2000 . . . . .	0.2 (at 400 Hz with 12 dB per octave rolldown from 400 to 2000 Hz)

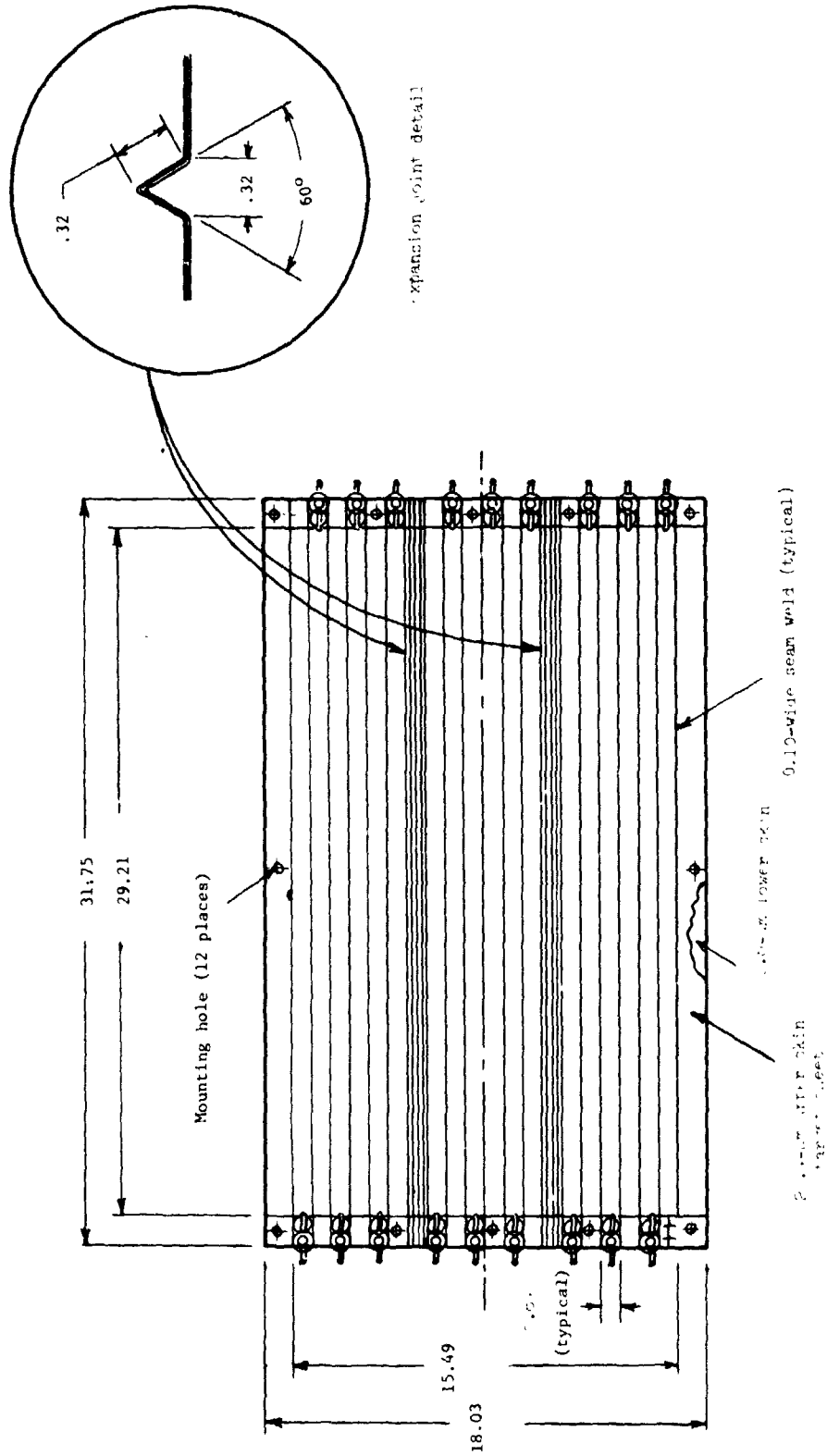


Figure III-1.- Sketch of pressurized cell detector panel. All dimensions are in centimeters unless otherwise noted.

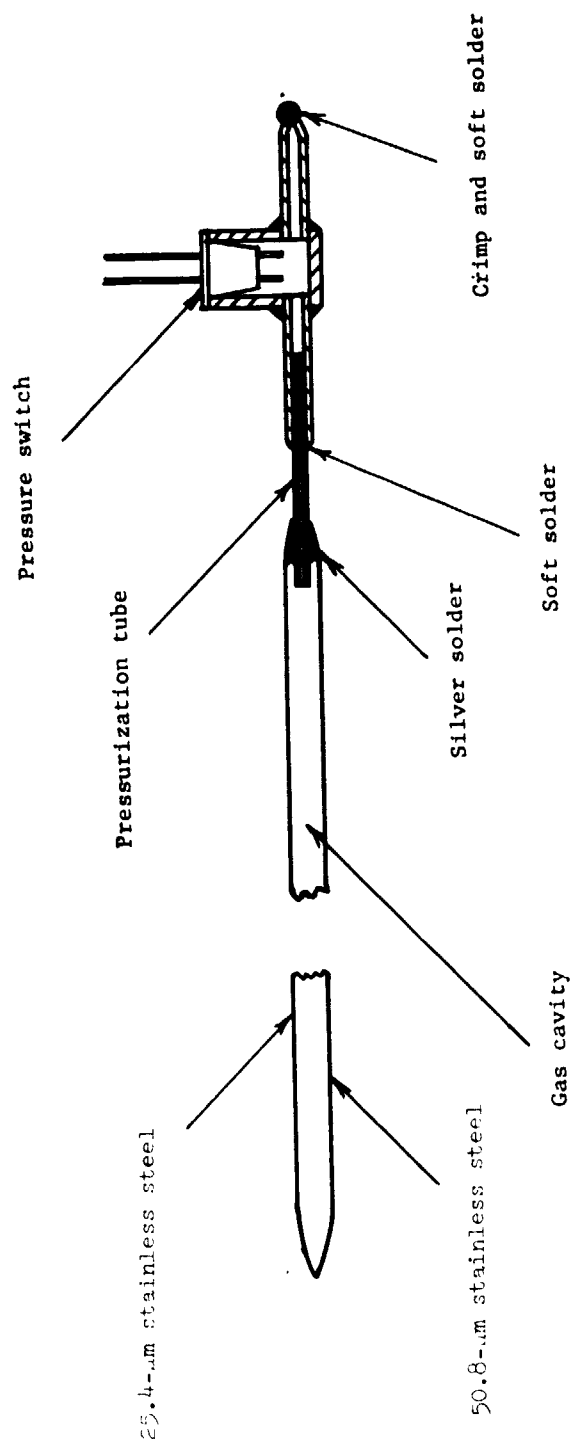
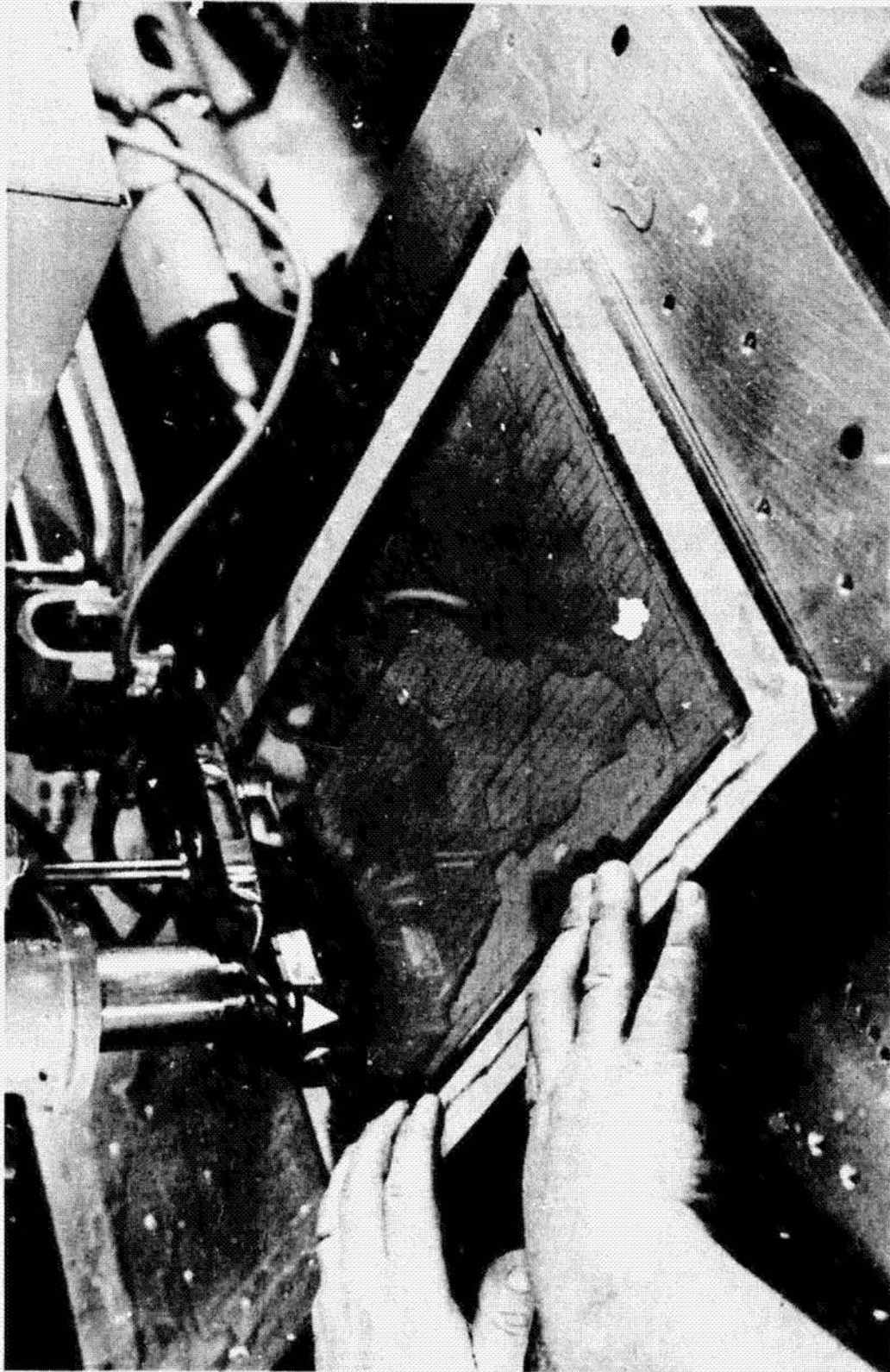
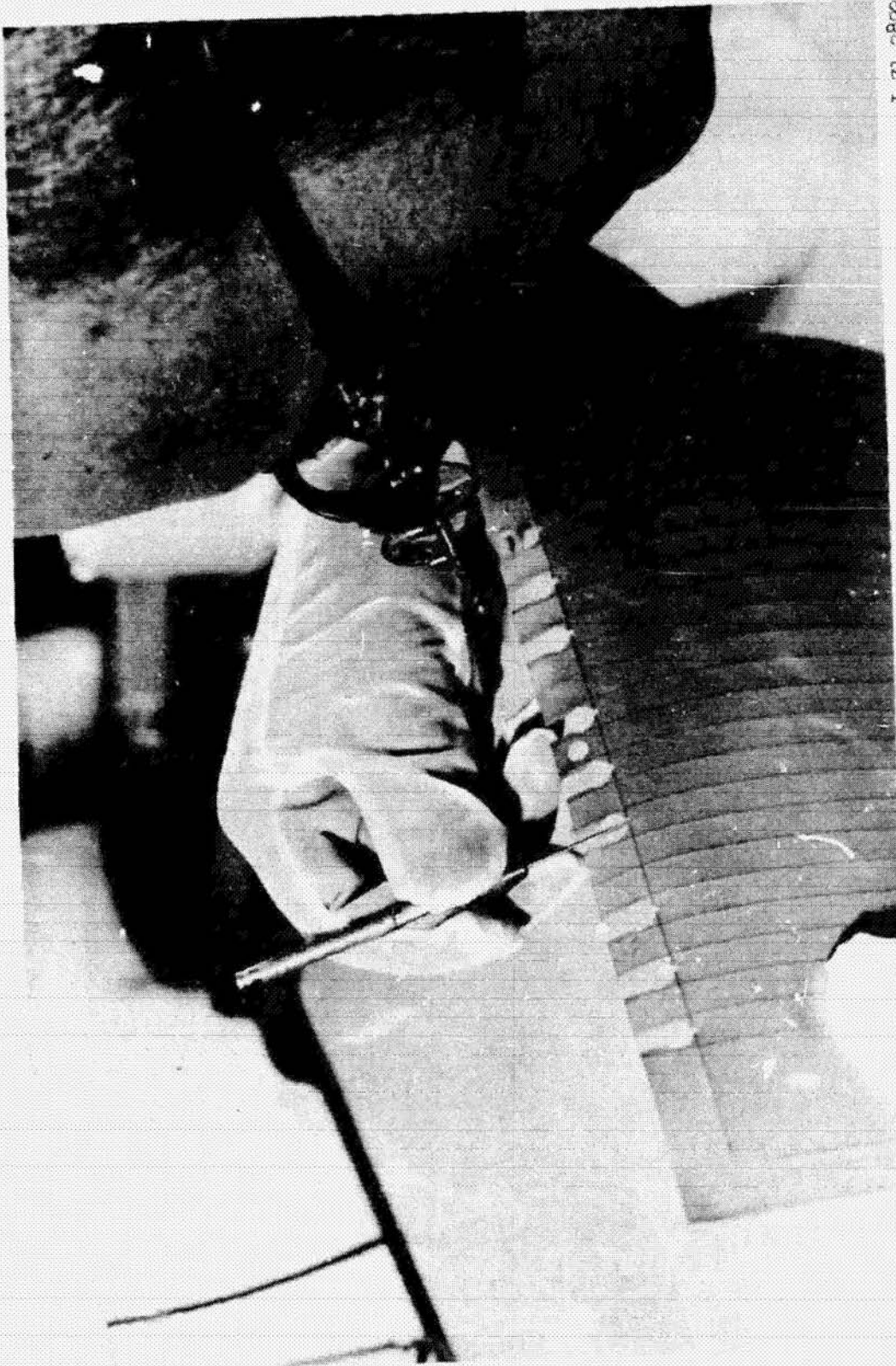


Figure III-2.- Schematic of pressure cell.



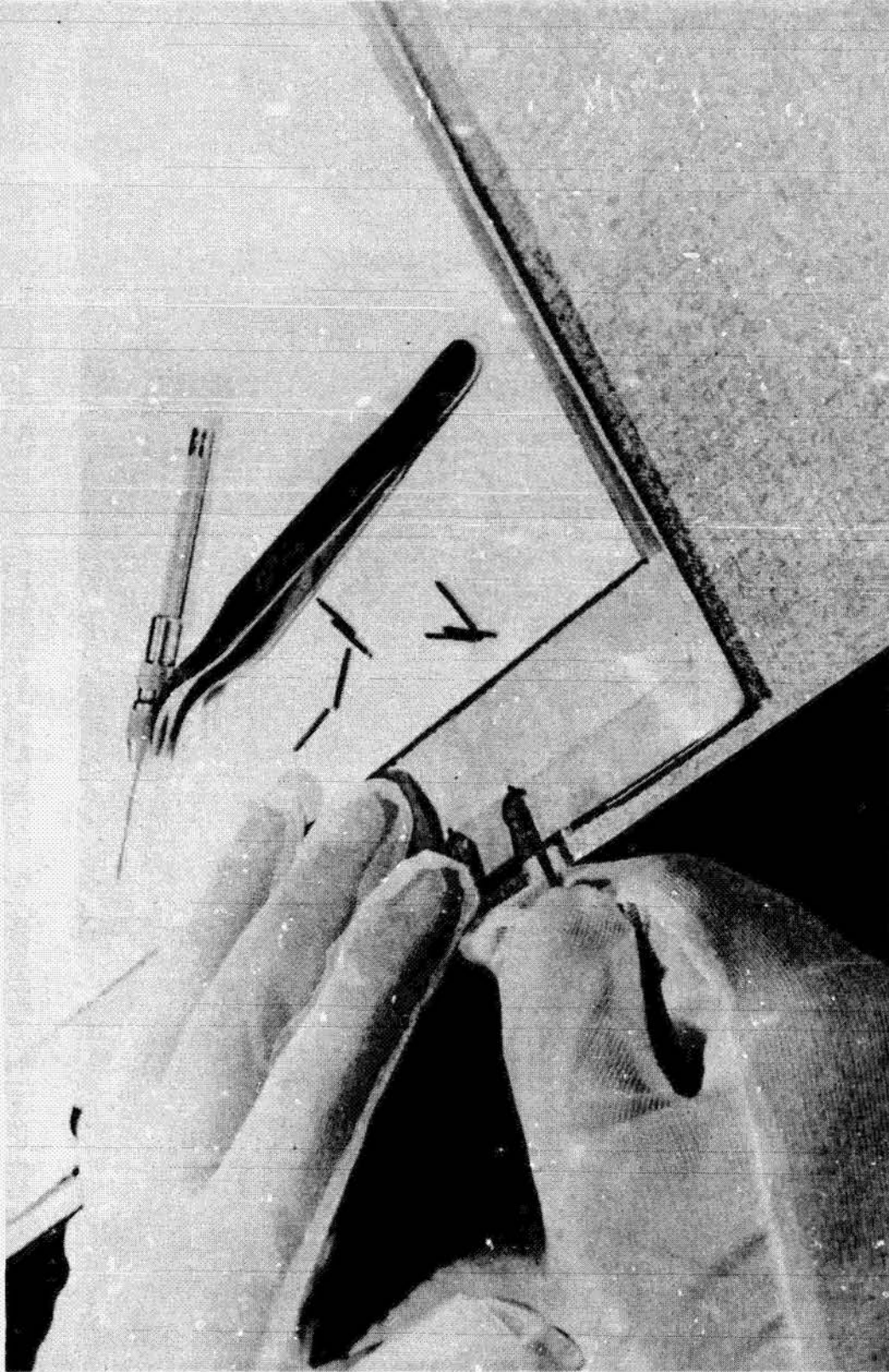
I-73-1094

Figure III-3.- Photograph showing 25- and 50- $\mu$ m stainless-steel sheets being welded together.



I-71-2892

Figure III-4.- Photograph showing preparation of holes in cells for pressurization tubes.



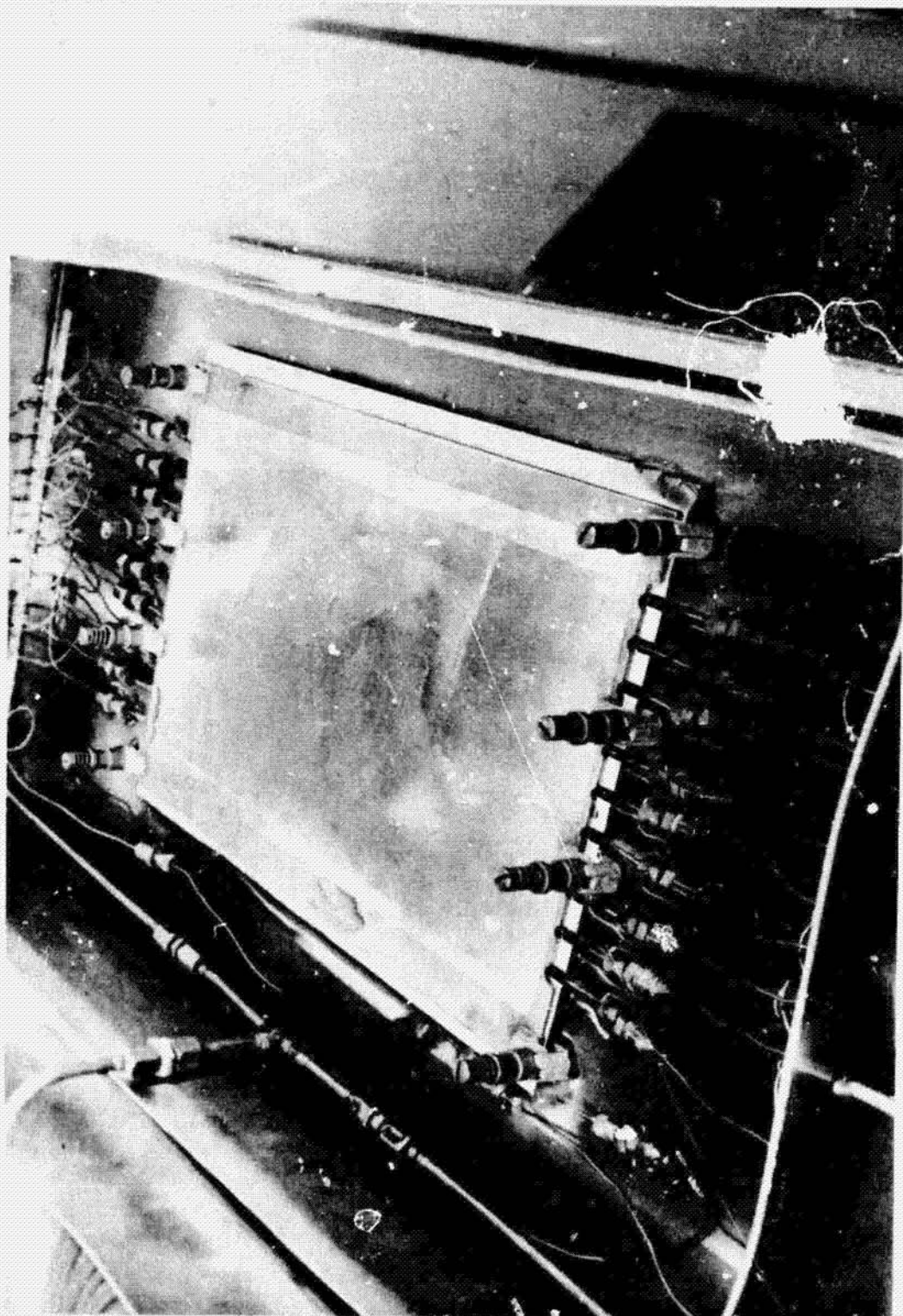
L-71-2888

Figure III-5.- Photograph of pressurization tube installation in panel.



L-71-2913

Figure III-6.- Photograph of pressurization tubes being silver soldered in cells.



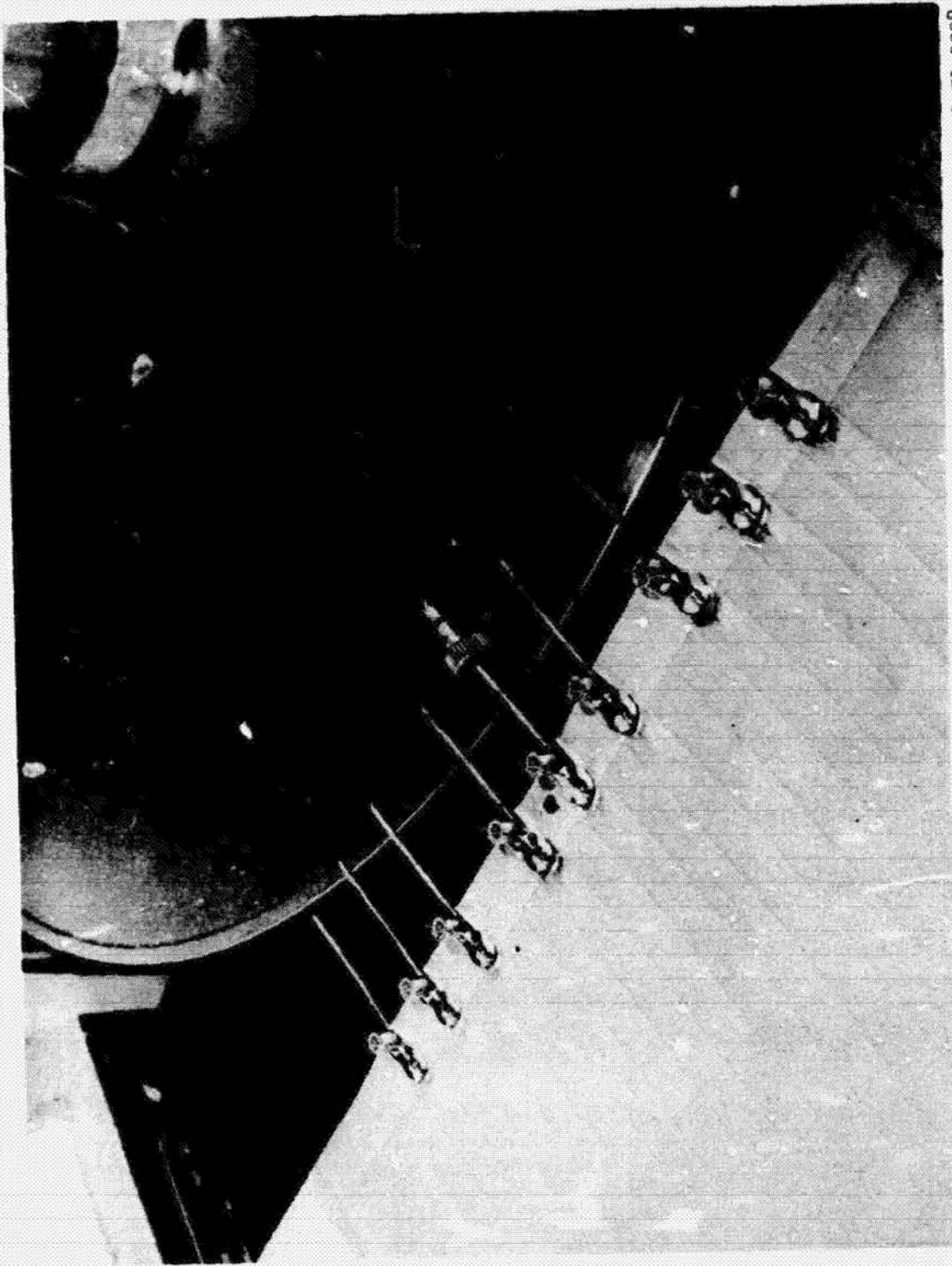
L-71-2919

Figure III-7.- Photograph of cells being flushed with boiling water.



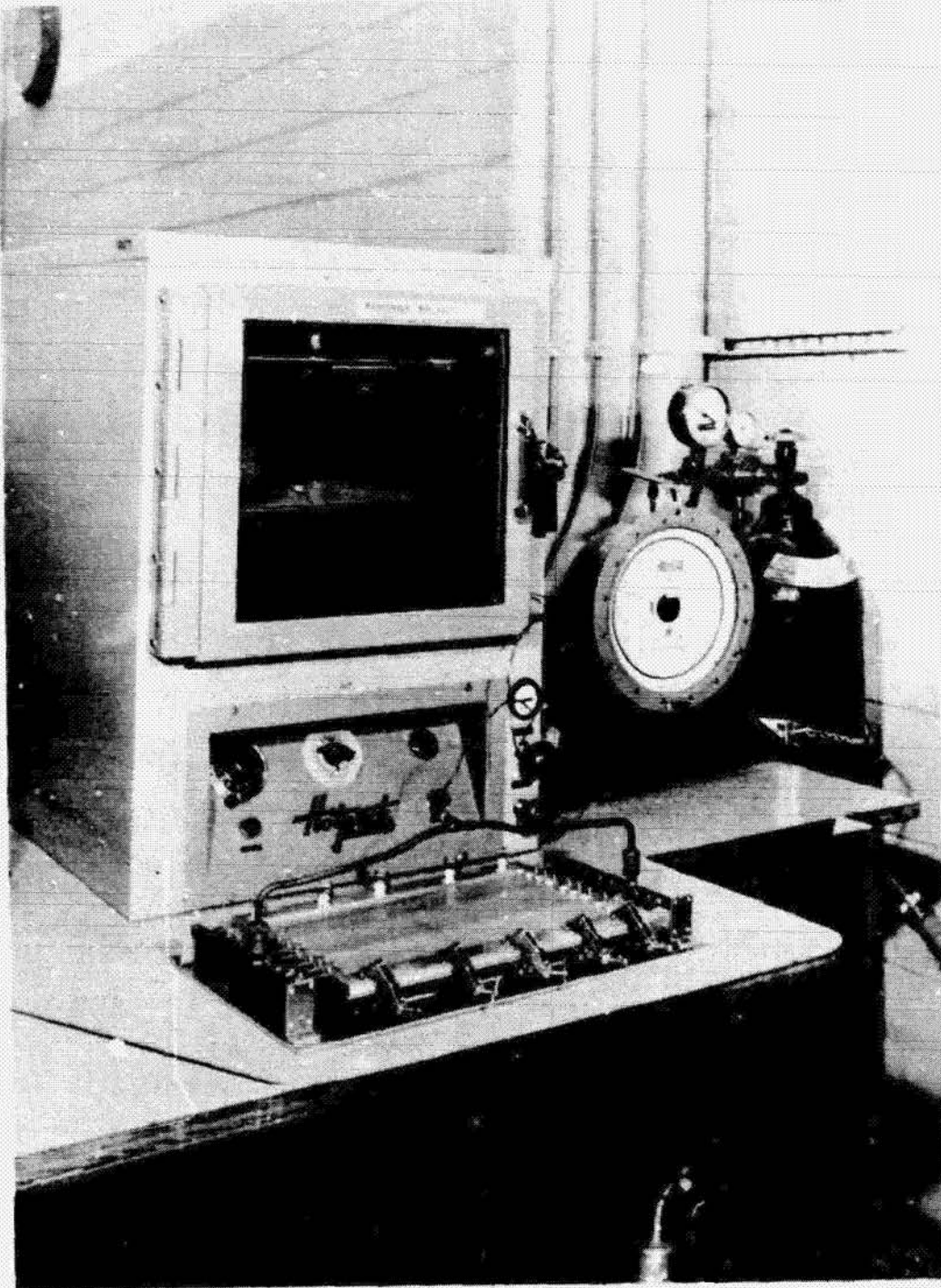
OK

Figure III-8.- Photograph of switch assemblies being soldered to pressurization tubes.



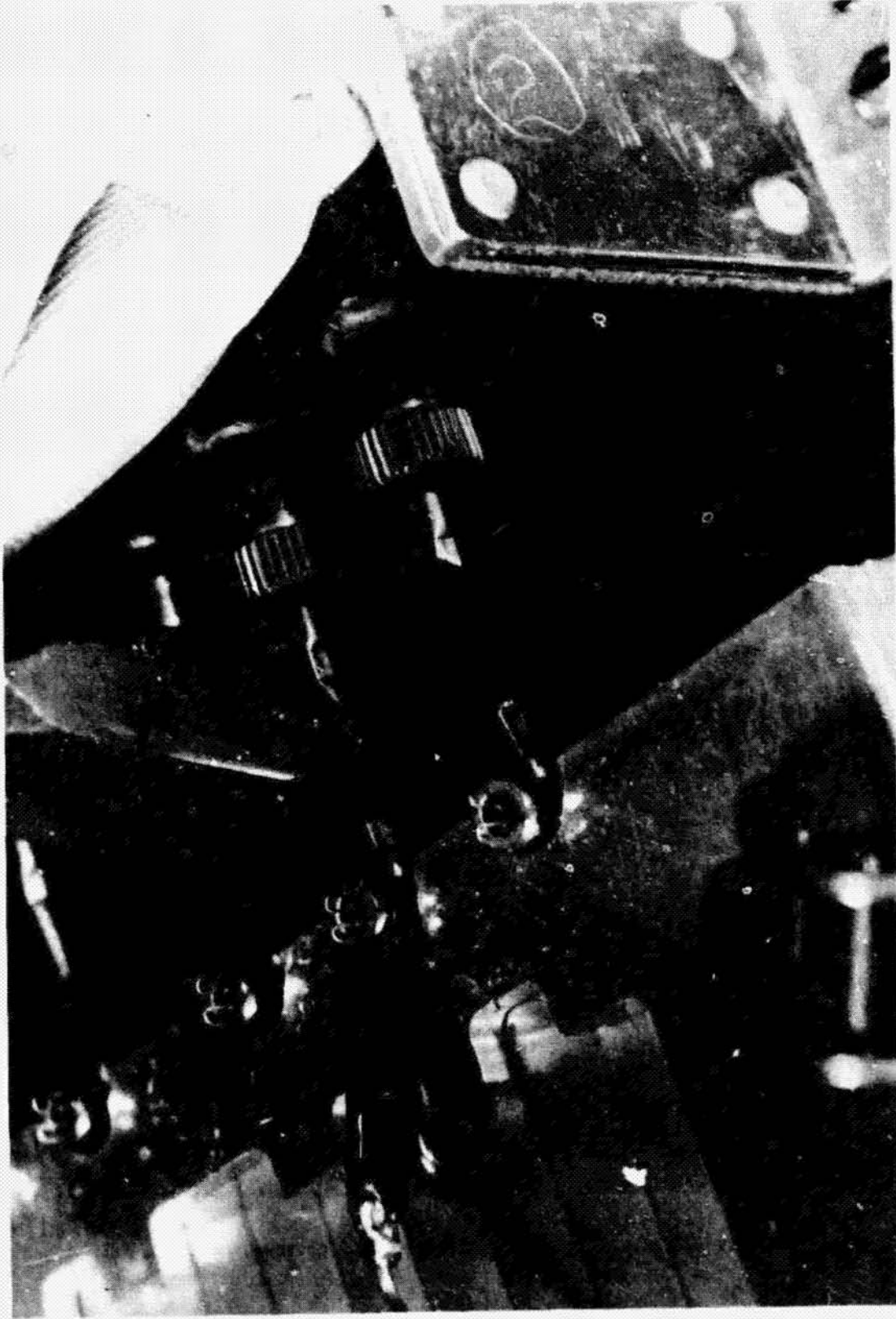
L-71-2928

Figure III-9.- Cell leak check after switch installation.



L-71-2907

Figure III-10.- Photograph of panel being pressurized.



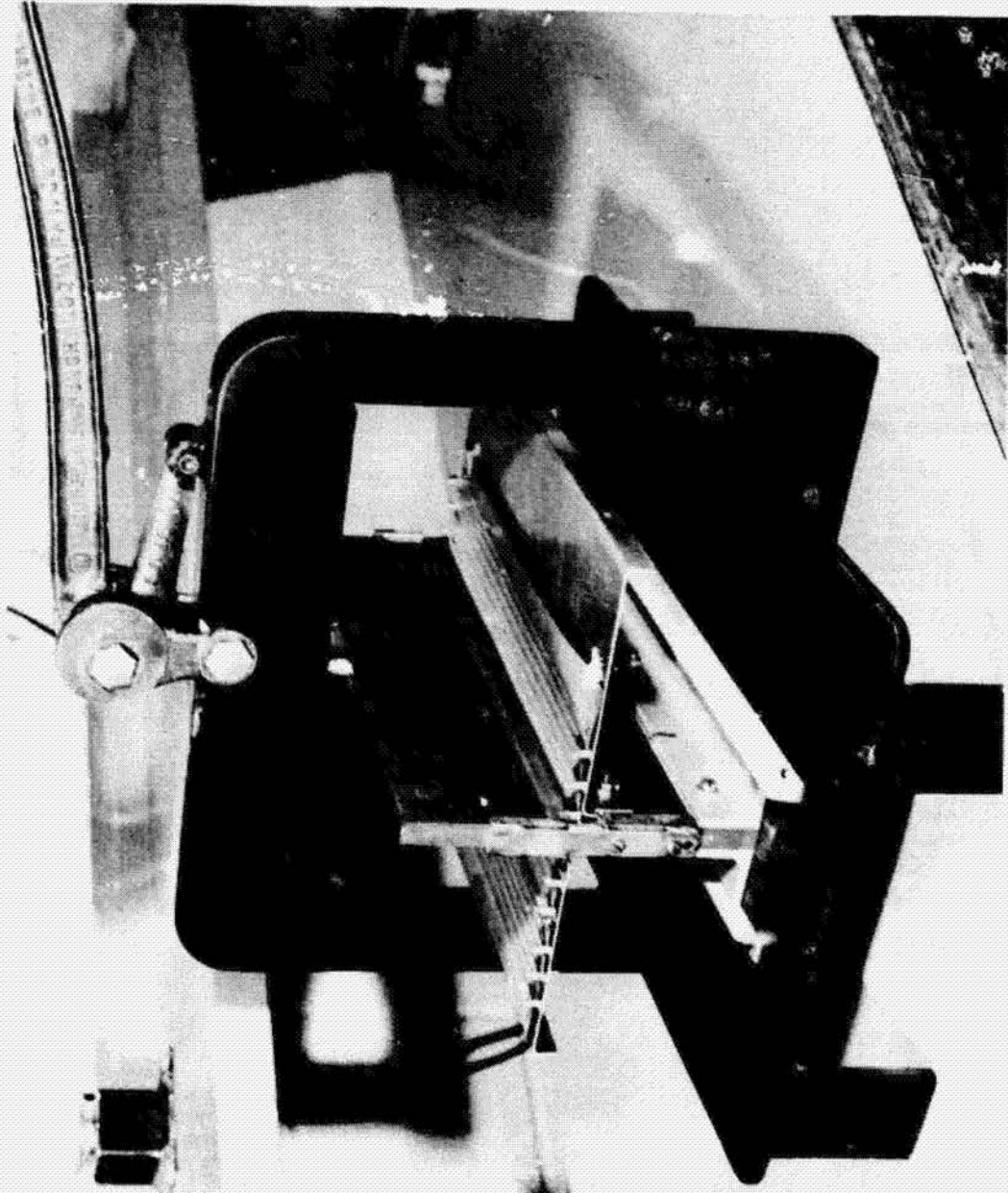
L-71-2887

Figure III-11. Photograph of individual cells being sealed after pressurization.



1-71-2909

Figure 111-12.- Panel installed in leak check facility



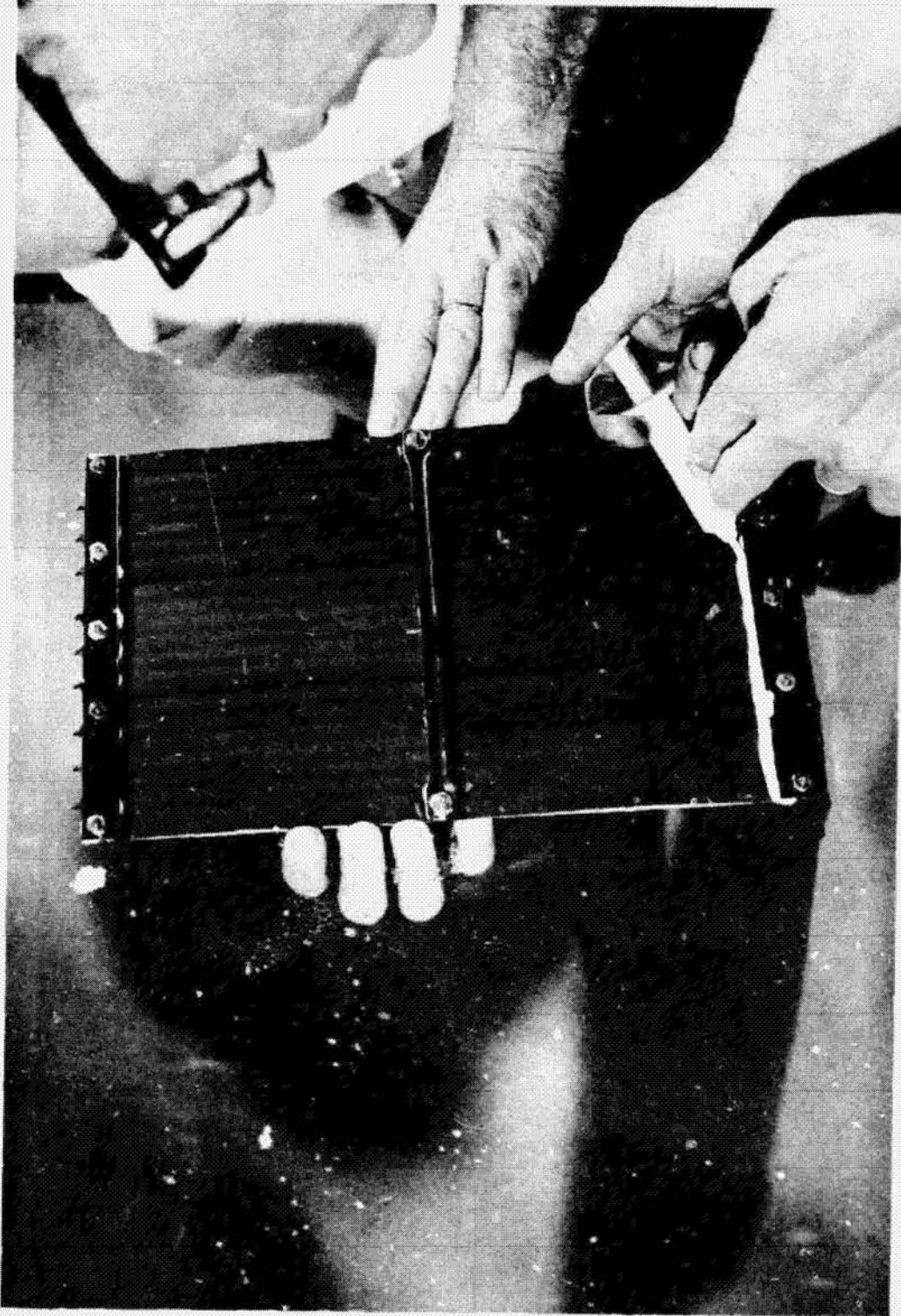
L-71-975

Figure III-13.- Expansion joint being pressed in sensor panel.



L-71-4300

Figure III-14.- Potting switch connections with RTV.



L-71-4299

Figure III-15.- Potting stiffener brackets to back of detector panel.

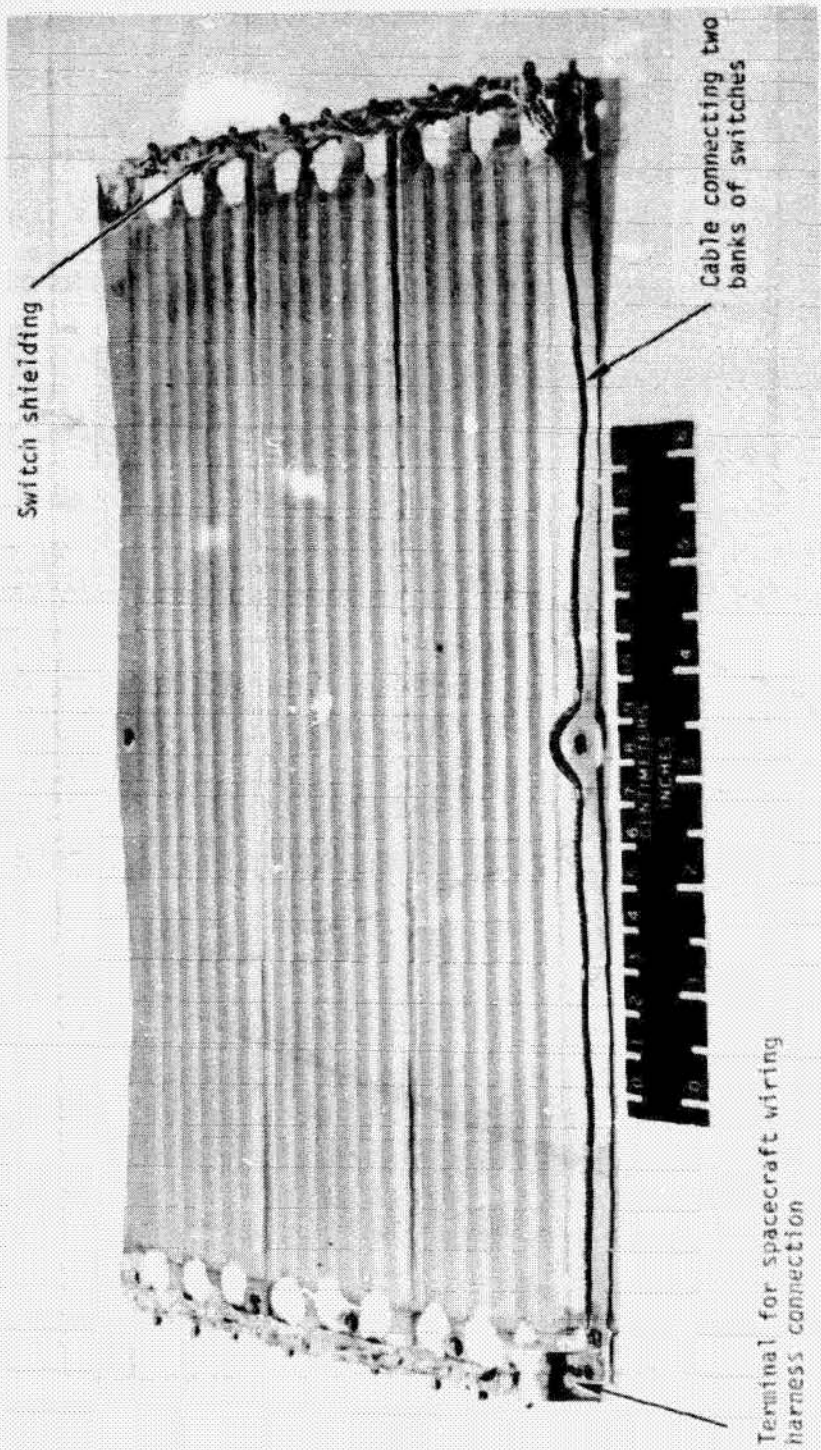


Figure III-16.- Photograph of completed pressurized cell detector panel.

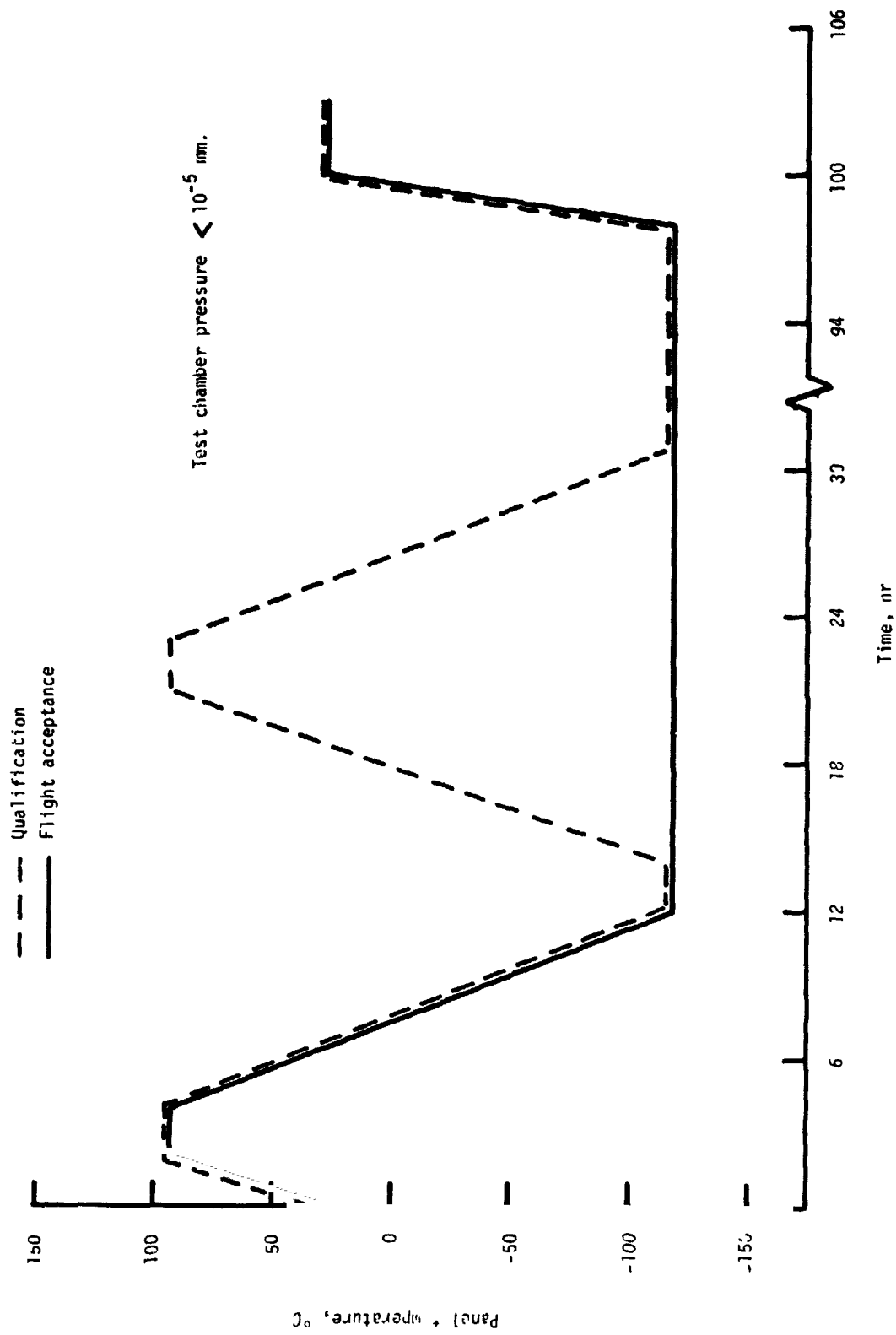


Figure III-17.- Detector panel temperature for qualification and flight-acceptance level tests.

#### **IV. PRESSURE MONITORING SYSTEM**

**By Leonard R. McMaster  
Langley Research Center**

**and**

**Carl D. Parker  
Research Triangle Institute**

#### **INTRODUCTION**

The large number of pressurized cells necessary to accomplish the meteoroid experiment on Pioneer 10 and 11 and the very small weight allowed for the experiment required the use of a unique sensor to detect penetrated pressure cells. At the beginning of the experiment design phase, an extensive survey of available pressure monitoring devices was made, but a developed system capable of meeting the functional weight and volume constraints placed on the experiment could not be identified. The pressure-diaphragm-operated microswitch-type sensor used successfully in the Explorer meteoroid satellites was too large and too heavy for this experiment. Additionally, a microswitch-type sensor required individual electrical leads between the sensors and the instrument electronics unit and, consequently, significantly increased the weight of the experiment.

As a result, a research effort was initiated at Langley Research Center to investigate the use of cold-cathode pressure-monitoring devices for application in meteoroid experiments. Theoretically, this type of sensor offered several unique features which made it very attractive for use in the Pioneer experiment. These features were (1) it could be made lightweight and (2) several switches could be wired in parallel; thus, the wire weight would be greatly reduced. Based on promising preliminary tests and the potential advantages offered, a decision was made to proceed with the development of a cold-cathode-type pressure switch optimized for this experiment.

#### **THEORY OF OPERATION**

A detailed description of the theory of operation of this type of sensor and some results of early tests in the research program are covered in reference IV-1. Some general details of how this device operates in the Pioneer experiment are given in the following paragraphs.

A gas in its normal state is an excellent insulator, but when an electric field of sufficient intensity is applied, the gas will become conductive. The voltage at which conduction will occur is a function of electrode geometry, electrode material, the gas being

used, the electric field, and gas pressure. For a given gas, electrode material, and electrode geometry, this relationship is illustrated by figure IV-1. At both higher and lower pressures, relatively larger voltages are required for breakdown. Thus, if the voltage impressed on the electrodes is above the minimum voltage  $V_1$  and the pressure  $p$  sufficiently high, a reduction in pressure to  $p_0$  will result in a change in conduction between the electrodes. This condition is evident in figure IV-1 where a voltage of  $V_2$  is impressed across a pair of electrodes in a gas at a pressure of  $p_4$ . In this dormant state, the current flow between the electrodes is essentially zero. If the pressure is allowed to decrease, a pressure  $p_3$  is reached where a glow discharge between the electrodes occurs and a significant current flow exists. This condition will exist until the pressure decreases to a pressure  $p_1$  at which point the glow discharge is no longer sustained and the current flow between the electrodes will again be essentially zero. In this manner, the cold-cathode device acts as an off-on-off switch and was so used in the Pioneer experiment.

#### ELECTRODE GEOMETRY

In the study of cold-cathode pressure-sensing devices for meteoroid experiment application (ref. IV-1) several electrode geometries were investigated. These studies indicated the optimum electrode geometry for a discharge tube to be a thin-wire cathode and coaxial cylinder anode with the cathode grounded, but it also showed a simple parallel-wire cathode-anode configuration to be an acceptable electrode geometry. Since parallel wire electrodes were simple, rugged, and commercially available, that electrode configuration was selected for future development and use in the experiment. The parallel rod electrode used in the experiment is shown in figure IV-2. This is a Kovar matched-expansion dual-lead terminal. This device was produced commercially for use as an electrical feedthrough in vacuum applications. The electrode assembly was soft soldered into a copper holder which becomes part of the pressurized cell gas cavity when installed as illustrated in figure IV-3. Figure IV-4 shows the components which make up a switch-tee assembly.

Numerous tests were conducted to establish Paschen characteristics of the pressure switch. The Paschen characteristics of the switch had to be defined in order to select the cell pressure and the switch voltage for proper switching action. Early attempts to establish the Paschen characteristics revealed that an initial ionization source was essential for reliable, repeatable pressure cell Paschen characteristics. A suitable isotope to provide the required ionization source was selected in view of the following criteria:

- (1) The half-life of the isotope had to be long to insure an adequate activity throughout the flight mission.

(2) The range of the particle emitted had to be long relative to electrode spacing and yet pose no hazard to personnel.

(3) A stable daughter was desired in the interest of simplicity, and

(4) The isotope had to be available in a convenient form compatible with the experiment.

Additionally, Pioneer specifications imposed the restrictions that

(1) No gamma emitters be used,

(2) The particle emission energy not exceed 7 MeV, and

(3) The total activity level not exceed 1  $\mu\text{Ci}$ .

Restrictions on the total activity required that each of the 234 switches in the experiment use less than  $1/234 \mu\text{Ci}$  and increased the importance of selecting an isotope with a convenient controllable form. At the time the selection was made, the total number of pressure cells had not been firmly established and the radioactivity level was limited to  $1/288 \mu\text{Ci}$ .

$\text{Ni}^{63}$  was selected from a survey of isotopes as the most suitable for the experiment. It has a half-life of 92 years, is a beta emitter with a decay of 67 KeV, a suitable range of approximately 5 cm in air and 0.0013 cm in copper, and a stable daughter ( $\text{Cu}^{63}$ ). It also poses no problem related to health hazards or Atomic Energy Commission regulations. A most important attribute was that it could be electroplated on the switch electrodes in precisely controlled, minute quantities. Reference IV-2 describes the  $\text{Ni}^{63}$  plating process and summarizes the  $\text{Ni}^{63}$  characteristics. The leakage current caused by betas leaving the cathode and arriving at the anode was calculated to be a negligible  $6 \times 10^{-15}$  amperes for worse case conditions. All electrode assemblies electroplated were checked to determine the amount of radioactivity plated and only those with  $1/288 \mu\text{Ci} \pm 15$  percent were used in the experiment.

### PRESSURIZING GAS SELECTION

Initial switch characterization tests were conducted with helium as the pressure cell working medium. Helium was selected because of previous experience in its use in meteoroid experiments and because techniques and equipment existed for detecting minute traces of this gas as required in pressurized cell leak tests. Later, the use of helium in the experiment was prohibited because one of the other scientific experiments on the Pioneer spacecraft was searching for helium as one of its scientific objectives and the use of helium would jeopardize the success of that experiment. An extensive program was then undertaken to identify another gas that would be acceptable for the meteoroid detection experiment.

The Paschen characteristics of cells pressurized with neon, nitrogen, argon, neon-nitrogen, and argon-nitrogen were established and evaluated in terms of switch firing levels, contamination sensitivity, thermal characteristics, and leak detection criteria.

In order to obtain a high reliability, it was necessary for the pressure cell to have a Paschen characteristic with a low minimum firing voltage and rise rapidly at pressures greater than or less than the minimum voltage and pressure. These characteristics provided the desired safety margin between the firing voltage  $V_3$  and the operating voltage  $V_2$  at both low and high pressures. (See fig. IV-1.)

Although stringent procedures were formulated and used to maintain cleanliness in the pressurized cell-switch system manufacture, it was desirable to use a gas the Paschen characteristics of which were not altered significantly by traces of moisture and air. This characteristic would make manufacture of the system easier and would also instill more confidence in the proper operation of the panel-switch system.

Two items were considered in evaluating thermal characteristics of the candidate gases. Calculation of pressure cell temperatures indicated that the cells would have to operate at temperatures as low as  $-164^{\circ}\text{C}$  at the Jupiter distance. It was, therefore, necessary that the Paschen characteristics be acceptable over a range of temperatures from room temperature to at least  $-164^{\circ}\text{C}$ . It was also desirable that the Paschen characteristics be acceptable to temperatures near that of liquid nitrogen,  $-196^{\circ}\text{C}$ , to allow the use of liquid nitrogen as the working medium for switch characterization and development tests.

Numerous switch characterization tests were conducted by using the candidate gases with varied results. It was found that the Paschen characteristics of the neon and neon-nitrogen gas were altered significantly by traces of air in the gas. The effects of these changes were to lower the Paschen curve at higher pressures and reduce the margin between switch firing voltage and operating voltage. The use of neon was eliminated on this basis. The nitrogen test data displayed a higher than desirable minimum voltage, but displayed a very desirable characteristic of increasing rapidly at pressures greater than or less than  $p_2$ . Argon test data indicated acceptable Paschen characteristics, but since argon liquefies at a temperature greater than liquid nitrogen temperature, the use of pure argon was eliminated. Tests were then run with argon-nitrogen mixtures in a ratio sufficient for the argon not to liquefy at  $-196^{\circ}\text{C}$ . Paschen data generated by use of such a mixture, 75 percent argon-25 percent nitrogen by volume, were acceptable, and this gas was selected as the pressurized cell gas. All pressurized cell detectors manufactured for flight were filled from a single container of gas. The results of a chemical analysis of the gas used are shown in table IV-1.

## PASCHEN CURVE DEFINITION

Numerous Paschen data were generated for the argon-nitrogen gas at both room and liquid nitrogen temperatures. Some typical data are shown in figure IV-5. Two techniques were used to obtain Paschen curve data. One technique was to set the pressure in a gas reservoir representing the pressure cell at a pressure sufficiently high so the switch would not fire at a given switch voltage. While holding the switch voltage constant, the pressure was slowly decreased and the pressure at which firing initiated was recorded. The other technique was to hold pressure constant and increase switch voltage until the switch fired. Both techniques were used to define the Paschen curve at room temperature and at cold temperature by immersing the gas reservoir and switch in liquid nitrogen. The data shown in figure IV-5 have some scatter. Such factors as electrode spacing, electrode surface roughness, and nonuniformities at the electrode ends due to a cutting operation in switch manufacture contribute to the scatter. The data shown are but a small part of the switch firing voltage-cell pressure data used to establish the switch operating voltage and cell pressure for the experiment. Adequate margins were allowed for the scatter found in the large data sample in setting voltage and pressure levels. Of the many hundred tests conducted in establishing the operating conditions of the gas-switch system, no switch failed to fire.

## DEFINITION OF PRESSURE SWITCH OPERATING CONDITIONS

The Paschen data represented by figure IV-5 were used to establish the switch voltage and cell pressure used in the experiment. The nominal switch voltage was defined by allowing a 100-volt margin above the highest firing voltage point observed in the liquid nitrogen temperature data at the bottom of the curve, that is, the highest minimum point. The highest minimum voltage observed was 425 volts. The electronic system was designed to provide 525 volts to the switch terminals.

The cell pressure was set at a level to insure the firing voltage in the dormant state in the space environment was greater than 1000 volts. This voltage would provide over 400 volts margin to insure no extraneous switch firing while the cell was pressurized with 525 volts impressed on the switch terminals. A large margin was desirable since there was significant scatter in the higher pressure Paschen data and since the pressure in the cells decreases, with a resultant drop in firing voltage, because of the cell expansion in a vacuum. The cells were pressurized to 1175 mm Hg to insure an adequate margin during flight. The firing voltages of cells in several panels were checked under vacuum conditions over a period of a year and this margin was found to be at least 500 volts. The switch voltage and panel pressure used in the experiment are shown with the Paschen data in figure IV-5.

## CONTAMINATION EFFECTS

A series of tests were conducted to determine whether either air or moisture in the pressurized cells would cause detrimental effects on the experiment operation. Although extreme care was taken in evacuating the cells before pressurization, it was hoped that an inadvertent inclusion of air or moisture would not result in an experiment malfunction.

Another series of tests was conducted to establish Paschen characteristics of a gas consisting of 63 percent argon, 21 percent nitrogen, and 16 percent air by volume. The results of these tests are shown in figure IV-6. Based on these data, it was concluded that any changes in the Paschen characteristics were insignificant, and even a sizable quantity of air in the cells would not cause the switch to function improperly.

To determine the effects of moisture on switch operation, several drops of distilled water were injected in a pressurized cell-switch test setup and pressurized with the argon-nitrogen gas and sealed. The pressure cell switch was then immersed in liquid nitrogen and, after reaching thermal equilibrium, was allowed to leak to a vacuum through a valving arrangement. It was found through several tests that the water froze and prevented gas flow in the switch-tee connection immediately after the leak to vacuum was established. However, after remaining connected to the vacuum system for a few minutes, the ice vaporized and the ensuing drop in switch-tee pressure caused the switches to fire in a normal manner. It was concluded that even large quantities of water in the cells would only delay a leak to vacuum and operation of the switch and would not result in an experiment malfunction during the mission.

## Ni<sup>63</sup> VARIATIONS

An analysis and experimental study was made to determine the adequacy of the quantity of Ni<sup>63</sup> deposited on the switch electrodes. The results of the analysis and supporting tests are covered in detail in reference IV-3. This analysis included estimates of the time required to exhaust the volume of gas in the switch housing through the small tube connecting this volume with the pressure cell. The analysis showed the shortest time required for the pressure to reduce from 100 mm to 1 mm Hg, the firing range of the switch, would be greater than 20 seconds. On the average, 94.5 electrons per second are available from the Ni<sup>63</sup> to initiate the ionization process. This quantity is adequate to initiate gas ionization and switch firing during the most rapid leak. Experimentally, it was not possible to induce switch failure to fire by initiating rapid leak rates.

The amount of Ni<sup>63</sup> plated on the electrodes used in the Pioneer experiment varied from 0.00255 to 0.00345  $\mu$ Ci (0.00300  $\mu$ Ci nominal). Tests were conducted to determine the variation in Paschen characteristics with large variations in the quantity of Ni<sup>63</sup>

plated on the electrodes. The results of these tests are shown in figure IV-7. The Paschen curves at both 25° C and liquid nitrogen temperature are essentially unchanged from the 0.00300  $\mu$ Ci units. These tests indicate the adequacy of the amount of Ni<sup>63</sup> used on the switch electrodes.

### SPUTTERING STUDY

To investigate the possibility of test firings sputtering electrode material and changing the pressure cell characteristics, a sample of cell-mounted transducers were forced to sputter in a continuous glow circuit that permitted approximately 1 watt of dissipation across the transducer for several seconds. Afterwards, leakage impedances were checked and observed to be still above  $10^{13}$  ohms and indicated that sputtered material had not created a significant metal film path between the electrodes. The firing voltages of the cells were observed to be approximately the same as before sputtering. The transducers were then removed from their housings and examined under a microscope for evidence of sputtering. In the most severe cases, the electrode surfaces, both anodes and cathodes, had a different finish; thus, some sputtering had occurred. Finally, the radioactivity of the transducers was measured and compared with previous readings. The cathodes were then removed and the anodes recounted. These results, presented in table IV-2, do not show any significant differences between the electrodes. These results also indicate that sputtering of electrode material including the Ni<sup>63</sup> electroplate did occur. Increasing the power dissipated and time did not significantly influence the results and suggests that the sputtering became localized on the electrodes and continued in the same area.

It is significant that although power dissipation in this sample was increased so that sputtering was caused to occur, it did not degrade the pressure cell performance. It is concluded, therefore, that the pressure cells could be fired in numerous tests without causing any degradation due to sputtering.

### CONCLUDING REMARKS

The cold-cathode device developed for the Pioneer experiment has been demonstrated to be a very reliable pressure switch. The only disadvantage of this off-on-off type switch is that it has no inherent storage of a penetration event and, as a result, it must be powered and monitored continuously by the instrument electronics system. This disadvantage is minor, however, since the instrument will remain on throughout the mission and full-time data coverage will be obtained.

## REFERENCES

- IV-1. McMaster, Leonard R.: **Sensor for Detecting Meteoroid Penetration of Pressurized Cells.** NASA TN D-6447, 1971.
- IV-2. Parker, C. D.: **Evaluation of a Gas Discharge Transducer and Associated Instrumentation Necessary for the Asteroid Belt Meteoroid Experiment.** Contract NAS1-9420, Res. Triangle Inst., Feb. 1971. (Available as NASA CR-111848.)
- IV-3. Parker, C. D.: **Experimental Program To Determine Long-Term Characteristics of the MDE Pressure Transducers.** Contract NAS 1-10175, Res. Triangle Inst., Jan. 1973. (Available as NASA CR-112273.)

**TABLE IV-1.- CHEMICAL ANALYSIS OF GAS**

Component	Result	Unit of measure
Nitrogen	24.5	Molar percent
Oxygen	1.0	Molar ppm
Carbon dioxide	<0.5	Molar ppm
Carbon monoxide	<1.0	Molar ppm
Nitrous oxide	<0.1	Molar ppm
Methane	<0.5	Molar ppm
Acetylene	<0.05	Molar ppm
Total hydrocarbons	<1.0	Molar ppm
Water	<0.15	Molar ppm
Water	-87° C	Dewpoint
Argon	Balance	Molar ppm

**TABLE IV-2.- SPUTTERING STUDY RESULTS**

Transducer	Power dissipated, W	Time, sec	Radioactivity, $\mu$ Ci		
			Initial	After sputtering	Anode only
1	0.76	15	3	0.8	0.4
2	.76	30	3	.7	.3
3	1.4	15	3	.9	.6
4	1.4	30	3	.8	.4
5	1.4	120	3	.8	.4

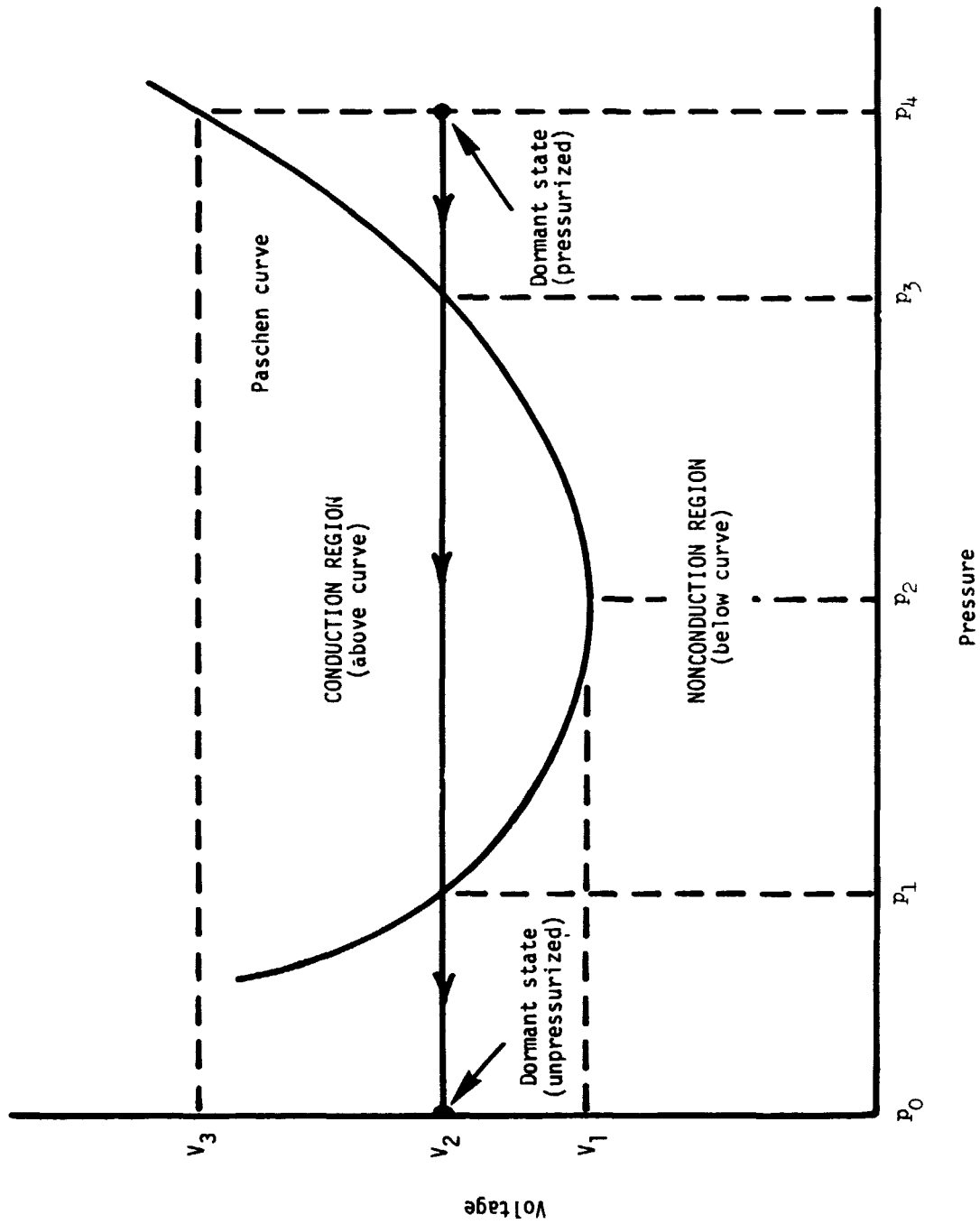


Figure IV-1.1.- Illustration of breakdown voltage as a function of gas pressure  $P$ .

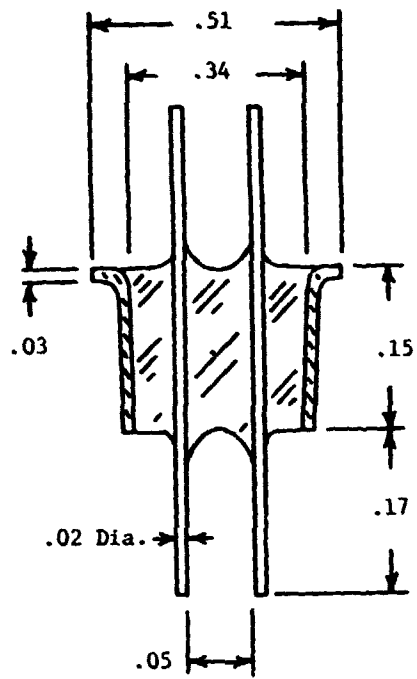


Figure IV-2.- Sketch of vacuum feedthrough used in pressure switch. Dimensions are in centimeters.

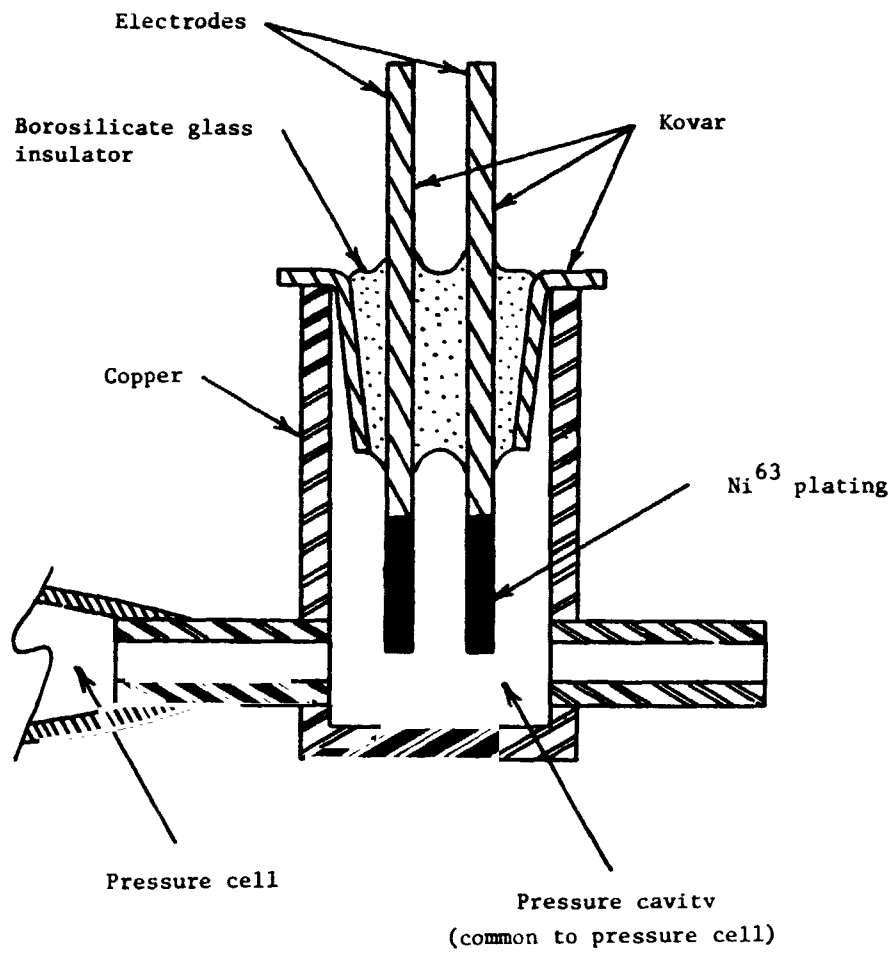
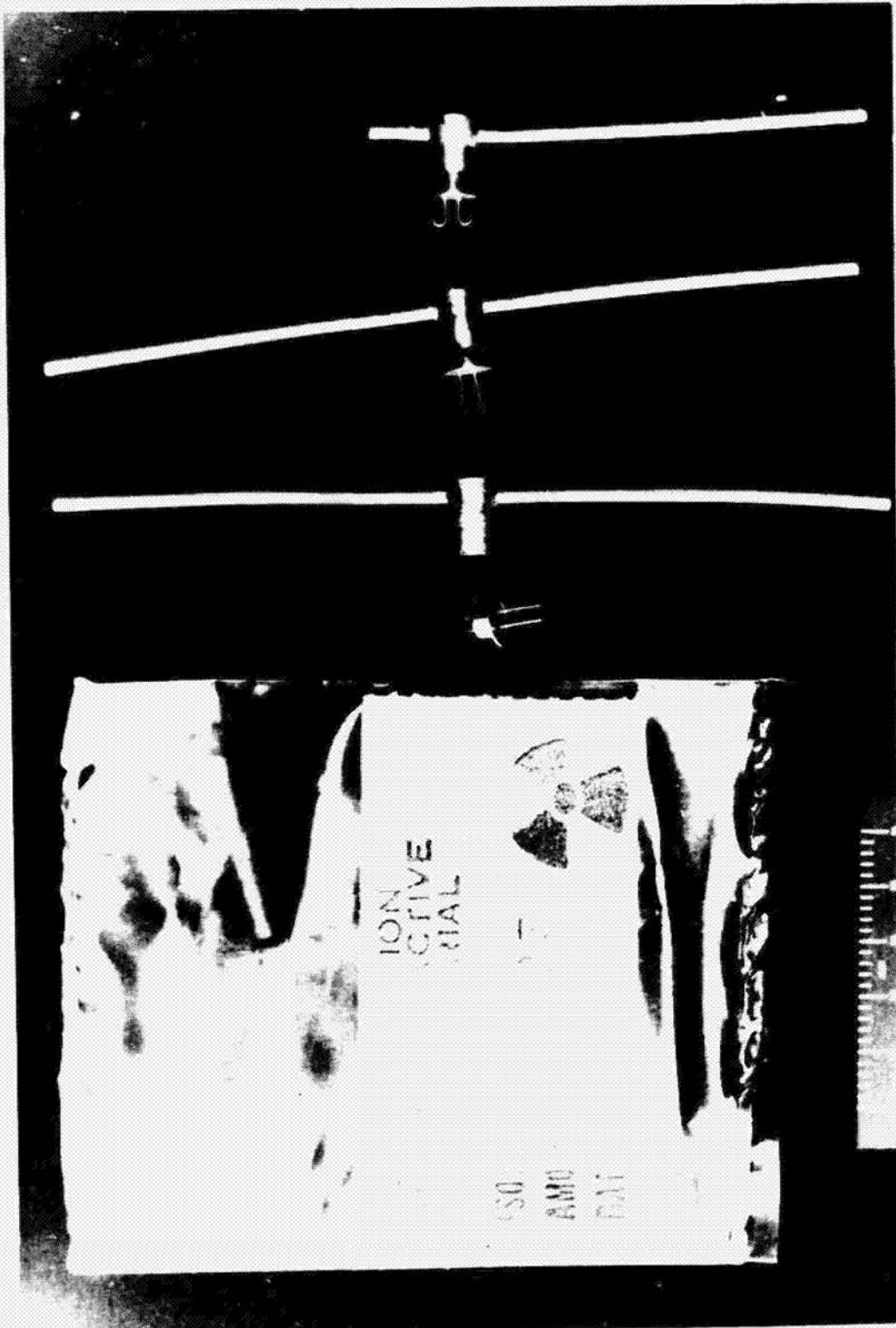


Figure IV-3.- Sketch of pressure switch assembly.



I-70-9054

Figure IV-4.- Photograph of pressure switch component parts before and after assembly.

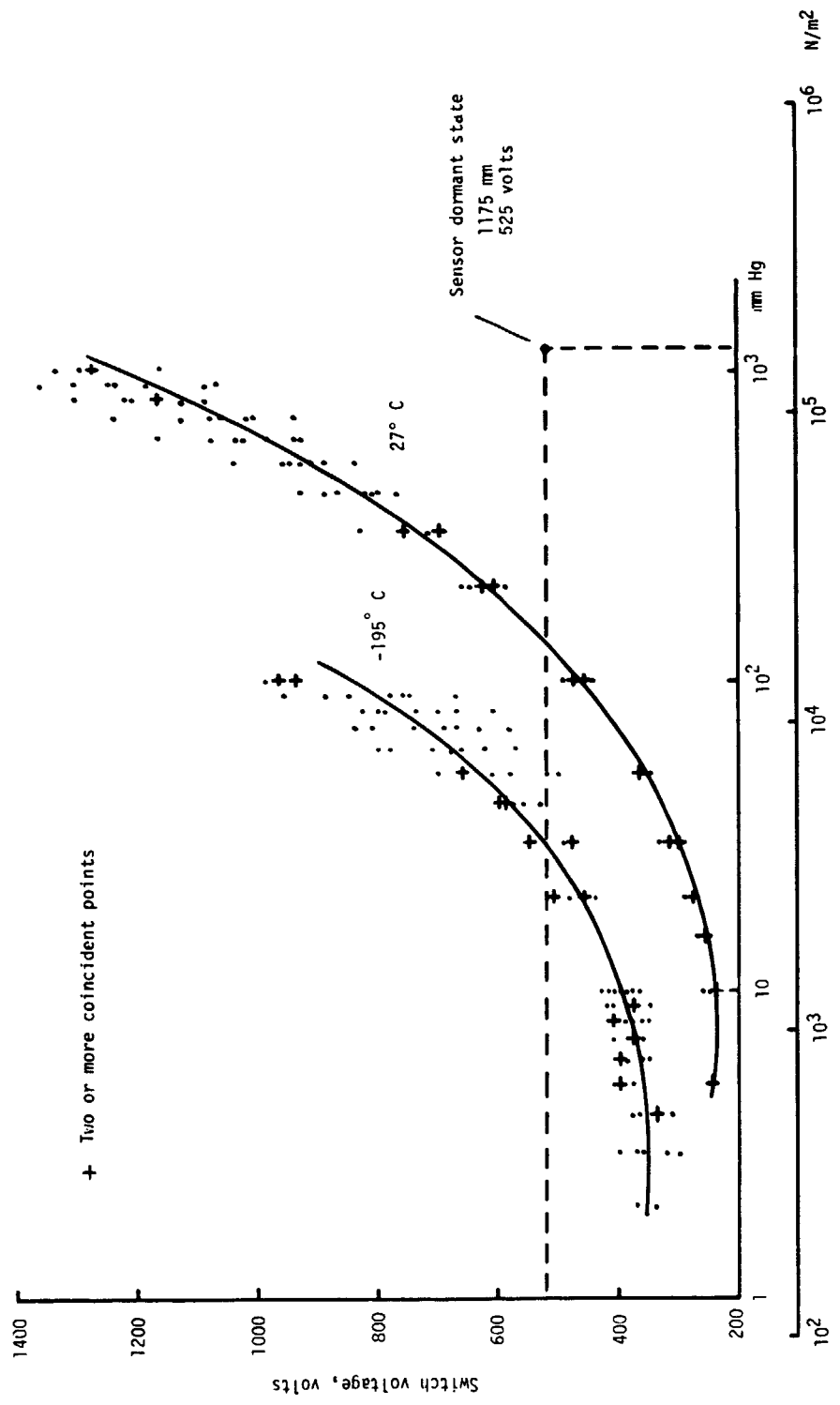


Figure IV-5.- Typical Paschen data for two gas temperatures.

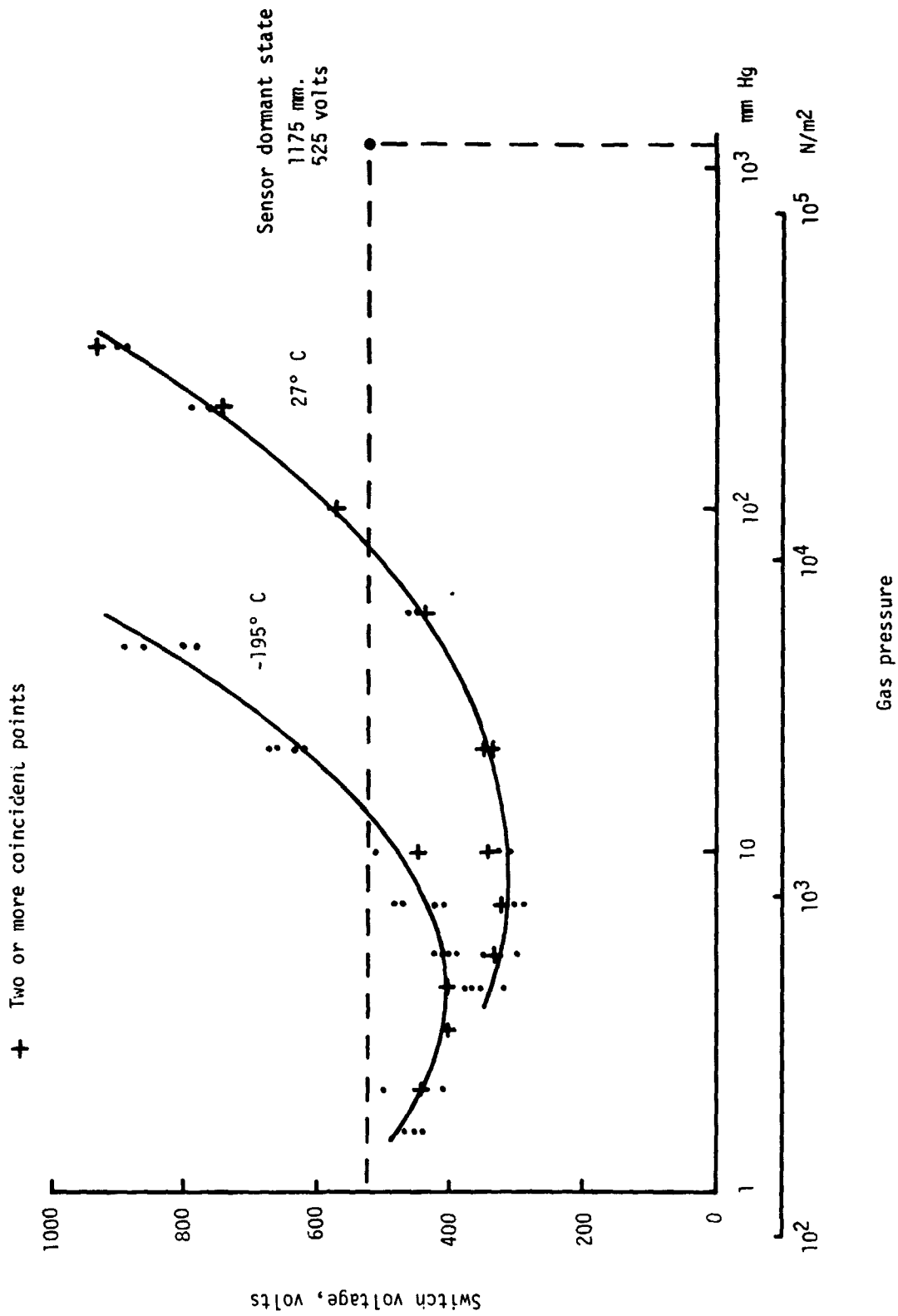


Figure IV-6.- Paschen curves for a 63 percent argon, 21 percent nitrogen, and 16 percent air mixture.

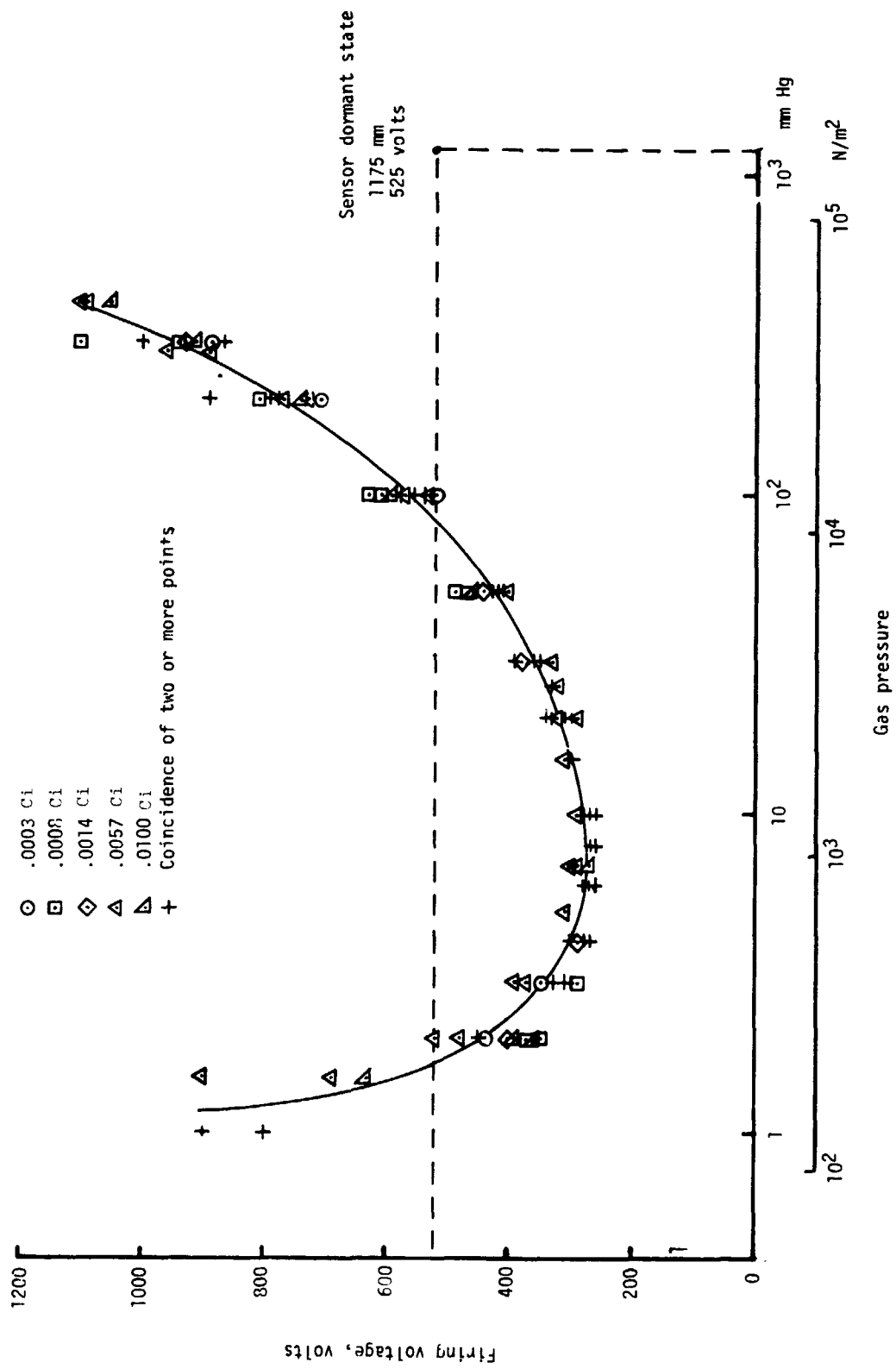


Figure IV-7.- Paschen characteristics with various quantities of NiO<sub>3</sub>. Gas temperature, 25° C.

## V. ELECTRONIC SYSTEM

By John Thomson  
Langley Research Center

### INTRODUCTION

As discussed in sections III and IV, each pressurized cell has a switch which, in the event of a penetration will signal the loss in cell pressure. The meteoroid detection experiment (MDE) electronics system detects the switch impedance change, conditions the resulting signal, registers and stores the count, and converts the stored count to a digital data word in the spacecraft telemetry system. The data from the experiment is the cumulative number of penetration events which have occurred. The spacecraft has communications coverage by the Deep Space Network (DSN) during the mission.

### SYSTEM OPERATION

The operation of the electronic system is dependent on a meteoroid penetration at a sensor panel and the functional control of the system by the spacecraft. Figure V-1 is a functional block diagram of the experiment. The experiment was divided into 13 panels of 18 switches each and 2 channels of electronics. Seven panels (126 switches) were connected to one of the channels and 6 panels (108 switches) were connected to the other channel. The two channels were used to improve the instrument reliability. The design and operation of both electronic system channels shown in figure V-1 are the same. The instantaneous conduction of any of the 234 individual sensor switches is detected and processed by the signal conditioner and registered in the event counter. The parallel output from the event counter is transferred to the storage register and then converted to serial digital data. The spacecraft supplies the necessary word gates and bit shift pulses to convert and time multiplex the data to the science frame of the spacecraft telemetry. The spacecraft also supplies the primary power for the instrument and an instrument on-off control signal. The data transmitted from the spacecraft will consist of the latest count in the storage register. The number of meteoroid penetrations is determined relative to previous readouts from the spacecraft.

### INSTRUMENT DESCRIPTION

The description of the penetration detector panels and associated switches and the placement of the panels on the spacecraft are described in other sections of this paper. Figure V-2 is a photograph of the electronic system assembly. The system is encased in a 7.5-cm-cube housing, weighs 409 grams, and requires a nominal 675 mW of primary

electrical power. Coaxial cable is used in the spacecraft wiring harness connecting the sensor panels to the electronic system to reduce the interference caused by radio-frequency radiation during switch conduction. The interface connections to the electronic system are shown in the block diagram of figure V-1. The physical layout of modules within the electronic system is shown in the photograph of figure V-3 and the detailed schematic of the system is shown in figure V-4. The two channels are indicated in figure V-3. Each of these channels contains a signal conditioner, event counter, and storage-register/converter. Where feasible, the system was designed by use of low power transistor-transistor logic (TTL) integrated circuits to minimize the power required by the instrument. One dc-dc converter, shown in figure V-3, distributes power to both channels of the system.

#### Signal Conditioner

The signal conditioner (fig. V-5) consists of a pulse shaper to detect a glow discharge in a sensor switch, an OR circuit to isolate the individual sensor panels, a time-controlled transmission gate to trigger the event counter and block all extraneous counts generated during switch conduction, and a reset generator to control the time the transmission gate is inhibited.

The pulse shaper (the bottom modules of fig. V-3 and the schematic diagram of fig. V-6) was designed to serve three functions. The first requirement of the circuit is to reduce the switch conducting power to a level which will keep the total instrument power within the limited power supplied to the instrument. The circuit was designed to limit the energy available at the switch during conduction. The  $0.01 \mu\text{F}$  capacitor stores 1.37 mJ of energy at 525 volts ( $CV^2/2$  where C denotes capacitance and V, the voltage) which allows conduction through the switch for 1.5 msec per ionization. The capacitor is recharged from the 525-V power supply through a 10-M $\Omega$  resistor in 100 msec. The resulting 1.5-percent duty cycle requires an average power during switch conduction of 15 mW. The 10-M $\Omega$  resistor also takes care of the circuit requirement to eliminate the possibility of a shorted switch causing a catastrophic failure of the experiment. A low impedance at a switch will drain a small amount (25 mW) of continuous power from the electronic unit. This level is well within the constraints of the power supply. A short at a switch will eliminate the associated panel from the experiment, but the 10-M $\Omega$  resistor isolates the faulty panel from the circuit. The resistive voltage divider and direct-current blocking capacitor take care of the last requirement of the circuit which is to match the impedance and voltage levels of the switch driving the circuit to the impedance and voltage levels of the TTL integrated circuits. In the standby condition of no switch conduction, the voltage across the voltage divider is zero. In full conduction the switch impedance drops to approximately 150 000 ohms and causes a 200-V pulse to be developed across the voltage divider. The series voltage divider reduces the high voltage of the

drive circuit to the 4-V positive going pulse required to drive the TTL inverter input of the OR circuit. The divider also matches the impedance of the inverter circuit to maintain a logical zero of less than 700 mV.

The OR circuit of the signal conditioner isolates the individual sensor pane's. When there is conduction in any of the pulse shaper circuits, the event will register at the transmission gate. The transmission gate (fig. V-5) is a basic set-reset flip flop. The leading edge of the OR circuit output sets the gate to an inhibited condition which triggers the event counter and starts the reset generator. The gate is inhibited for 85 minutes to eliminate extraneous counts during switch conduction from entering the event counter. The inhibit period was determined by an analysis to determine the maximum cell leak-down time which could be expected during the mission. This analysis is presented in section VIII of this paper. After 85 minutes, a pulse from the reset generator resets the transmission gate and readies the gate for the next penetration event.

The reset generator is controlled from the output of the transmission gate. When the gate is in a reset condition, the output voltage level (5 V) holds the 10-stage binary counter in a reset-inhibited state. When a penetration signal sets the transmission gate, the output voltage level drops to zero and enables the reset generator to count the 0.1-Hz pulses from the low-frequency clock. At the end of 512 counts (85 minutes), the counter output resets the transmission gate and enables the gate for the next event.

The low-frequency clock (0.1 Hz) is an astable multivibrator using complementary metal oxide semiconductor field-effect transistors (MOS-FET). The MOS-FET transistors were used in the circuit to keep the power drain from the instrument to a minimum. The high gate impedance of MOS-FET also improved the wave shape of the extremely slow clock pulse. In addition to supplying the clock pulse to the reset generator counter, the clock also supplies the load pulse to the storage register.

#### Event Counter

The event counter (fig. V-7) is a 5-bit ripple-through counter that registers the number of penetration events. The counter does not utilize a reset capability; therefore, the transmitted count is relative to the counter state prior to each spacecraft interrogation. A flip-flop in a latched condition is used for channel identification, a logical 0 for channel 1 and a logical 1 for channel 2. The channel identification appears as a sixth bit of data from the event counter.

#### Storage-Register/Converter

The storage-register/converter (fig. V-8) consists of a shift register that stores the event count and converts the stored count to a serial digital output. In addition, the unit has a level converter and two buffer stages. The parallel output from the event

counter is coupled to the storage register every 10 seconds by a load pulse from the low frequency clock of the reset generator. The shift register is controlled by the word gate levels and the bit shift pulses from the spacecraft digital telemetry unit. The presence of the word gate level inhibits the parallel inputs from the event counter and enables the six-bit shift pulses associated with the word gate time interval to the clock inputs of the shift register. The shift register then cycles through the six data bits and shifts the parallel data to serial digital data to be time multiplexed in the digital telemetry unit of the spacecraft. The level converter is required to make the instrument compatible with the spacecraft telemetry system. The buffer stages in the bit shift and word gate lines, a Pioneer requirement, are for the protection of the spacecraft in case of a voltage fault in the instrument.

#### dc-dc Converter

The instrument is supplied with primary power from the spacecraft power bus. The power conversion is accomplished by the dc-dc converter, the right-hand module of figure V-3, and the schematic diagram of figure V-9. The converter was developed under contract with Wilmore Electronics Co., Inc., Durham, North Carolina. The system converts the spacecraft primary power of 28 V dc to instrument voltages of 525 V dc to bias the sensor switches, 10 V dc to operate the low frequency clock, and 5 V dc to operate the integrated circuits. The converter can be turned on and off by external control.

#### DATA PROCESSING

The spacecraft has a number of telemetry formats that can be selected by ground command. These formats concern data from the scientific instruments and engineering data on the performance of spacecraft systems. To simplify the data format description, it is assumed that the engineering data for the spacecraft trajectory is automatic and that the MDE is only involved with the main and subcommutated (subcom) science telemetry format.

The science main frame is composed of 192 bits divided into 64 telemetry words of 3 bits per word. The science subcom word of the main frame consists of two consecutive words, 6 bits. The science subcom formats are essentially a single frame of science information composed of 384 bits divided into 64 telemetry words of 6 bits per word. For every main frame telemetered, one word of the science subcom frame is telemetered. The spacecraft accepts the two digital words from the MDE instrument as two telemetry words in the science subcom frame. The two words, equally spaced, are then telemetered in the science subcom word of the science main frame. The spacecraft has the capability of transmitting at various bit rates ranging from 2048 bits per second, command controlled down to 16 bits per second, in factors of two depending on range and

receiving antenna used. The data readout for the experiment will be every 6 to 768 seconds depending on the transmission bit rate selected. For the prime data period the data readout is expected to be in 24-second cycles. The MDE telemetry format in the science subcom of the spacecraft is shown in table V-1. The computer program converts the two digital words in the science subcom word of the main frame to a decimal number and prints the resulting numbers as shown in table V-2. The on-off status of the experiment is displayed as a single bit in the engineering format titled C-1, word 24, bit 6.

### TEST PROGRAM

The test program for the experiment and spacecraft was set up in three phases. During the first phase, the Design Verification Unit (DVU) was fabricated by using flight-type hardware and tested to verify design feasibility, parts suitability, and fabrication methods. The prototype unit, used for phase two testing, was fabricated by using flight components and was completely representative of the flight instrument. The prototype unit was exercised and evaluated in all operating modes under conditions simulating 150 percent of launch and flight environment to insure functional capability during launch and flight conditions. The third phase was the flight-acceptance testing of all flight units to prove their acceptability for flight. Four flight-acceptable units were fabricated, two flight units and two backup units.

The ground support equipment (GSE) shown in figure V-10 was specially designed to exercise the electronic system for all testing prior to launch. The GSE provides an accurate simulation of the Pioneer spacecraft and supplies power and control functions for all unit level testing and trouble shooting. The GSE also injects an artificial signal into the sensor output to duplicate hits at the sensors and processes the telemetry data for a nixie lamp display or recording on an oscillograph. The functional block diagram of figure V-11 shows the GSE experiment system used for unit level testing. Figure V-12 depicts the oscillograph format used during unit level testing to record the profiles and signal amplitudes.

A test that verified the operation of the electronic system was performed before, during, and after the temperature and thermal-vacuum tests and before and after all other environmental tests. Basically, the test consists of injecting the equivalent of 72 sensor hits to the unit under test to establish that the instrument is functioning satisfactorily. Essentially, the same test is used for spacecraft level testing. However, the GSE only supplies the equivalent of sensor hits to verify that the electronic system is operational following adverse effects from the test environment. The spacecraft supplies the power and control of the instrument as in actual flight and the data are displayed on the computer printout. The GSE automatic sequence is used for all testing with the exception of the counter-inhibit verification which uses the manual mode of operation. A meggar test

was used to verify the sensor panel integrity. (This test involves the use of a special instrument which measures resistance in megaohms). The meggar test is gross, but it has been determined that a good cell will have an impedance of  $10^{11}$  ohms while an open circuit will indicate  $10^{12}$  ohms or more. This meggar test also verifies the isolation of the sensor panels from the high-gain antenna.

### Functional and Design Verification Tests

The DVU unit was fabricated by using unscreened components that were equivalent to the anticipated flight components and the engineering model of the dc-dc converter. The DVU unit was tested in the sequence shown in table V-3. The unit level functional and design verification tests were performed at Langley Research Center (LRC) and verified the conformance to design, assessed the performance, and established operating criteria. The physical properties, interface, magnetic moment, and electromagnetic interference tests were performed at Ames Research Center (ARC) and verified the ability of the unit to meet design specifications. The mechanical and electrical integration and limited instrument performance tests were performed at TRW Systems Inc. (TRW) on the engineering model spacecraft and verified the electrical and mechanical interface, instrument and data-subsystem compatibility, and the computer software program. The DVU unit verified the instrument requirements, demonstrated that the design goals were met, and that the spacecraft and instruments were compatible. There were four modifications to the experiment as a result of the functional and design verification testing.

During the initial functional checkout of the unit, the integrated logic circuits were susceptible to noise. The noise susceptibility was reduced by decoupling the logic supply voltage line and rerouting the signal return lines. The magnetic moment measurement exposed a magnetic cable on the sensor panels. The magnetic moment of the panels was reduced to below specification level by replacing the copper-coated iron (copper-clad) coaxial cable with a silver-coated copper coaxial cable.

Two problems were discovered during the electromagnetic interference testing at the unit level. The first problem was that with the switches firing, the panels were generating an interference signal above the Military Standard 462 specification level as shown in figure V-13. The radiation was reduced to below specification level by wrapping the sensor switches and lead wires with aluminum-coated Mylar. The second problem was in the electronic unit. The electromagnetic interference (EMI) testing showed that the dc-dc converter had a critical frequency of approximately 9 MHz as shown in figure V-14. The conducted radiation was reduced to below specification level by capacitively balancing the power lines.

### Unit Level Qualification Tests

The prototype unit, a counterpart of the flight instrument, was fabricated by using flight hardware and was space qualified through the testing sequence shown in table V-3. The unit level testing was performed at LRC and the spacecraft systems level testing was performed at TRW on the prototype spacecraft.

Environmental test specifications.- The following specified environments were used for flight qualifying the electronic system for the Pioneer 10 and 11 spacecraft using the Atlas/Centaur launch vehicle.

**Vibration test:** The vibration was applied along each of the orthogonal axes as shown in figure V-2 for a 1 g sine sweep from 10 to 2000 Hz and a sinusoidal and random motion vibration as listed in tables V-4 and V-5.

**Acceleration test:** The unit was mounted on the acceleration table at an angle of 90° from the vertical spin axis which allowed the 3 minute 48 g acceleration level to be applied to the unit along the same axis as it was applied to during launch acceleration.

**Shock test:** The unit was subjected to a half-sinusoidal shock level of 50 g for a duration of 6 msec along each of the orthogonal axes. The unit was dropped three times per axis at this level.

**Temperature test:** The unit, while operating, was subjected to temperature extremes of -29° C and 38° C.

**Humidity test:** The unit was exposed to a temperature of 30° C and a relative humidity of 95 percent for a period of 24 hours.

**Thermal-vacuum test:** The operating unit was subjected to an 34-hour, -29° C temperature soak, and a 84-hour 38° C temperature soak at a vacuum of  $10^{-5}$  mm of mercury.

Unit level qualification test results.- The prototype unit had a total of four failures at the end of unit level testing. The failures were: one operator fault, one design deficiency, and two defective TTL integrated circuits. Detailed failure analyses were run and precautions were taken to minimize the possibility of reoccurrence.

### Unit Level Flight Acceptance Tests

All flight units were tested in the sequence shown in table V-3 and were determined to be acceptable for flight. The backup units were not tested at the spacecraft level.

**Environmental test specifications:** The following test specifications were for flight acceptance of the instrument for the Pioneer 10 and 11 flights using the Atlas/Centaur launch vehicle.

**Vibration tests:** The vibration was applied along each of the orthogonal axes shown in figure V-2 for a 1 g sine sweep from 10 to 2000 Hz and a sinusoidal and random motion vibration as listed in tables V-6 and V-7.

**Temperature tests:** The unit while operating, was subjected to temperature extremes of  $-18^{\circ}\text{C}$  and  $32^{\circ}\text{C}$ .

**Thermal-vacuum test:** The operating unit was subjected to a 84-hour,  $-18^{\circ}\text{C}$  temperature soak and a 84-hour,  $32^{\circ}\text{C}$  temperature soak at a pressure of  $10^{-5}$  mm of mercury.

Unit level flight acceptance test results.- All unit level testing was completed on the flight and backup unit with a total of two failures. The failures were caused by an operator error and a defective TTL integrated circuit. Detailed failure analyses were run and precautions were taken to minimize the possibility of reoccurrence.

#### Spacecraft Level Tests

The following section is a brief description of the spacecraft level testing that was performed at the spacecraft contractor's (TRW) laboratories. The engineering-model spacecraft and the DVU were used for mechanical and electrical interface testing, limited instrument tests, and for proofing the procedures. The prototype spacecraft and instrument were used to complete all testing at the qualification environmental levels and were also used for proofing the test procedures. The flight spacecraft and instrument followed the prototype sequence of testing but at flight-acceptance environmental levels.

Limited instrument performance test.- An end-to-end systems test was used to verify the compatibility of the instrument with the data subsystem of the spacecraft and to verify the correctness of the computer software.

Integrated system test.- An end-to-end test of the complete system was used to verify satisfactory operation of the instrument.

Spacecraft EMI determination.- A measurement of the electromagnetic signature of the spacecraft was used to evaluate the effect of EMI on the spacecraft bus.

Detailed instrument performance test.- An end-to-end test for a detailed examination of the operation of each experimenter's instrument with all instruments and subsystems operating was performed.

Radioisotope thermoelectric generator (RTG), spacecraft, and instrument integration test.- A performance monitoring test was performed to establish the compatibility of the radioisotope thermoelectric generator, spacecraft and instrument with the radioisotope thermoelectric generator (RTG) configured for flight.

Spacecraft magnetic field susceptibility test.- A performance monitoring test was made to observe the effect on the operation of the spacecraft and the instruments when the spacecraft is placed in a magnetic field of up to 20 gauss peak to peak.

Spin test.- A performance monitoring test was made to verify the operation of all systems with the spacecraft rotating at 180 revolutions per minute.

Functional test.- A functional checkout of the spacecraft systems was made to verify operation after all prior testing.

Vibration test.- A performance monitoring test was made to verify operation of spacecraft systems after being exposed to qualification or flight-acceptance level vibrations.

Thermal-vacuum test.- A performance monitoring test was performed to verify complete spacecraft functional capabilities under simulated flight environment. Simulated sun levels at 0.9 AU and 5.5 AU at a pressure of  $10^{-4}$  mm Hg are used for this test.

Post environmental instrument performance test.- A detailed instrument performance test was made after the spacecraft and instrument have successfully completed all environmental tests.

Launch site integrated system test.- An end-to-end test was made to verify the satisfactory operation of the instrument upon arrival at Eastern Test Range.

Launch site detailed instrument performance test.- A final detailed examination of the operation of the instrument was made before committing to launch.

Spacecraft level test results.- The prototype instrument was successfully qualified for flight on the prototype spacecraft and the flight instruments were found to be acceptable on the flight spacecraft.

TABLE V-1.- TELEMETRY FORMAT

Science subcom word	7						39					
Bit	1	2	3	4	5	6	1	2	3	4	5	6
Weighting	$2^0$	$2^4$	$2^3$	$2^2$	$2^1$	$2^0$	$2^0$	$2^4$	$2^3$	$2^2$	$2^1$	$2^0$
Type data	0 Event count						1 Event count					
	Channel 1						Channel 2					

TABLE V-2 - DATA FORMAT

Experiment identification	Decimal number	Channel identification *
/L/	XX	0
/L/	XX	1
/L/	**XX	0
/L/	**XX	1

\* 0 indicates channel 1; 1 denotes channel 2.

\*\* Indicates change in value compared with last readout.

TABLE V-III.- INSTRUMENT TEST SEQUENCE

	Unit level										Spacecraft level																				
Unit	Functional	Design verification	Physical properties	Interface	Magnetic moment	Electromagnetic interference	Thermal	Acceleration	Shock	Vibration	Humidity	Thermal-vacuum	Panel/instrument integration	Mechanical integration	Electrical integration	Limited instrument performance	Integrated systems	Detailed instrument performance	Electromagnetic interference	RTG/spacecraft/instrument integration	Magnetic field susceptibility	Spin	Functional	Vibration	Thermal-vacuum	Post environmental	Integrated systems	Launch-site integrated systems	Launch-site detailed instrument	Functional	
DVU	X	X	X	X	X	X	X	X	X	X	X	X	X	X	X	X	X	X	X	X	X	X	X	X	X	X	X	X	X	X	X
Prototype	X	X	X	X	X	X	X	X	X	X	X	X	X	X	X	X	X	X	X	X	X	X	X	X	X	X	X	X	X	X	X
Flight	X	X	X	X	X	X	X	X	X	X	X	X	X	X	X	X	X	X	X	X	X	X	X	X	X	X	X	X	X	X	X

**TABLE V-4.- SINUSOIDAL VIBRATION**

[Sweep rate, 2 octaves/minute]

Axis	Frequency range, Hz	Acceleration, g units (0 peak)
Z-Z and Y-Y	5 to 22	*0.4
	22 to 50	10.0
X-X	50 to 200	6.0
	5 to 18	*0.4
	18 to 150	6.5
	150 to 200	9.0

\*Units are inches double amplitude instead of g units.

**TABLE V-5.- RANDOM MOTION VIBRATION**

[Test duration, 2 minutes/axis]

Axis	Frequency range, Hz	Power spectral density, g <sup>2</sup> /Hz
All	20 to 60	Increases at 12 dB/octave to 0.2 at 60 Hz
	60 to 1500	0.2
	1500 to 2000	Decreases at 12 dB/octave from 0.2 at 1500 Hz

**TABLE V-6.- SINUSOIDAL VIBRATION**

[Sweep rate, 4 octaves/minute]

Axis	Frequency range, Hz	Acceleration, g units (peak)
Z-Z	5 to 40	13.5
	40 to 70	6.5
	70 to 200	3.5
X-X	5 to 150	4.5
	150 to 200	5.5
Y-Y	5 to 60	4.5
	60 to 90	8.5
	90 to 200	2.0

**TABLE V-7.- RANDOM MOTION VIBRATION**

[Test duration, 1 minute/axis]

Axis	Frequency range, Hz	Power spectral density, g <sup>2</sup> /Hz
All	20 to 60	Increases at 12 dB/octave to 0.089 at 60 Hz
	60 to 1500	0.089
	1500 to 2000	Decreases at 12 dB/octave from 0.089 at 1500 Hz

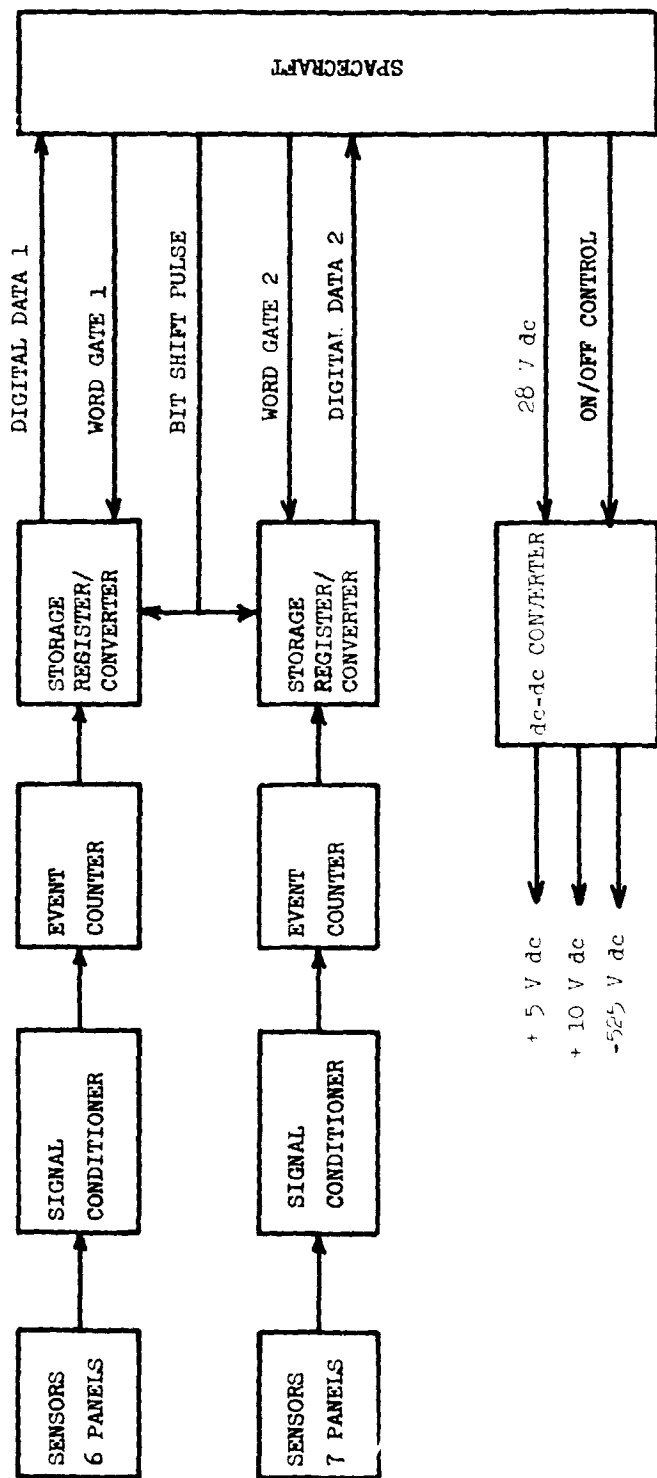
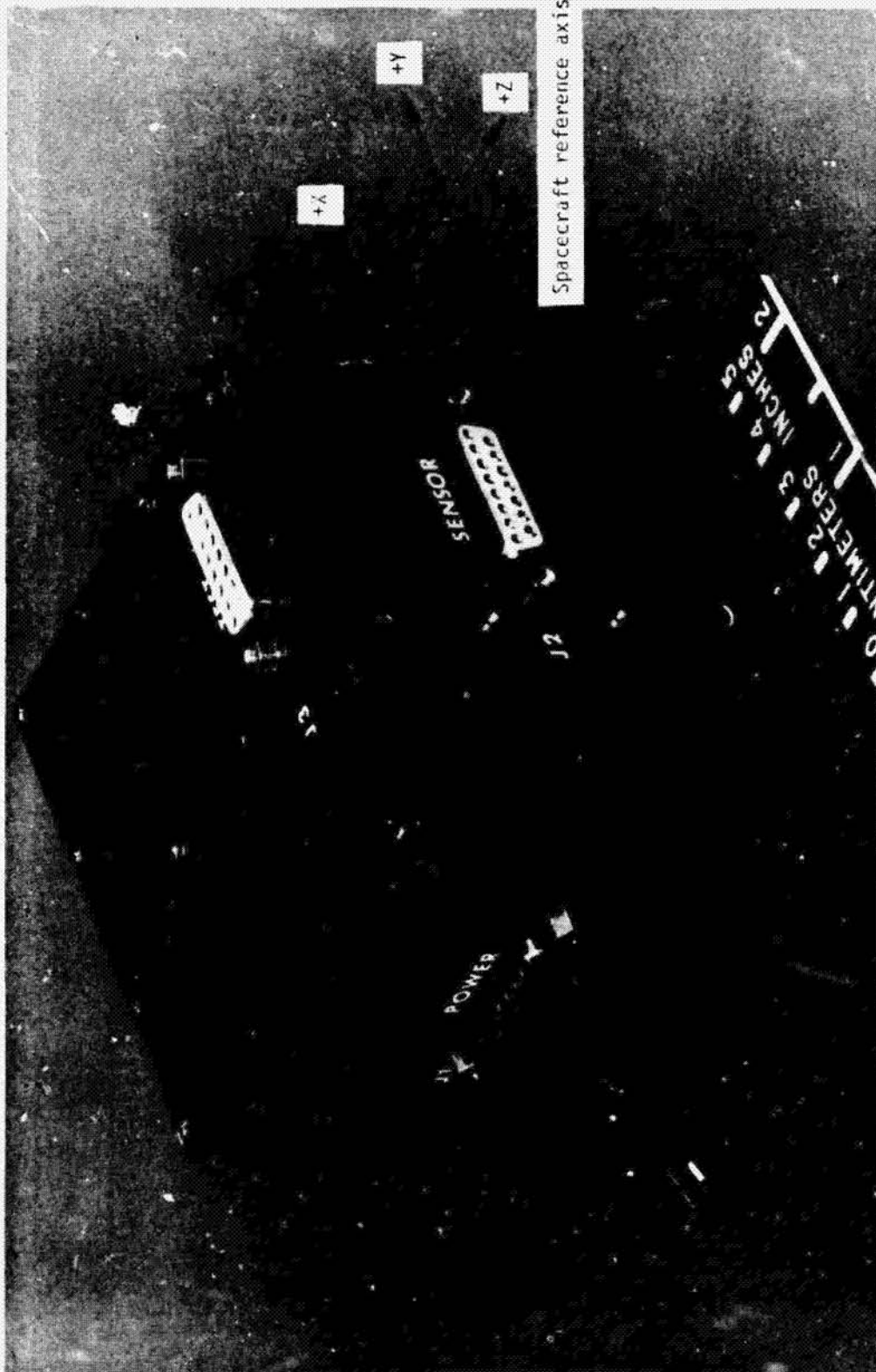


Figure V-1.- Meteoroid detection experiment functional block diagram.



L-71-1134

Figure V-2.- Instrument electronic system assembly.

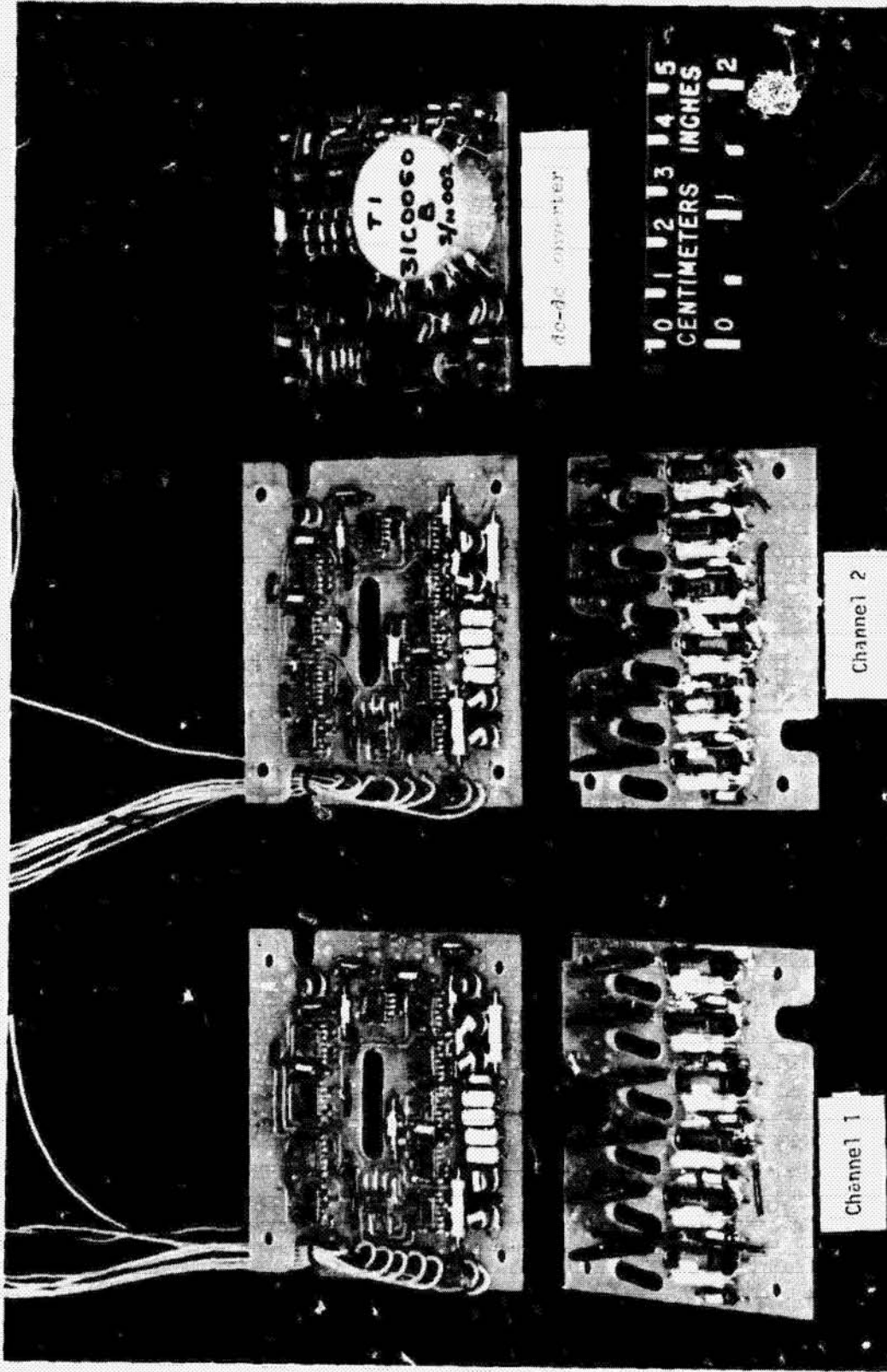


Figure V-3.- Electronic system module.

I-70-9062

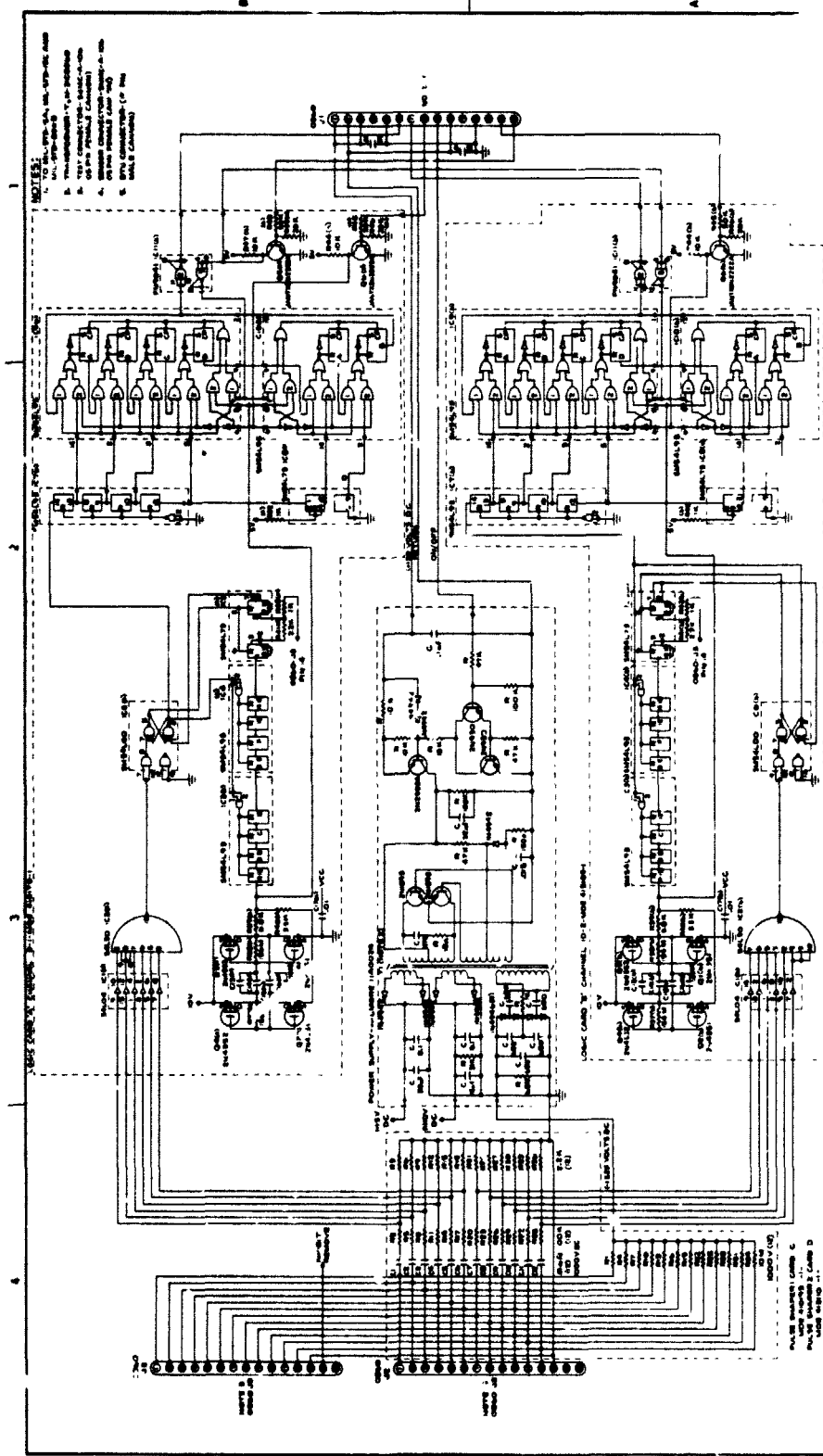


Figure V-4.- Schematic of electronic system.

REPRODUCIBILITY OF THE ORIGINAL PAGE IS POOR

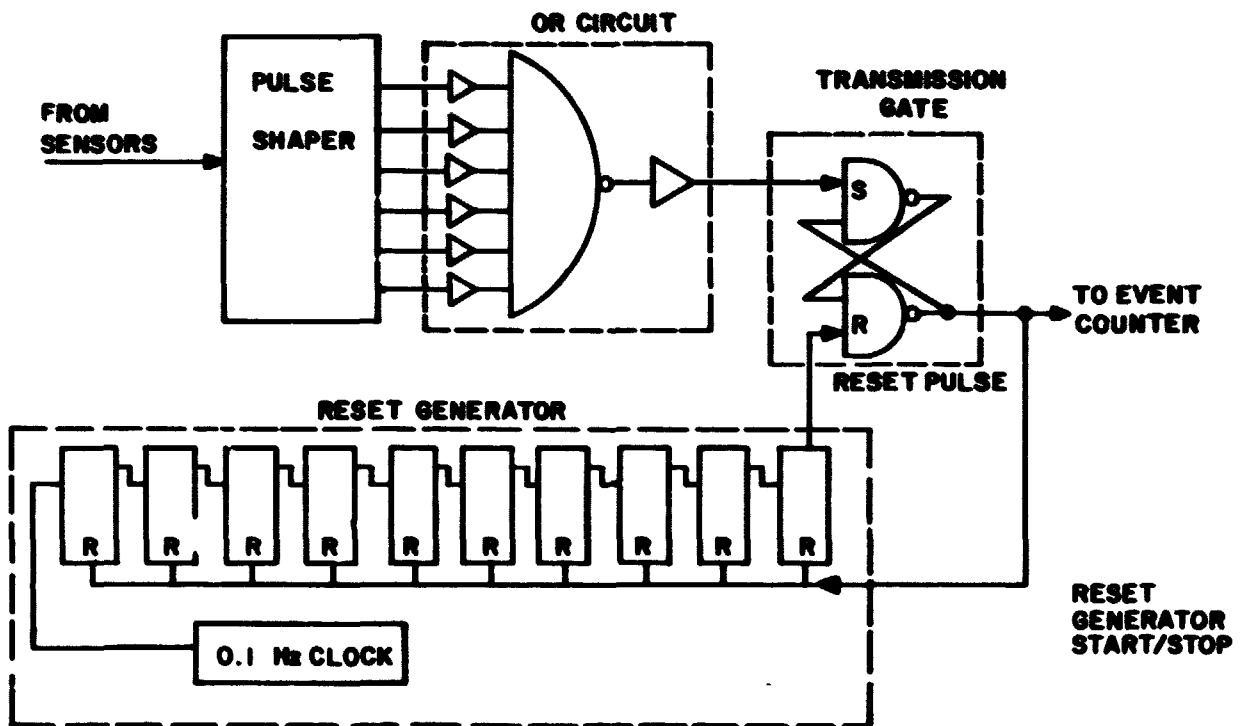


Figure V-5.- Signal conditioner.

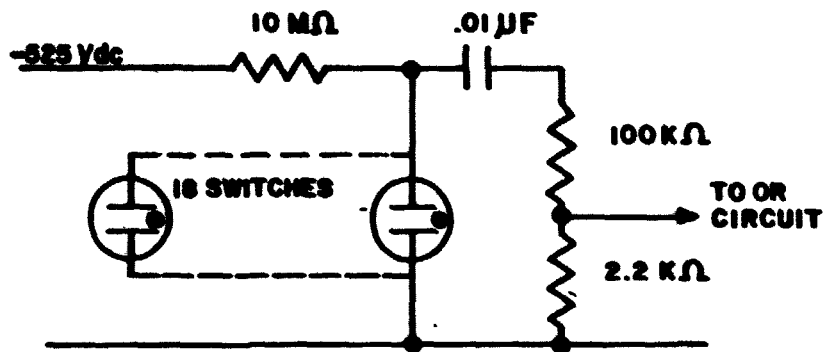


Figure V-6.- Pulse shaping circuit.

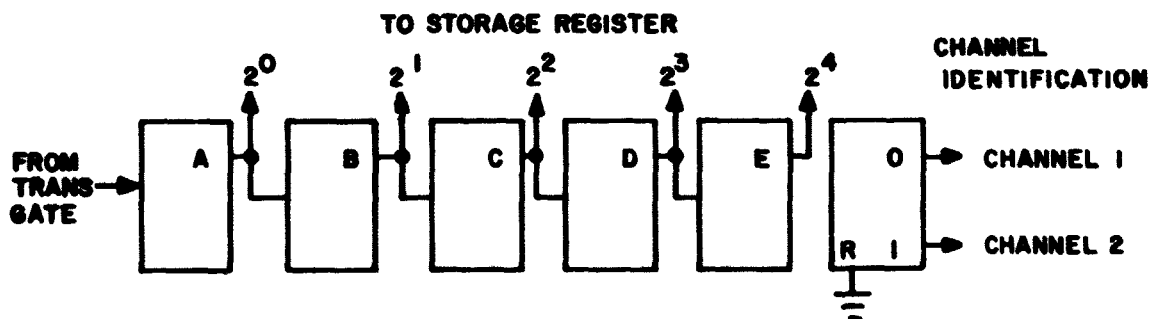


Figure V-7.- Event counter. A, B, C, D, E denote circuits; R denotes reset.

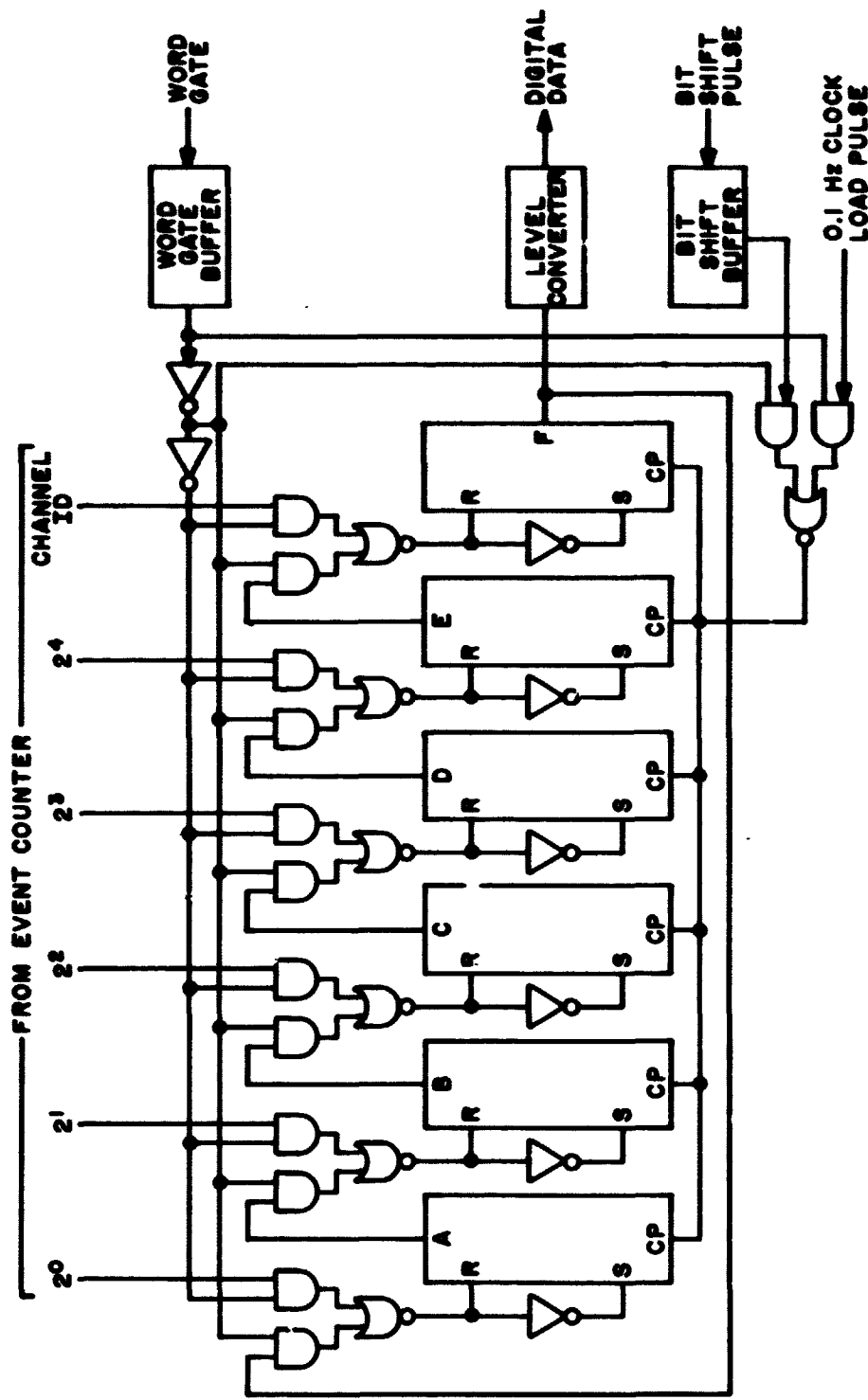
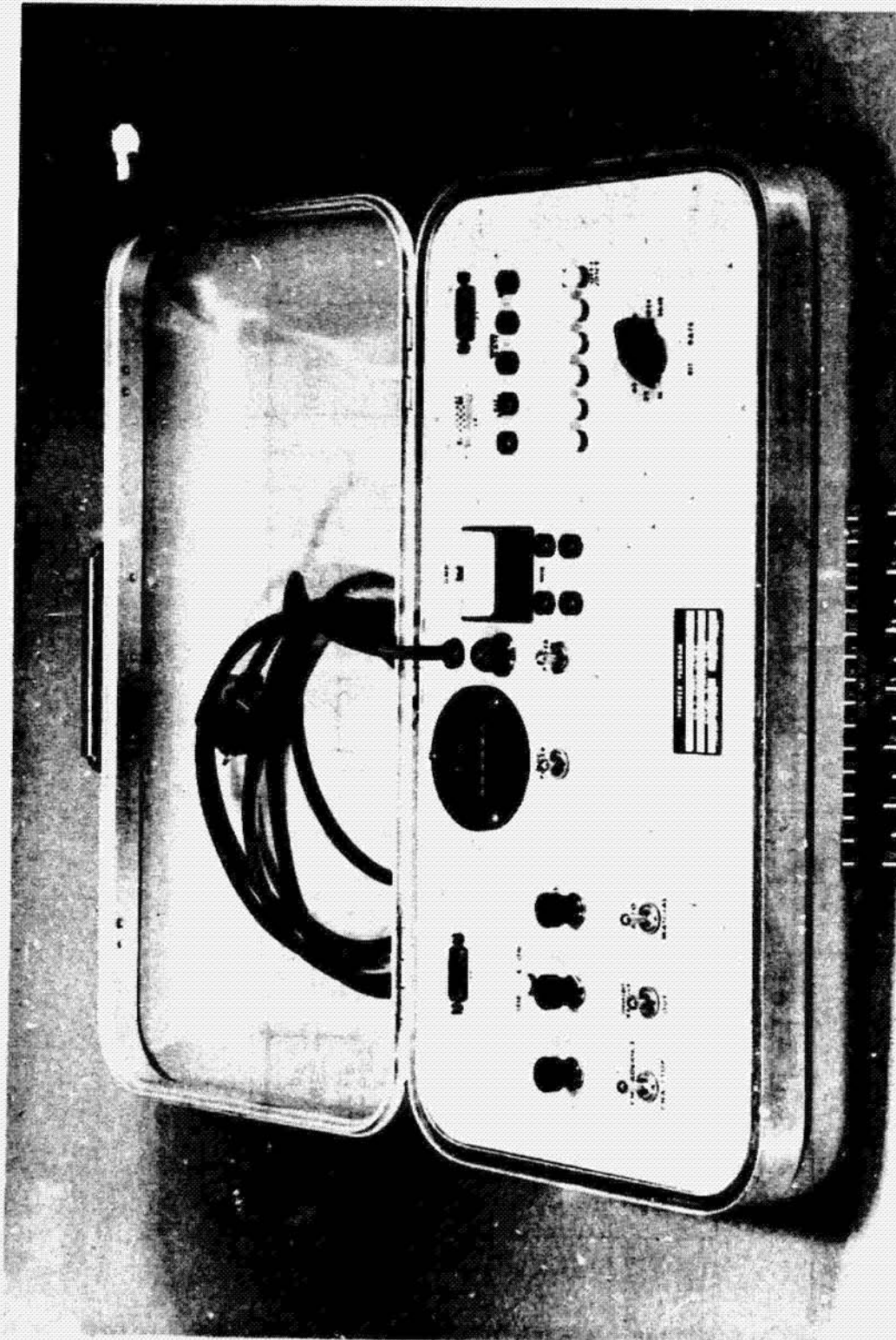


Figure V-8.- Storage-register/converter. R denotes reset; S denotes set; CP denotes clock pulse; A, B, C, D, E denote circuits.





L-70-9063

Figure V-10.- Ground support equipment.

Ground support equipment

Experiment

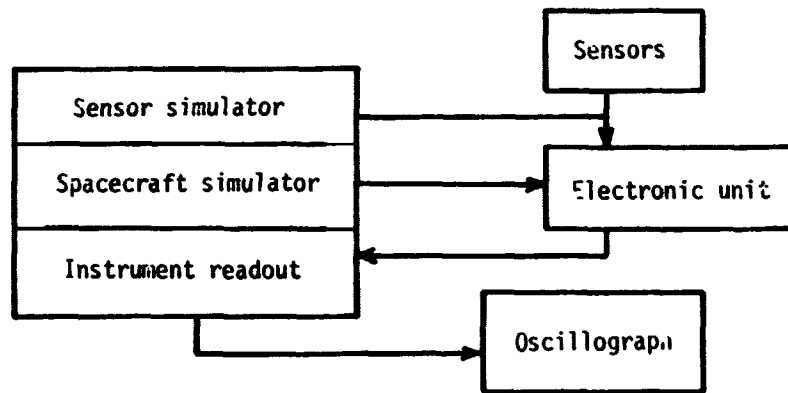


Figure V-11.- Functional block diagram of ground support equipment and experiment.

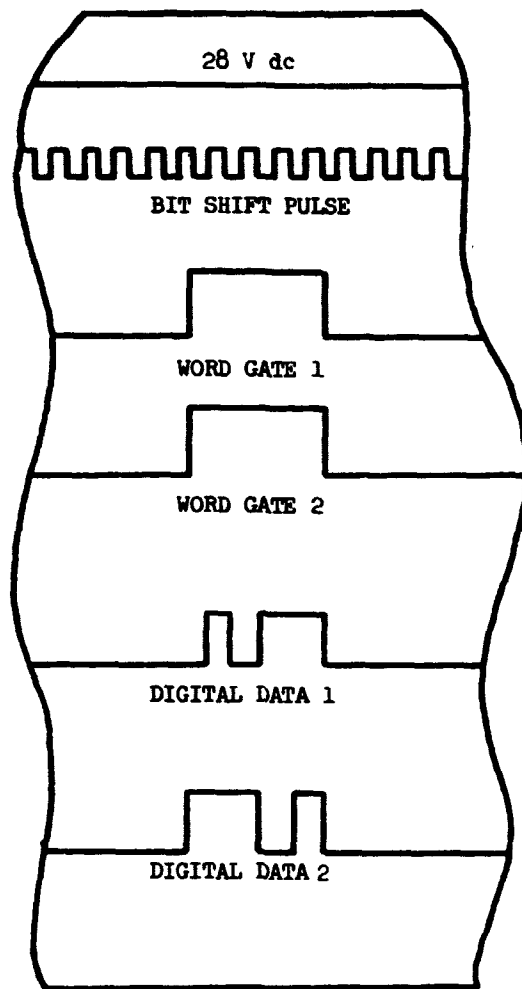


Figure V-12.- Oscilloscope record format for electronic unit under test.

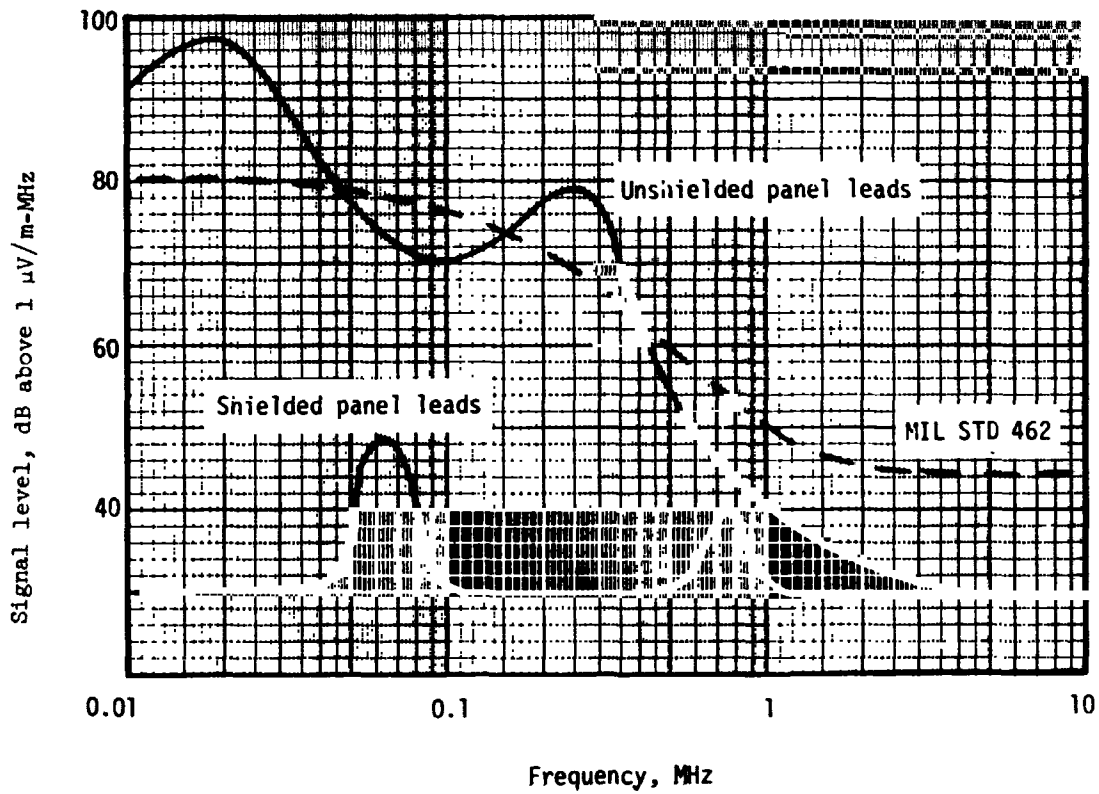


Figure V-13.- EMI broad band radiated.

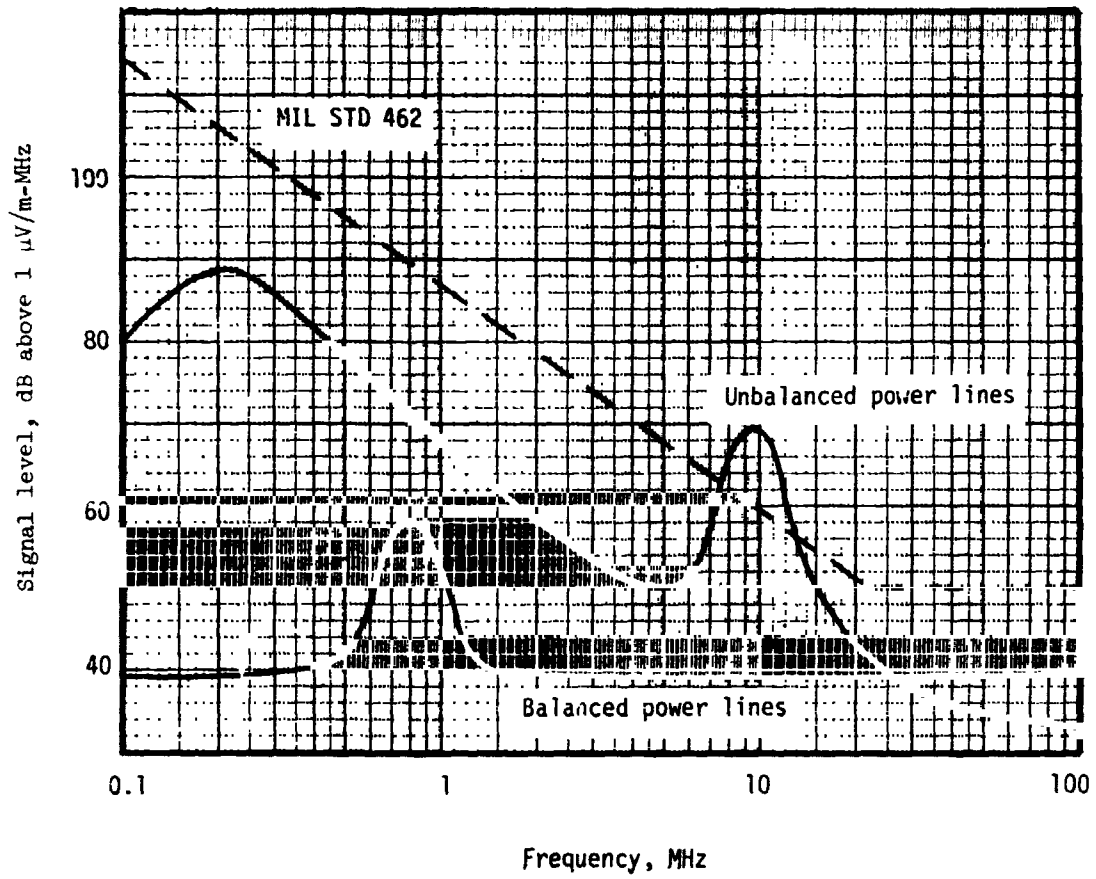


Figure V-14.- EMI broad band conducted.

## VI. PRESSURIZED PANEL LIFE TESTS

By Carl D. Parker  
Research Triangle Institute

### TEST DESCRIPTION

To verify the adequacy of the design and fabrication of the pressurized cell panels for the Pioneer missions, a number of panels were subjected to a long-term test under simulated space thermal and vacuum conditions. Eight pressurized cell panels were used in these tests. Pressurized cell panels were of flight quality with the following exceptions. The switch potting on one panel was not applied according to flight hardware procedures, and several cells were not leak tight. However, these cells were deactivated prior to beginning the test. The status of the life test panels is summarized in table VI-1. Tests were conducted under vacuum conditions of less than  $40 \times 10^{-3}$  mm Hg with four panels maintained at room temperature ( $27^{\circ}$  C) and four panels maintained at liquid nitrogen temperature ( $-195^{\circ}$  C). The physical setup of the test apparatus is indicated by the sketch in figure VI-1 and the photographs in figure VI-2.

The life test was designed to verify that pressurized cell switches would not inadvertently fire with voltage applied to the terminals, but had the ability to fire if a leak should occur. The test consisted of applying 600 volts continuously across each switch and monitoring for switch firings while the panel ambient environment was maintained at less than  $40 \times 10^{-3}$  mm Hg. Additionally, at predetermined intervals, the voltage on each switch was increased until the switch fired. The test schedule of the 138 active cells is shown in table VI-2. The criteria for a successful completion of tests were that (1) no switch firings occur during the period when the 600 volts were continuously applied, (2) no switch firings occur at less than 1000 volts when the voltage level was being raised in the test firing mode, and (3) in this test firing mode each switch fire as the voltage was increased beyond 1000 volts. Any deviations from these criteria would be considered a failure and subject to further investigation.

Each panel used in these investigations had been subjected to all tests to which flight panels were routinely subjected. Prior to installation in the test facility, the leakage impedance of each individual cell was checked at 1000 volts and was determined to be greater than  $10^{13}$  ohms. The individual cells were fired in an ambient pressure of 760 mm Hg and then fired under vacuum conditions of less than  $40 \times 10^{-3}$  mm Hg on several occasions over a period of 10 days.

## TEST RESULTS

The eight pressure panels committed to the long-term experiment were monitored continuously for erroneous firings. Periodically, individual cells were caused to fire by increasing the applied voltage. The cell firing schedule is presented in table VI-2. Table VI-3 summarizes the firing results from the eight test panels. Each table summarizes data from a single panel. Tabulated for each cell are averaged values of firing voltage at room temperature with atmospheric pressure and room temperature with vacuum pressure prior to the long-term test, long-term test firing voltage averages, and room temperature with vacuum pressure and room temperature with atmospheric pressure firing voltages after the long-term test. The number of data samples included in each average is also tabulated since it varied significantly from cell to cell. (The weekly firings yielded more data than the monthly firings, for example.) These tabulations summarize the effects of immersing the cells in a vacuum and in a cold temperature. As results with development panels had previously indicated, subjecting the cells to a vacuum lowers the firing voltage (the cells expand and the gas density reduces) and the low temperature increases the firing voltages. The significant observations are that the voltages remain at a reasonably uniform and satisfactory level for all conditions and are reasonably repeatable after a year of testing. The uniformity of results obtained before and after the long-term experiment is excellent.

Variations in period-to-period firing voltages are illustrated in figure VI-3. The cells selected (panel 092, cells 2 and 10) are from the liquid nitrogen temperature weekly firing group because more data are available and the low-temperature firing voltages tend to be less uniform from period to period. These results show significant but acceptable variations in firing voltages throughout the experiment. The variations appear to be random and not significantly correlated from cell to cell. A similar plot is presented in figure VI-4 for two cells from the weekly, room-temperature group. The cell firing voltages from the weekly, monthly, and quarterly groups were plotted on probability paper, and these plots were examined for any obvious data distribution. A few distributions appeared to be reasonably normal; however, most of the plots did not indicate anything other than a random distribution.

The most significant results from the long-term experiment are that the switch firing voltages remained at a satisfactory value throughout the experiment and, with one exception which will be discussed in a subsequent paragraph, no extraneous firing events occurred. Furthermore, when the experiment was terminated, all the active pressure cells were found to be in excellent condition; none had leaked or deteriorated in any observable way during the long-term experiment.

## DISCUSSION OF AN ANOMALY

Soon after the beginning of the long-term experiment, pressure cell number 11, panel 114 (weekly group, liquid nitrogen temperature) registered a significant decrease in firing voltage. Within 1 month, the recorded weekly voltages decreased from approximately 1500 volts to approximately 1000 volts. Eventually, it fired during routine monitoring and continued to fire occasionally. It was removed from the long-term experiment by removing the voltage excitation; however, it was caused to fire occasionally during routine weekly firings by increasing the applied voltage until a firing event occurred. Firing voltages observed during these firing events were satisfactory.

When the long-term experiment was terminated, cell 11 of panel 114 was examined carefully for an anomaly. The cell was fully pressurized and its firing voltage was satisfactory. This panel was unique in one respect. The external connections to the switch electrodes in the other seven test panels were coated with RTV during fabrication at Langley Research Center. The RTV was carefully primed and applied in such a way as to eliminate any voids in the insulating RTV in accordance with standard procedures. Panel 114, by contrast, was received at the Research Triangle Institute without the RTV coating. Consequently, RTV was applied to the external part of the switch electrodes of panel 114 at Research Triangle Institute without priming.

When cell 11 was examined, it was observed that the spacing between the external, negative electrode and the switch housing (positive, ground potential) was significantly less than in other electrodes examined. The spacing was approximately 0.51 mm whereas others examined were approximately 0.89 mm. This close spacing, coupled with the pointed geometry of the electrode, was favorable to breakdown. Furthermore, the RTV coating was defective and a large void existed between the electrode and the switch housing. Figure VI-5 is a photograph showing the electrode geometry after the RTV was removed.

For spacecraft applications, electrical insulation must fit tightly onto the conductors and be free of voids, both within the insulation and between the insulation and the conductor. This absence of voids is necessary to prevent the trapping of gas between the insulation and the conductor. A gas-filled void existing in an insulating material of higher dielectric constant will have an electric field many times greater than would exist in the gas alone or in a perfect solid insulator. When there are voids, the accumulation of gas from the surrounding material may make the volume near high voltage components sufficiently conductive so that breakdown will readily occur. When RTV is used, it is normally thinned to reduce viscosity and allow its application without void. These precautions were not taken with the RTV application to panel 114 and a void is known to have existed

between the high voltage cathode and ground. Approved procedures were strictly followed in applying RTV to the other test panels and all flight panels.

#### CONCLUDING REMARKS

The only anomaly occurring in the long-term tests was the firing of cell 11 of panel 114. It was concluded that the electrical breakdowns noted during the 600-volt monitoring phases of the test were external to the cell. It was further concluded that the conditions conducive to such an occurrence were unique to panel 114 and the anomaly noted was not characteristic of the flight panels.

TABLE VI-1.- TEST PANEL DESCRIPTIONS

Serial	Switch potting	Cell status
092	Flight quality	Cell 5 inactive
114	Not flight quality	All cells active
125	Flight quality	Cell 17 inactive
154	Flight quality	All cells active
137	Flight quality	Cell 1 inactive
146	Flight quality	Cells 4 and 9 inactive
151	Flight quality	Cells 6 and 7 inactive
161	Flight quality	All cells active

TABLE VI-2.- PRESSURE CELL FIRING SCHEDULE

[Numbers indicate pressure cell number; unscheduled indicates those cells which were not fired according to a predetermined schedule but were fired at the beginning and at the conclusion of the test.]

Panel	Firing schedule for periods, weeks, of -					
	1	4	12	24	48	Unscheduled
092	1, 2, 10	3, 11, 12	4, 6, 13	7, 14, 15	8, 9, 16	17, 18
114	3, 11, 12	4, 5, 13	6, 14, 15	7, 8, 16	9, 17, 18	2, 10
125	4, 5, 13	6, 14, 15	7, 8, 16	9, 18, 10	1, 2, 11	3, 12
154	6, 14, 15	7, 8, 16	9, 17, 18	1, 2, 10	3, 11, 12	4, 5, 13
137	2, 3, 10	4, 11, 12	5, 6, 13	7, 14, 15	8, 9, 16	17, 18
146	5, 11, 12	6, 7, 13	8, 14, 15	1, 2, 16	3, 17, 18	10
151	5, 8, 13	9, 14, 15	1, 2, 16	3, 17, 18	4, 10, 11	12
161	9, 14, 15	10, 11, 16	1, 17, 18	2, 3, 12	4, 5, 8	6, 7, 13

TABLE VI-3.- SUMMARY OF FIRING RESULTS

Cell	Average voltage for room-temperature— atmosphere tests	Number of samples	Average voltage for room-temperature— vacuum tests	Number of samples	Average voltage for long-term test	Number of samples	Average voltage for room-temperature— vacuum tests	Number of samples	Average voltage for room-temperature— atmosphere tests	Number of samples
Panel 092 (LN <sub>2</sub> temperature)										
1	1340	1	1187	3	1307	48	1140	3	1330	2
2	1390	1	1213	3	1526	48	1180	3	1385	2
3	1340	1	1200	3	1440	14	1187	3	1360	2
4	1380	1	1243	3	1430	6	1213	3	1375	2
5	1400	1	1217	3	1392		1180	3	1360	2
6	1410	1	1233	3	1468		1270	3	1400	2
7	1450	1	1287	3	1497	3	1270	3	1405	2
8	1450	1	1240	3	1497	3	1233	3	1420	2
9	1390	1	1190	3	1478	4	1186	3	1366	2
10	1390	1	1217	3	1466	14	1213	3	1360	2
11	1430	1	1213	3	1497	14	1253	3	1410	2
12	1400	1	1210	3	1440	6	1207	3	1360	2
13	1320	1	1183	3	1394	4	1177	3	1325	2
14	1370	1	1243	3	1475	4	1253	3	1365	2
15	1360	1	1195	2	1450	3	1220	3	1365	2
16	1380	1	1203	3	1507	3	1203	3	1375	2
17	1330	1	1157	3	1373	3	1170	3	1330	2
Panel 114 (LN <sub>2</sub> temperature)										
1	1610	1	1435	2	1777	3	1383	3	1570	2
2	1640	1	1500	2	1705	48	1403	3	1335	2
3	1590	1	1445	2	1726	14	1437	3	1575	2
4	1580	1	1420	2	1745	14	1407	3	1590	2
5	1530	1	1400	2	1665	6	1403	3	1560	2
6	1660	1	1465	2	1728	4	1490	3	1575	2
7	1570	1	1395	2	1723	4	1360	3	1545	2
8	1690	1	1520	2	1907	3	1510	3	1705	2
9	1650	1	1405	2	1683	3	1370	3	1600	2
10	1600	1	1350	2	1771	48	1607	3	1660	2
11	1670	1	1475	2	1766	14	1433	3	1650	2
12	1660	1	1475	2	1638	6	1330	3	1640	2
13	1590	1	1390	2	1638	6	1503	3	1690	2
14	1730	1	1530	2	1742	6	1503	3	1470	2
15	1450	1	1325	2	1623	4	1393	3	1525	2
16	1630	1	1335	2	1650	3	1447	3	1660	2
17	1710	1	1460	2	1333	3				

TABLE VI.3.- SUMMARY OF FIRING RESULTS - Continued

Cell	Average voltage for room-temperature-atmosphere tests	Number of samples	Average voltage for room-temperature--vacuum test--	Number of samples	Average voltage for long-term test	Number of samples	Average voltage for room-temperature--vacuum tests	Number of samples	Average voltage for room-temperature--atmosphere tests	Number of samples
Panel 125 (LN <sub>2</sub> temperature)										
1	1440	1	1200	2	1383	3	1210	3	1410	2
2	1320	1	1135	2	1377	3	1143	3	1295	2
3	1400	1	1135	2	1360	3	1130	3	1265	2
4	1330	1	1135	2	1185	4	1160	3	1300	2
5	1430	1	1165	2	1437	4	1233	3	1300	2
6	1500	1	1255	2	1455	14	1260	3	1450	2
7	1440	1	1140	2	1417	6	1137	3	1375	2
8	1410	1	1170	2	1437	6	1190	3	1360	2
9	1400	1	1145	2	1370	4	1143	3	1430	2
10	1370	1	1185	2	1393	4	1207	3	1350	2
11	1410	1	1195	2	1433	3	1237	3	1370	2
12	1400	1	1145	2	1403	3	1157	3	1240	2
13	1370	1	1205	2	1453	4	1223	3	1360	2
14	1320	1	1155	2	1378	14	1160	3	1265	2
15	1400	1	1115	2	1401	14	1197	3	1335	2
16	1470	1	1220	2	1420	6	1207	3	1345	2
17										
18	1440	1	1155	2	1358	4	1177	3	1350	2
Panel 137 (room temperature)										
1										
2	1540	1	1310	2	1319	4			1385	2
3	1560	1	1305	2	1279	4			1455	2
4	1400	1	1260	2	1334	14			1350	2
5	1390	1	1170	2	1155	6			1290	2
6	1490	1	1320	2	1265	6			1460	2
7	1500	1	1300	2	1275	4			1460	2
8	1470	1	1275	2	1240	3			1375	2
9	1420	1	1305	2	1300	3			1470	2
10	1430	1	1360	2	1269	4			1425	2
11	1480	1	1335	2	1320	14			1430	2
12	1420	1	1265	2	1272	14			1395	2
13	1440	1	1270	2	1273	6			1415	2
14	1430	1	1265	2	1268	4			1410	2
15	1420	1	1285	2	1265	4			1420	2
16	1410	1	1200	2	1197	3			1365	2
17	1480	1	1310	2	1273	3			1465	2
18	1400	1	1590	2	1577	3			1670	2

TABLE VI 3. - SUMMARY OF FIRING RESULTS - Continued

Cell	Average voltage for room-temperature-atmosphere tests	Number of samples	Average voltage for room-temperature-vacuum tests	Number of samples	Average voltage for long-term test	Number of samples	Average voltage for room-temperature-atmosphere tests	Number of samples
Panel 146 (room temperature)								
1	1750	1	1450	2	1448	4	1670	2
2	1500	1	1270	2	1253	4	1460	2
3	1540	1	1290	2	1260	3	1480	2
4								
5	1440	1	1235	2	1209	48	1790	2
6	1460	1	1235	2	1236	14	1435	2
7	1400	1	1205	2	1190	14	1375	2
8	1410	1	1195	2	1185	6	1365	2
9								
10	1470	1	1275	2	1260	3	1415	2
11	1420	1	1265	2	1215	48	1395	2
12	1420	1	1240	2	1238	48	1395	2
13	1410	1	1195	2	1141	14	1290	2
14	1400	1	1190	2	1185	6	1340	2
15	1400	1	1170	2	1207	6	1370	2
16	1410	1	1200	2	1205	4	1365	2
17	1390	1	1195	2	1137	3	1340	2
18	1 30	1	1170	2	1117	3	1350	2
Panel 151 (room temperature)								
1	1370	1	1180	2	1178	6	1350	2
2	1490	1	1155	2	1245	6	1445	2
3	1460	1	1220	2	1205	4	1370	2
4	1380	1	1230	2	1157	3	1315	2
5	1380	1	1165	2	1151	48	1320	2
6								
7								
8	1440	1	1210	2	1204	48	1390	2
9	1350	1	1115	2	1162	14	1305	2
10	1470	1	1275	2	1213	3	1395	2
11	1480	1	1300	2	1237	3	1420	2
12	1340	1	1215	2	1220	3	1390	2
13	1300	1	1140	2	1136	48	1305	2
14	1370	1	1160	2	1159	14	1305	2
15	1400	1	1165	2	1168	14	1355	2
16	1480	1	1255	2	1242	6	1400	2
17	1430	1	1220	2	1188	4	1345	2
18	1410	1	1135	2	1125	4	1315	2

TABLE VI-3.- SUMMARY OF FIRING RESULTS - Concluded

Cell	Average voltage for room-temperature--atmosphere tests	Number of samples	Average voltage for room-temperature--vacuum tests	Number of samples	Average voltage for long-term test	Number of samples	Average voltage for room-temperature--vacuum tests	Number of samples	Average voltage for room-temperature--atmosphere tests	Number of samples
Panel 154 (LN <sub>2</sub> temperature)										
1	1530	1	1285	2	1440	4	1297	3	1420	2
2	1490	1	1275	2	1503	4	1283	3	1420	2
3	1540	1	1355	2	1520	3	1353	3	1520	2
4	1440	1	1330	2	1437	3	1320	3	1480	2
5	1550	1	1345	2	1493	3	1347	3	1470	2
6	1570	1	1340	2	1488	48	1357	3	1450	2
7	1470	1	1320	2	1505	14	1337	3	1460	2
8	1630	1	1420	2	1609	14	1437	3	1590	2
9	1670	1	1415	2	1544	6	1440	3	1600	2
10	1460	1	1295	2	1445	4	1280	3	1435	2
11	1520	1	1310	2	1500	3	1317	3	1470	2
12	1460	1	1290	2	1433	3	1207	3	1445	2
13	1440	1	1290	2	1440	3	1270	3	1390	2
14	1520	1	1325	2	1513	48	1303	3	1445	2
15	1490	1	14.5	2	1474	42	1330	3	1415	2
16	1460	1	1320	2	1492	14	1317	3	1465	2
17	1540	1	1345	2	1508	6	1327	3	1485	2
18	1420	1	1230	2	1403	6	1217	3	1425	2
Panel 161 (room temperature)										
1	1560	1	1235	2	1237	6	1470	2	1470	2
2	1800	1	1430	2	1330	4	1485	2	1485	2
3	1570	1	1320	2	1270	4	1395	2	1395	2
4	1590	1	1255	2	1303	3	1455	2	1455	2
5	1530	1	1305	2	1260	3	1450	2	1450	2
6	1540	1	1300	2	1283	3	1460	2	1460	2
7	1580	1	1365	2	1350	3	1520	2	1520	2
8	1610	1	1365	2	1287	3	1455	2	1455	2
9	1630	1	1360	2	1344	48	1545	2	1545	2
10	1610	1	1365	2	1409	14	1600	2	1600	2
11	1620	1	1380	2	1368	14	1555	2	1555	2
12	1530	1	1320	2	1298	4	1435	2	1435	2
13	1610	1	1330	2	1343	3	1500	2	1500	2
14	1580	1	1365	2	1331	46	1460	2	1460	2
15	1570	1	1370	2	1360	48	1485	2	1485	2
16	1560	1	1340	2	1306	14	1565	2	1565	2
17	1640	1	1335	2	1270	6	1495	2	1495	2
18	1640	1	1320	2	1322	6	1480	2	1480	2

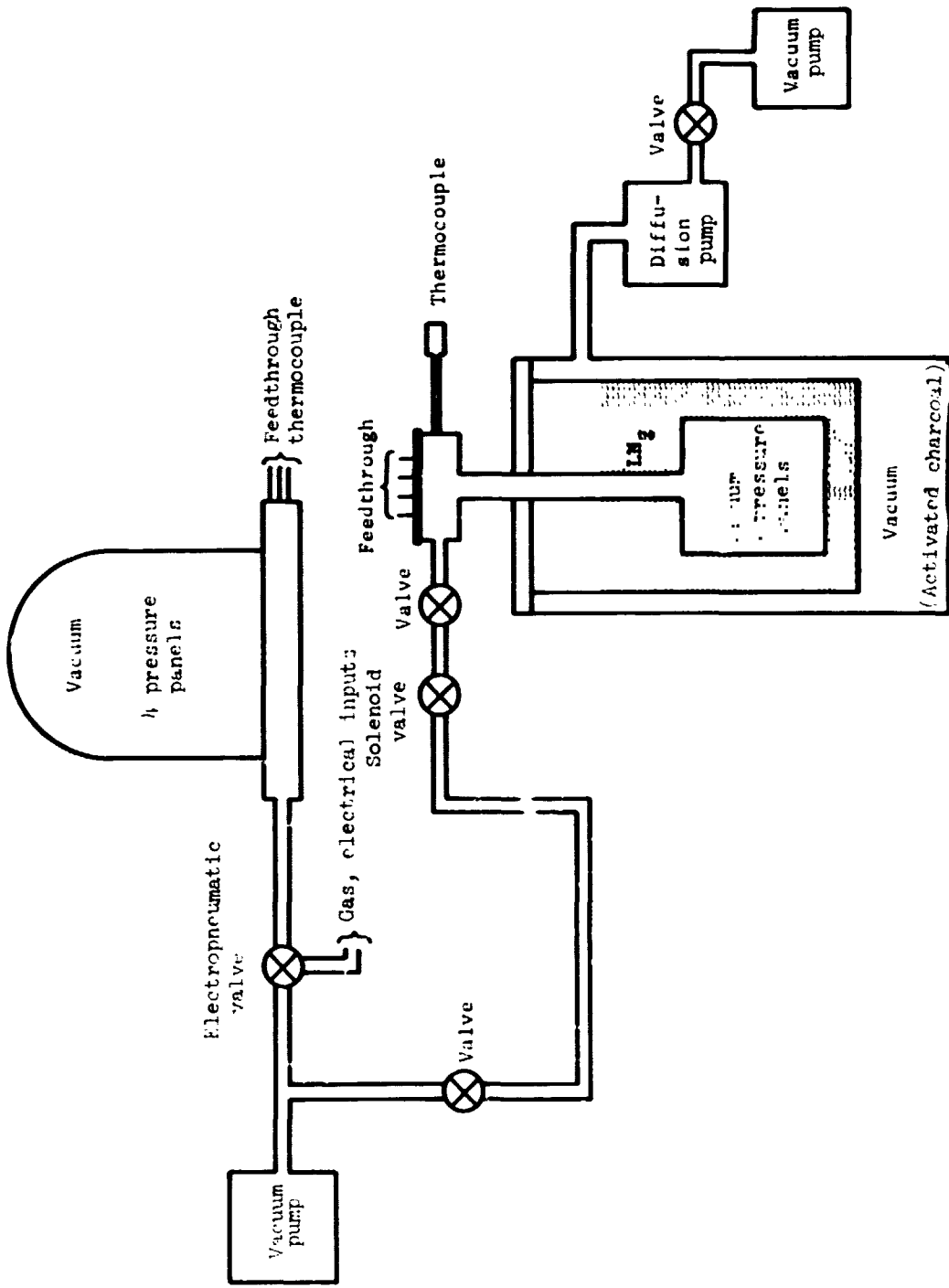
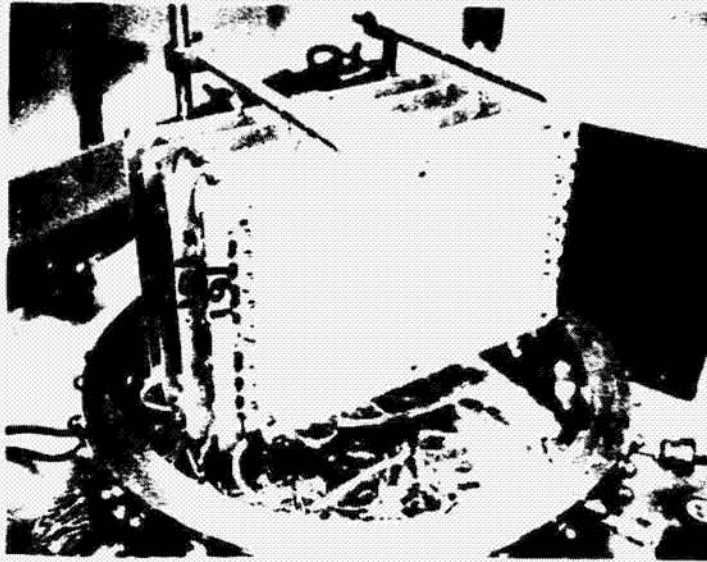
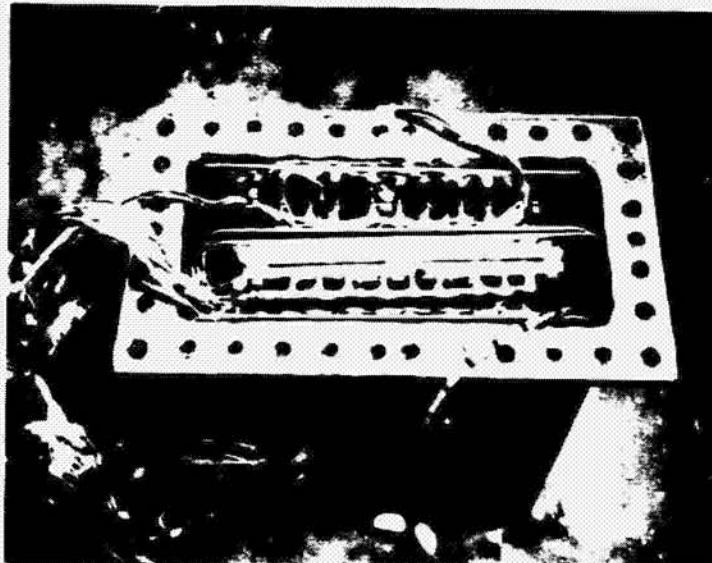


Figure VI-1.- Sketch of test setup.



(a) Photograph of room temperature test panels after completion of long-term test.



L-74-1120

(b) Photograph of LN<sub>2</sub> temperature panels in cold-vacuum chamber after completion of long-term test.

Figure VI-2.- Photographs of panels installed in test facility.

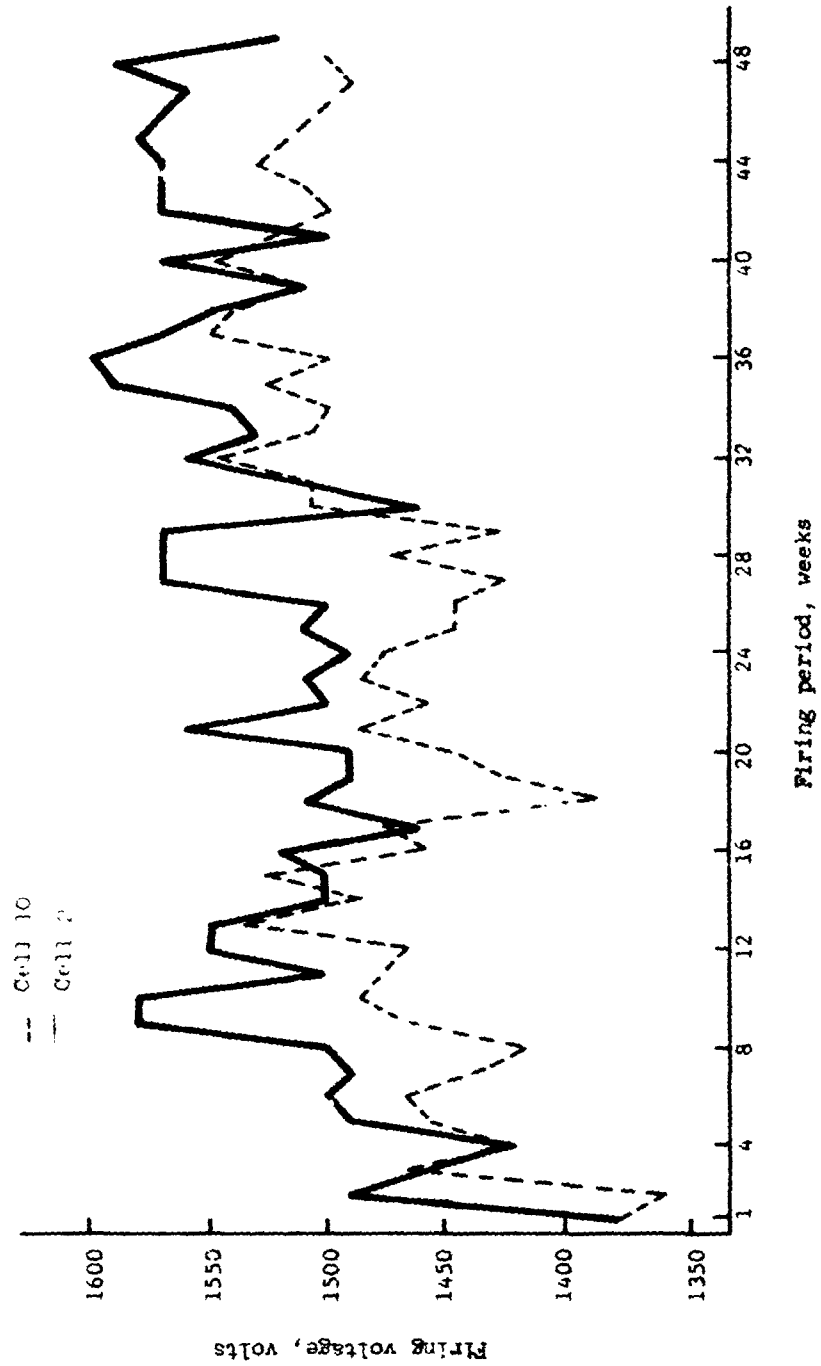


Figure VI-3.- Weekly  $\text{In}_2$  temperature firing voltages. Panel 092.

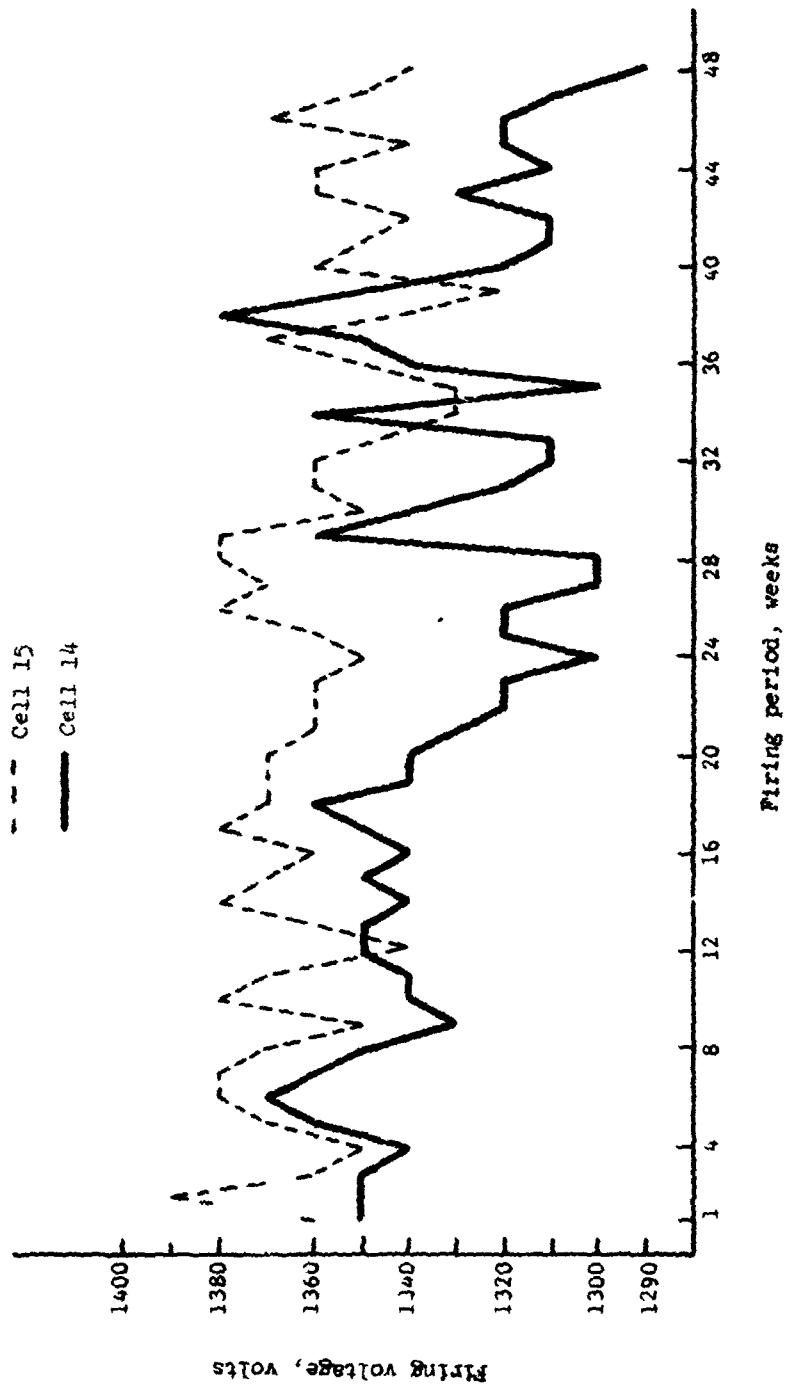
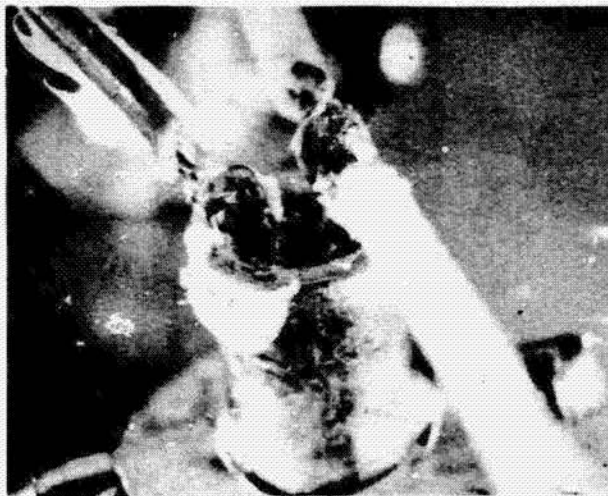


Figure VI-4.- Weekly room temperature firing voltages, Panel 116.



L-74-1135

Figure VI-5.- Photograph of external electrodes of  
cell 11 panel 114 after removal of RTV.

## VII. SIMULATION OF HEAVY ION AND PROTON IRRADIATION EFFECTS ON PRESSURE SWITCH OPERATION

By Larry Monteith  
North Carolina State University

### INTRODUCTION

Two possible radiation effects which could result in spurious outputs from the Meteoroid Detection Experiment (MDE) gas discharge transducer are suggested. The radiation-induced ionization could be collected in the applied field and result in a voltage pulse across the transducer. Secondly, the induced ionization could reduce the field required to sustain avalanche multiplication. A detailed analysis of either effect is beyond the scope of this discussion; however, a simple analysis will be presented later as a means to interpret the data.

Without a detailed model for the interaction of irradiation with the gas discharge transducer and without reliable data on the heavy ion and proton energy and fluence expected in flight, a purely empirical test program was devised to simulate worst case conditions. Four gas discharge transducers were exposed to a pulsed beam of 576 MeV protons at an average flux near  $10^{10}$  protons/cm<sup>2</sup>-sec. These energy and flux levels were considered to be high relative to the levels expected in flight. The peak flux was nearly 200 times the average flux and the pulse width was approximately 100 microseconds and occurred at 55 Hz. The proton flux covered an area of 6.5 cm<sup>2</sup>. The uniformity of the beam was assessed visually and the average flux rate was monitored by a Faraday cup.

The gas discharge transducers were connected electrically as illustrated in figure VII-1. Briefly, most of the measurements consisted of an electronic switch or gate which was actuated with a voltage pulse greater than 2 volts. The switch turned on a lamp as an indication of breakdown of the gas discharge transducer. The lamp glow was used as an indication that the transducer had discharged. In addition, the voltage across the 2200-ohm resistor during the proton pulse was observed on occasion when an oscilloscope was used. The applied voltages across the transducer included both avalanche and nonavalanche conditions.

### EXPERIMENTAL RESULTS

By using the electronic switch as an indicator for transducer discharge, four transducers were exposed to 575 MeV protons with fluxes covering the range from  $10^9$  to  $10^{10}$  protons/cm<sup>2</sup>-sec. The results are shown in table VII-1. From these data it is

obvious that the proton flux had an effect upon the firing or discharge voltage of the transducer in the test configuration. Even though the magnitude of the voltage decrease is hundreds of volts, the percent change is the order of 10 percent or less of the firing voltage without radiation. This condition is evident from figure VII-2 where the effect of the proton flux on the firing voltage is not very pronounced. Over the limited range of data a straight-line relationship on the log-log plot appears to be an adequate fit. Then

$$V_f = \Phi^{-n}$$

where  $n \approx 0.07$  by fitting a straight line to the data. The major features of this result are that the firing voltage  $V_f$  is reduced in a highly ionizing radiation environment; however, the effect of ionizing radiation on the firing voltage is not substantial over the range of the experiment. In fact, under the test conditions, the radiation would have no effect upon the performance of the discharge transducer as a pressure switch in the mode of operation intended for flight.

In an attempt to study charge collection of ionizing radiation, the oscilloscope was used to observe the voltage developed across the 2200-ohm resistor in figure VII-1. The observed voltage pulses were on the order of tens of millivolts. When the voltage division across the  $10^5$ -ohm resistor is considered, the voltage developed across the transducer during the proton pulse was on the order of volts at the maximum flux rate. Shown in figure VII-3 is the magnitude of the current pulse through the 2200-ohm resistor as a function of applied field. It is obvious that the collected charge during the proton pulse will not be sufficient to develop the 2 volts necessary to switch the electronic circuit and yield a false firing. This condition was verified by actually observing the firing event as the applied voltage was increased across the transducer. However, the firing event was always coincident with the proton flux which further substantiated the firing voltage.

As expected the collected charge is linearly related to the flux as shown in figure VII-4. Therefore, it may be assumed that during the 100-microsecond pulse of protons, the ion-electron density reaches steady state. Therefore, the conductivity of the gas should be controlled by the flux  $\Phi$ , the lifetime of the ion electron pairs, and the mobility of the ions and electrons. In addition, the instantaneous flux should be considered instead of the average flux in the interpretation of the results.

## ANALYSIS

The primary consideration has to be the simulation and how it relates to the space environment. Again, a worst-case analysis is used. The major factor will be the energy loss by the protons in traversing the transducer. The mass stopping power as a function of energy for protons is available from numerous sources. The energy loss per unit path

length is related to the mass stopping power by

$$\frac{1}{\rho} \frac{\partial E}{\partial x} = \frac{\partial E}{\partial \xi}$$

where

$\rho$  density of absorbing medium

$\frac{\partial E}{\partial x}$  rate of energy loss per unit path length

$\frac{\partial E}{\partial \xi}$  mass stopping power

For protons  $\frac{\partial E}{\partial \xi}$  varies from approximately 0.2 MeV mg<sup>-1</sup>-cm<sup>2</sup> at 1 MeV to 0.002 MeV mg<sup>-1</sup>-cm<sup>2</sup> at 1 GeV. At 576 MeV,  $\frac{\partial E}{\partial \xi}$  is also near 0.002 MeV mg<sup>-1</sup>-cm<sup>2</sup>.

The rate of energy loss could be increased by going to lower energies; however, the flux decreased for lower energies faster than the increase in  $\frac{\partial E}{\partial \xi}$ . Therefore, by using the high energy, maximum ionization density in the gas was achieved.

Proton simulation is rather obvious. If the predominant energy of the protons encountered in space is near 1 MeV, the simulation should be scaled by the ratio of  $\frac{\partial E}{\partial \xi}$  at 1 MeV to  $\frac{\partial E}{\partial \xi}$  at 576 MeV and the flux for worst case simulation reduced by this factor. Specifically, at 30 MeV,  $\frac{\partial E}{\partial \xi} = 0.015$  MeV mg<sup>-1</sup>-cm<sup>2</sup> and at 576 MeV,  $\frac{\partial E}{\partial \xi} = 0.002$  MeV mg<sup>-1</sup>-cm<sup>2</sup>.

Using an average flux of  $3 \times 10^{10}$  protons/cm<sup>2</sup>-sec corresponds to an instantaneous flux near  $10^{12}$  protons/cm<sup>2</sup>-sec. Therefore, the 576-MeV irradiations approximate the ionization effects of 30-MeV protons with a flux rate near  $10^{11}$  protons/cm<sup>2</sup>-sec. Obviously, these levels are far in excess of the flux rates expected during flight.

When heavy ions are considered, the rate of energy loss can be related to the rate of energy loss by protons by

$$\left. \frac{\partial E}{\partial x} \right|_{\text{ion}} = z^2 \left. \frac{\partial E}{\partial x} \right|_{\text{proton}}$$

where  $z$  is the charge state of the ion. One matter of little concern is the fact that  $z$  changes as the ion slows down. Obviously, the worst case occurs when the ion is fully

ionized. Thus, for carbon,  $z = 6$  or

$$\left. \frac{\partial E}{\partial x} \right|_{\text{ion}} = 36 \left. \frac{\partial E}{\partial x} \right|_{\text{proton}}$$

represents an example. Therefore, when ionization effects are considered, a flux of protons simulates a flux of fully ionized carbon ions at the same energy by reducing the proton flux by 36. Proton fluxes near  $10^{12}$  protons/cm<sup>2</sup>-sec at 576 MeV can be used to simulate approximately  $10^{10}$  carbon ions/cm<sup>2</sup>-sec at 576 MeV with the ions fully ionized. Clearly, this value is far in excess of the heavy ion flux expected in flight.

A brief analysis of the experimental results is given; however, there has been no significant attempt at a detailed model. Indeed, such a model would not add a great deal to the study. Regarding the decrease in firing voltage with ionization due to protons, there is no simple explanation of the observation. One expects the firing voltage to be relatively independent of residual ion-electron density for a dilute concentration. Basically, avalanche breakdown depends upon the fact that the field must impart enough energy to the ionized electrons to insure that during their lifetime they can create one or more electron-ion pairs. Of course, there is the problem that in the total absence of electron-ion pairs, electrode phenomena must initiate avalanche and consequently one may expect that irregularities in electrode geometry may cause unreliable firing. With ion-electron pairs available in the gas, the avalanche process then becomes essentially a gas-dynamic process and the firing voltage should be relatively insensitive to the density of ion-electron ionized pairs. The observations indicate a dependence; however, it is a very small dependence since  $V_f \propto \Phi^{-1/13}$

For the collection of ionized charge, the maximum voltage developed across the transducer is on the order of a few volts even at the very high flux rates. Unfortunately, ionization outside the transducer near the electrical connections could be responsible for most of the charge collected. However, the small voltage magnitude probably negates the need to give further consideration to the observations. A very simple analysis of charge collection within the transducer predicts about the voltage magnitude observed; however, the assumptions necessary to provide a tractable model make it difficult to be very definite regarding any conclusions about the origin of the voltage pulse.

#### CONCLUDING REMARKS

From the experiments two conclusions appear to be reasonable. The simulation of ionizing is far in excess of what is expected because of either protons or heavy ions. Secondly, the effects of the ionizing radiation upon the performance of the gas discharge transducer does not result in spurious signals which can be interpreted as impact events.

TABLE VII-1.- TRANSDUCER FIRING VOLTAGES FOR VARIOUS PROTON FLUX RATES

Transducer number	Flux rate, protons/cm <sup>2</sup> -sec	Firing voltages, volts
37	0	1520, 1540, 1550, 1560
	$0.36 \times 10^{10}$	1490, 1500, 1510
	$1.6 \times 10^{10}$	1450, 1450, 1450
	$3.3 \times 10^{10}$	1280, 1290, 1310, 1320
36	0	1350, 1360, 1370, 1400
	$3.4 \times 10^{10}$	1140, 1200
19	0	1430
	$3.3 \times 10^{10}$	1090, 1100
4	0	1490
	$0.19 \times 10^{10}$	1460, 1460, 1460
	$0.42 \times 10^{10}$	1420, 1420, 1420
	$0.68 \times 10^{10}$	1370, 1370, 1370
	$1.7 \times 10^{10}$	1250, 1250, 1250
	$3.4 \times 10^{10}$	1200, 1210, 1230

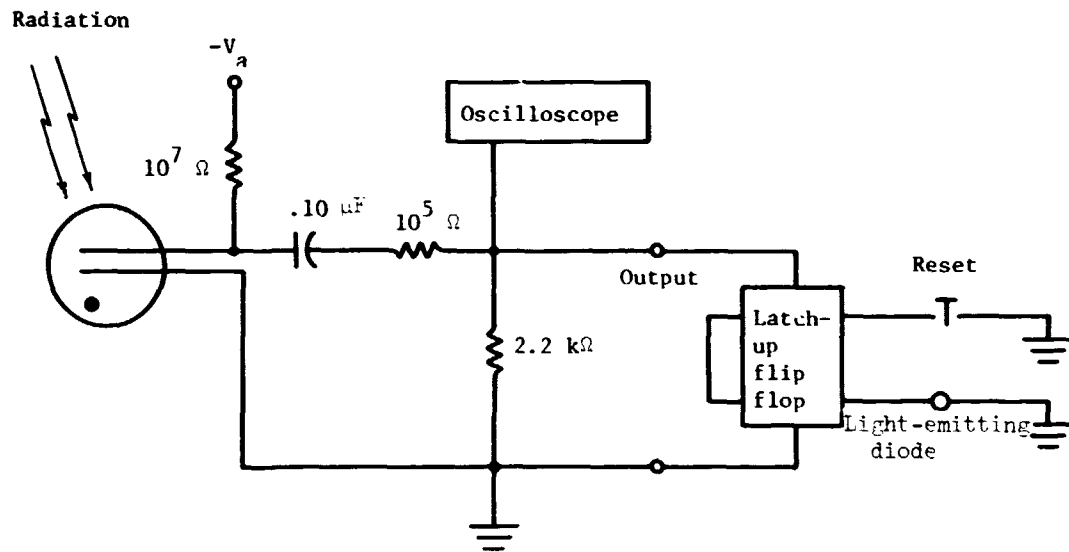


Figure VII-1.- Schematic of electrical circuit used in irradiation tests.  $V_a$ , applied voltage.

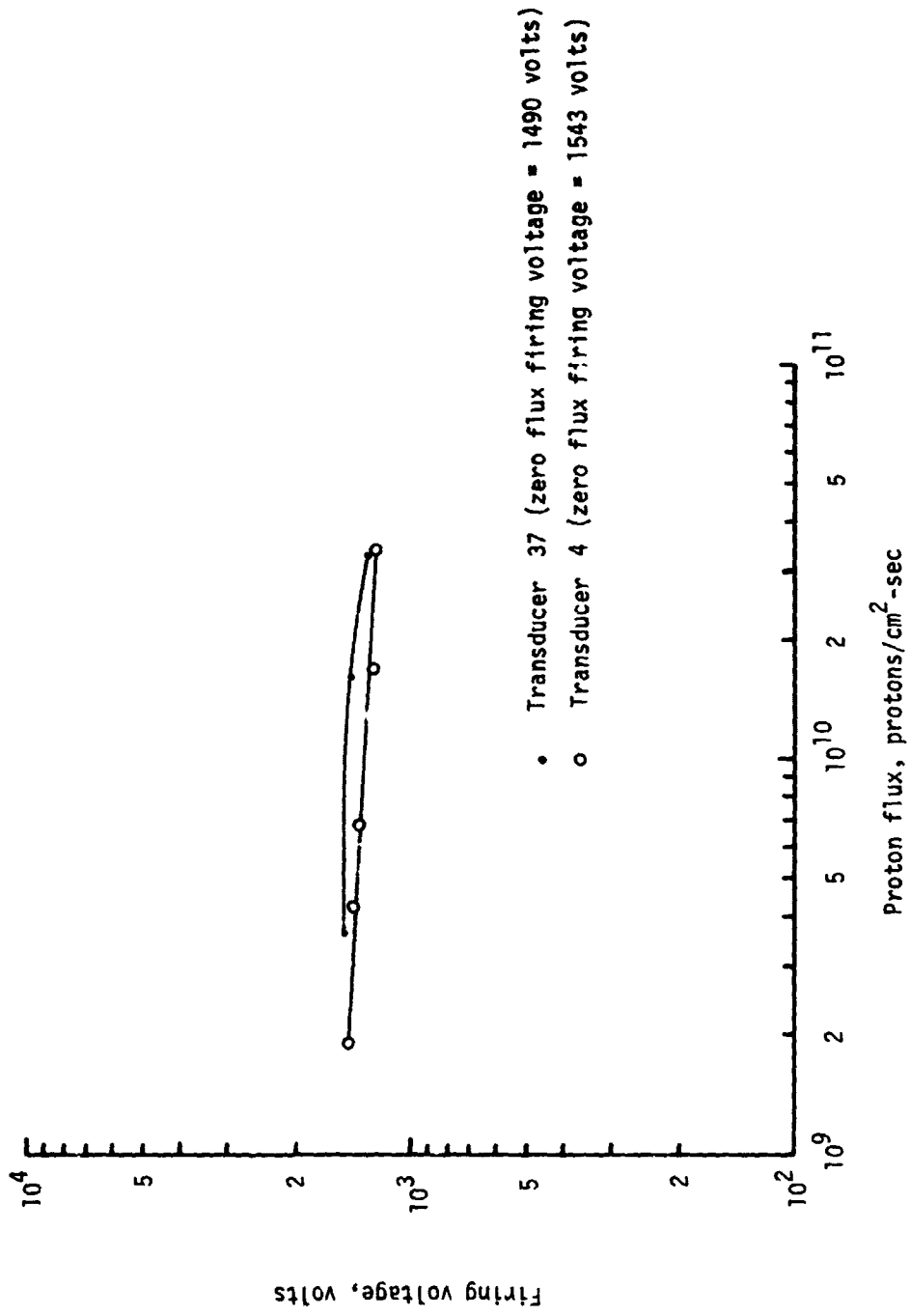


Figure VII-2.- Variation of firing voltage with proton flux.

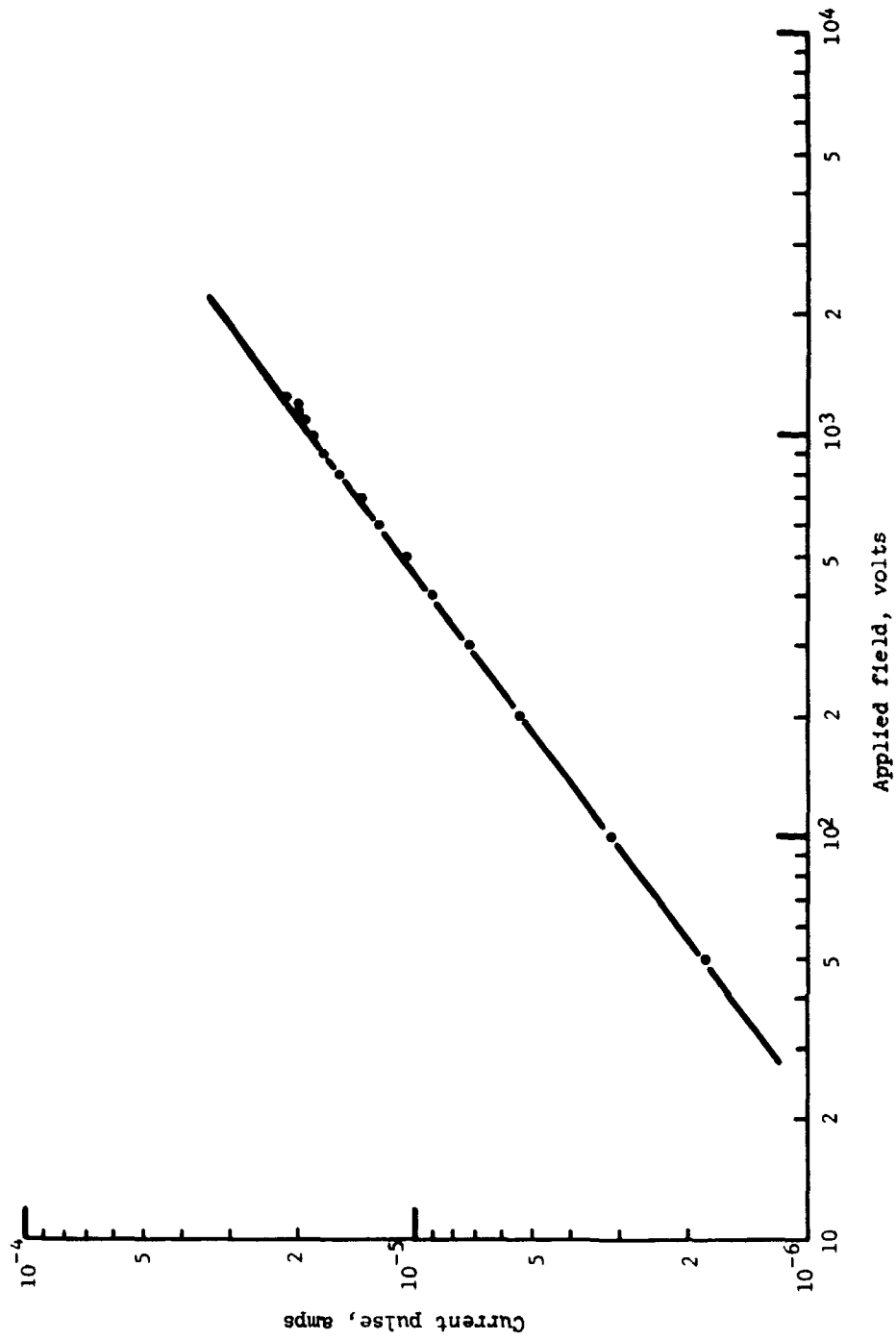


Figure VII-3.- Peak values of current pulse through the 2.2 kΩ resistor as a function of applied field.  
 $\Phi \approx 3 \times 10^{10}$  protons/cm<sup>2</sup>-sec; proton energy,  $E_p = 576$  MeV.

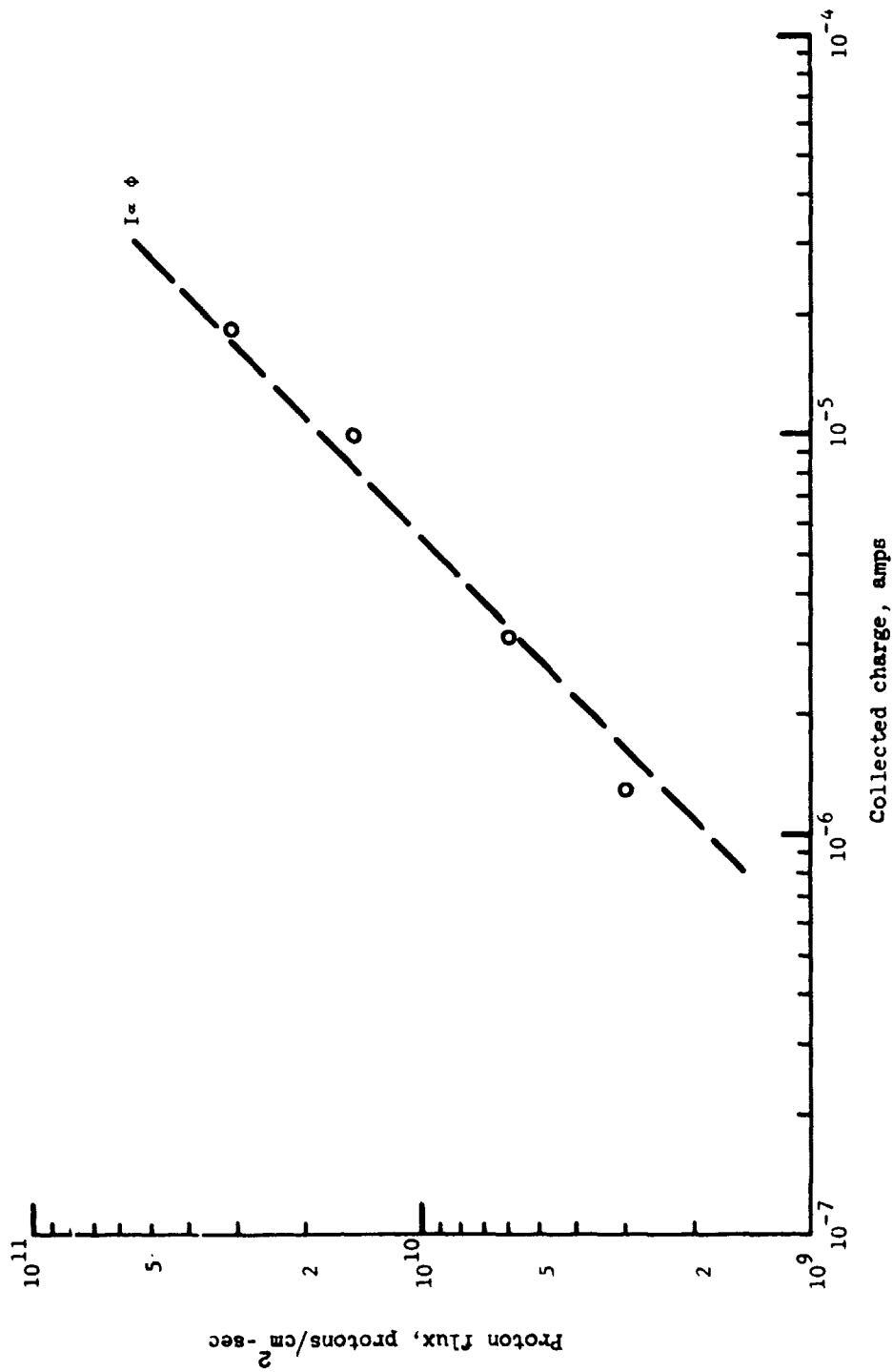


Figure VII-4.- Proton flux as a function of collected charge.  $V_g = 1000$  volts.



## VIII. CALCULATION OF THE LEAK-DOWN TIMES FOR PRESSURIZED CELL METEOROID PENETRATION DETECTORS

By Donald H. Humes  
Langley Research Center

### INTRODUCTION

The nature of the pressure switch and associated circuitry used in the experiment system made it necessary to inhibit the event counter at the first firing pulse of a switch to prevent the oscillating firing action of the switch from resulting in multiple counts from a single penetration event. A trade-off was involved in selecting the inhibit time used. It was desirable to have a long inhibit time to allow the cell pressure to decay and the switch firing to cease before the counter was enabled to count subsequent events, but it was also desirable to keep the inhibit time short since the instrument could not respond to additional legitimate penetration events while in the inhibit mode.

An analysis was made by using a model of the interplanetary meteoroid environment, spacecraft trajectory information, switch firing characteristics, and a representative penetration equation to calculate the expected frequency of penetration events and the resulting switch firing durations. This analysis based on penetration and switch firing duration probabilities is presented in this section.

### SYMBOLS

- A            cross-sectional area of penetration hole
- d            diameter of near-threshold penetration hole
- $f_1(P_\infty, t)$     hole diameter function for meteoroid penetration
- $f_2(\theta, \rho, v, P_\infty)$     meteoroid penetration function for infinitely thick plates which takes into consideration the meteoroid parameters,  $m$ ,  $\theta$ ,  $\rho$ , and  $v$ .
- $f_3(d, t)$     meteoroid penetration function for infinitely thick plates which takes into consideration the diameter of the hole which would be produced in a thin plate
- $g(\theta)$        meteoroid impact angle probability density function

$h(\rho)$	meteoroid density probability density function
$j(v)$	meteoroid impact velocity probability density function
$\left. \begin{matrix} K_0, K_1, K_2, \\ K_3, K_4, K_5 \end{matrix} \right\}$	constants
$k$	Boltzmann's constant
$M$	molecular weight of gas in pressurized cell
$m$	mass of meteoroid
$N$	number of molecules in container
$N_A$	Avogadro's number
$N_d$	number of holes of diameter $d$ and larger in a cell wall
$N_{d,0}$	number of holes in a cell wall
$N_{P_\infty}$	number of craters of depth $P_\infty$ and greater in a plate
$P_\infty$	depth to which a meteoroid can penetrate an infinitely thick plate
$p$	gas pressure in a pressurized cell
$p_0$	initial gas pressure in a pressurized cell
$Q_d$	probability that the first hole in a pressurized cell will be of diameter $d$ or larger
$Q_\tau$	probability that a pressurized cell will leak down in time $\tau$ or shorter
$T$	absolute temperature of gas in a pressurized cell
$t$	wall thickness of a pressurized cell
$V$	volume of a pressurized cell

$v$	meteoroid impact velocity
$v_0$	minimum meteoroid impact velocity
$v_1$	maximum meteoroid impact velocity
$\alpha, \beta, \eta, \Omega$	constants
$\theta$	meteoroid impact angle
$\rho$	meteoroid density
$\rho_0$	minimum meteoroid density
$\rho_1$	maximum meteoroid density
$\sigma$	meteoroid mass distribution index, constant
$\tau$	time
$\Phi$	flux density of molecules on a container wall
$\phi$	cumulative flux of meteoroids of mass $m$ and greater
$\phi_p$	number of craters of depth $P_\infty$ and greater produced in a unit area in a unit time

## DEVELOPMENT OF A GENERAL PROBABILITY EQUATION FOR METEOROID DETECTOR LEAK-DOWN TIMES

### Approach

When a pressurized container is punctured in a vacuum environment, the gas leaks out through the punctured orifice by viscous flow until the mean free path in the container begins to approach the dimensions of the orifice. When the mean free path exceeds the dimensions of the orifice, the flow is molecular. A transition flow region exists between the viscous and molecular regions. Comprehensive theories have been developed for the viscous and molecular regions, but none exists for transition flow. The theories show that the time required for the pressure to drop a given amount is greater in molecular flow than in viscous flow.

Simple calculations show that when a near-threshold penetration is produced in the Pioneer 10 and Pioneer 11 pressurized cell meteoroid detectors, the gas will escape by molecular or transition flow. The leak-down times for the Pioneer detectors were calculated in this paper by using molecular flow theory because it applies in the case of very small holes and is conservative for larger holes; that is, it predicts longer leak-down times than actually occur.

The approach taken in this analysis is to estimate first the size hole that a meteoroid of given mass, velocity, density, and impact angle will produce in a cell wall. Next the hole size distribution caused by meteoroids in the cells is calculated by using the distributions of meteoroid masses, velocities, densities, and impact angles. The probability that the first hole produced in a cell, the hole through which it leaks down, will be larger than a certain size is calculated from the hole size distribution. Finally, the leak-down time is related to the hole size so that the probability that a meteoroid penetration of a cell will result in a leak-down time less than a certain time can be calculated.

#### Size of Holes Produced by Meteoroids

Because of the distribution of meteoroid masses (ref. VIII-1), most of the holes produced by meteoroids in single-wall pressurized cells will be the result of near-threshold penetrations; that is, the holes will be small because the meteoroid was just able to penetrate the wall. The size of the near-threshold penetration hole must depend on the mass, velocity, density, impact angle, and other meteoroid parameters as well as the thickness and material of the cell wall. Although empirical equations for the size of the hole that a projectile will produce in a thin plate have been published (ref. VIII-2), they apply only to the case where the projectile easily penetrates the plate and leaves a hole with a diameter larger than the plate thickness. There are no theories and no empirical equations to predict the size of near-threshold penetration holes.

In order to simplify the analysis, it was assumed that for near-threshold penetrations, the diameter  $d$  of the hole produced in a plate by a hypervelocity particle depends only on (1) the depth  $P_{\infty}$  to which the particle would have penetrated a semi-infinite plate of the same material and (2) the thickness of the plate encountered  $t$ . This simplifying assumption is expressed as

$$d = f_1(P_{\infty}, t) \quad (1)$$

Experiments conducted to test the validity of this assumption are discussed in a later section of this paper.

**Calculation of Hole Size Distribution Resulting  
From Meteoroid Penetrations**

From equation (1), the number of holes of a given diameter and larger produced in a pressurized cell exposed to the meteoroid environment depends on the number of craters of some depth and larger that would be produced in a semi-infinite plate. If the depth to which a meteoroid penetrates an infinite plate depends only on the meteoroid mass, velocity, density, and impact angle (ref. VIII-3) the number of craters of depth  $P_\infty$  and greater produced in a unit area during a unit time is

$$\phi_p = \int_0^{\pi/2} \int_{\rho_0}^{\rho_1} \int_{v_0}^v \int_m^\infty \frac{\partial \phi}{\partial m} g(\theta) h(\rho) j(v) d\theta d\rho dv dm \quad (2)$$

where  $\partial \phi / \partial m$  is the differential mass-flux distribution function,  $g(\theta)$  is the meteoroid impact angle probability density function,  $h(\rho)$  is the meteoroid density probability density function,  $j(v)$  is the meteoroid velocity probability density function, and  $m = f_2(\theta, \rho, v, P_\infty)$  is the penetration equation for semi-infinite plates. For a development of equation (2), see reference VIII-4.

If the penetration equation for semi-infinite plates is of the form

$$P_\infty = K_0 m^\alpha v^\beta \rho^\eta (\cos \theta)^\Omega$$

as is suggested in reference VIII-5, so that

$$m = K_1 P_\infty^{1/\alpha} v^{-\beta/\alpha} \rho^{-\eta/\alpha} (\cos \theta)^{-\Omega/\alpha}$$

where  $m$ ,  $v$ ,  $\rho$ , and  $\theta$  are the meteoroid mass, velocity, density, and impact angle, respectively, and if the meteoroid mass-flux relationship is

$$\phi = K_2 m^{-\sigma}$$

as is suggested in reference VIII-6, so that

$$\frac{\partial \phi}{\partial m} = K_3 m^{-\sigma-1}$$

where  $\phi$  is the cumulative flux of meteoroids of mass  $m$  and greater and  $\sigma$  is a constant which will be called the meteoroid mass distribution index, then  $\phi_p$  is

$$\phi_p = \frac{K_3 K_1^{-\sigma}}{\sigma} P_\infty^{-\sigma/\alpha} \int_0^{\pi/2} \int_{\rho_0}^{\rho_1} \int_0^{v_1} (\cos \theta)^{\Omega\sigma/\alpha} g(\theta) \rho^{\eta\sigma/\alpha} h(\rho) v^{\beta\sigma/\alpha} j(v) d\theta d\rho dv \quad (3)$$

For any given meteoroid velocity probability density function, meteoroid density probability density function, and meteoroid impact angle probability density function, and for given values of the constants  $\alpha$ ,  $\beta$ ,  $\sigma$ ,  $\eta$ , and  $\Omega$

$$\phi_p = K_4 P_\infty^{-\sigma/\alpha} \quad (4)$$

where  $K_4$  is a constant for any particular case.

Note in equation (4) that the distribution of crater sizes depends on the distribution of meteoroid masses but is independent of the distributions of meteoroid velocity, density, and impact angle. If, for instance, different velocity distributions  $j(v)$  are used, the constant  $K_4$  would change, but the exponent on  $P_\infty$ , which determines the relative number of various size craters, would remain the same. The relative number of craters of various sizes depends on the mass distribution of meteoroids and the exponent of mass in the penetration equation, but is independent of the distributions of impact velocity, impact angle, and meteoroid density.

If equation (4) is multiplied by an area-time product, the result is the number of craters of depth  $P_\infty$  and greater  $N_{P_\infty}$ ; that is,

$$N_{P_\infty} = K_5 P_\infty^{-\sigma/\alpha}$$

But  $d = f_1(P_\infty, t)$  from equation (1) so that  $P_\infty = f_3(d, t)$  and the number of holes of diameter  $d$  and greater  $N_d$  in a cell of thickness  $t$  is

$$N_d = K_5 [f_3(d, t)]^{-\sigma/\alpha} \quad (5)$$

Equation (5) is the hole size distribution caused by meteoroids.

The probability that the first hole produced by a meteoroid in a pressurized cell will be of diameter  $d$  or larger is

$$Q_d = \frac{N_d}{N_{d,0}} \quad (6)$$

where  $N_{d,0}$  is the number of holes of all sizes which is  $N_d$  obtained in equation (5) when  $d$  is set equal to zero. Upon substitution  $Q_d$  becomes

$$Q_d = \frac{[f_3(d,t)]^{-\sigma/\alpha}}{[f_3(0,t)]^{-\sigma/\alpha}} \quad (7)$$

#### Calculation of Cell Leak-Down Time

The flux density of molecules on the wall of a container at low pressure is given in reference VIII-7 to be

$$\Phi = \frac{N}{V} \left( \frac{N_A kT}{2\pi M} \right)^{1/2} \quad (8)$$

where  $N$  is the number of molecules in a container of volume  $V$ ,  $N_A$  is Avogadro's number,  $k$  is Boltzmann's constant,  $T$  is the temperature of the gas, and  $M$  is the molecular weight of the gas. Multiplying both sides of equation (8) by  $A \Delta\tau$  gives the number of molecules striking a given area in a small interval of time; that is,

$$\Phi A \Delta\tau = \frac{NA}{V} \left( \frac{N_A kT}{2\pi M} \right)^{1/2} \Delta\tau \quad (9)$$

If the area in equation (9) is the area of a hole, then the molecules striking this area pass through the container wall and the difference in the number of molecules in the container is (by assuming that no molecules enter from the outside and that the outgassing from the interior of the container is negligible)

$$\Delta N = -\Phi A \Delta\tau$$

so that

$$\frac{\Delta N}{\Delta\tau} = -\frac{NA}{V} \left( \frac{N_A kT}{2\pi M} \right)^{1/2} \quad (10)$$

By the perfect gas law

$$N = p \frac{V}{kT}$$

and when the gas leaks out slowly so that the temperature of the remaining gas is constant, the change in the number of molecules in the container is related to the change in pressure

$$\frac{\Delta N}{\Delta \tau} = \frac{\Delta p}{\Delta \tau} \frac{V}{kT} \quad (11)$$

Substituting equation (11) into equation (10) and rearranging terms gives

$$\frac{\Delta p}{p} = -\frac{A}{V} \left( \frac{N_A kT}{2\pi M} \right)^{1/2} \Delta \tau$$

By integrating this equation, the leak-down equation becomes

$$\log_e \frac{p}{p_0} = -\frac{A}{V} \left( \frac{N_A kT}{2\pi M} \right)^{1/2} \tau \quad (12)$$

where  $p$  is the pressure in the container at time  $\tau$ , and  $p_0$  is the initial pressure at  $\tau = 0$ .

Equation (12) is the leak-down equation for a container with an orifice, a perfect hole with no length. The holes in a real container wall have length and some of the molecules entering the hole strike the hole wall and are directed back into the container. By using the Dushman approximation of the Clausing factor (ref. VIII-7), which accounts for the molecules that return, the leak-down equation for a container with a tube is

$$\log_e \frac{p}{p_0} = -\frac{1}{V} \frac{1 + \frac{3}{4} \frac{t}{d}}{\pi} A \left( \frac{N_A kT}{2\pi M} \right)^{1/2} \tau \quad (13)$$

Equation (13) can be rewritten as

$$d^3 + ad + b = 0 \quad (14)$$

where  $d$  is the diameter of the hole and  $a$  and  $b$  are

$$a = \left[ \frac{4V \log_e \frac{p}{p_0}}{\pi \tau \left( \frac{N_A kT}{2\pi M} \right)^{1/2}} \right]$$

$$b = \frac{3}{4} t \left[ \frac{4V \log_e \frac{p}{p_0}}{\pi \tau \left( \frac{N_A kT}{2\pi M} \right)^{1/2}} \right]$$

Solving the cubic equation (14) for  $d$  gives the diameter of the hole which will cause the container to leak down from  $p_0$  to  $p$  in time  $\tau$

$$d = \left( -\frac{b}{2} + \sqrt{\frac{b^2}{4} + \frac{a^3}{27}} \right)^{1/3} + \left( -\frac{b}{2} - \sqrt{\frac{b^2}{4} + \frac{a^3}{27}} \right)^{1/3} \quad \left( \frac{b^2}{4} + \frac{a^3}{27} \geq 0 \right) \quad (15)$$

$$d = \left( -\frac{2a}{3} \right) \cos \left[ \frac{\cos^{-1} \left( -\frac{b/2}{\sqrt{-a^3/27}} \right)}{3} \right] \quad \left( \frac{b^2}{4} + \frac{a^3}{27} < 0 \right) \quad (16)$$

When equations (15) and (16) are substituted into equation (7), the result is the expressions for the probability that a meteoroid penetration of a cell will produce a hole which will result in a leak-down time of  $\tau$  or shorter. These expressions are

$$Q_\tau = \frac{\left[ f_3 \left\{ \left[ \left( -\frac{b}{2} + \sqrt{\frac{b^2}{4} + \frac{a^3}{27}} \right)^{1/3} + \left( -\frac{b}{2} - \sqrt{\frac{b^2}{4} + \frac{a^3}{27}} \right)^{1/3} \right], t \right\} \right]^{-\sigma/\alpha}}{\left[ f_3(0,t) \right]^{-\sigma/\alpha}} \quad \left( \frac{b^2}{4} + \frac{a^3}{27} \geq 0 \right) \quad (17)$$

$$Q_\tau = \frac{\left[ f_3 \left\{ \left[ \left( -\frac{2a}{3} \right) \cos \left( \frac{\cos^{-1} \left( -\frac{b/2}{\sqrt{-a^3/27}} \right)}{3} \right) \right], t \right\} \right]^{-\sigma/\alpha}}{\left[ f_3(0,t) \right]^{-\sigma/\alpha}} \quad \left( \frac{b^2}{4} + \frac{a^3}{27} < 0 \right) \quad (18)$$

Equations (17) and (18) are the general solution to the problem of a pressurized cell leaking down after a penetration of the wall by a meteoroid. In order to obtain the particular solution for the case of the Pioneer 10 and Pioneer 11 pressurized cell meteoroid detectors, it is necessary to determine (1) the function  $f_3(d,t)$  which is the near-threshold hole size equation for stainless steel, (2) the upper and lower threshold pressures for the transducer  $p_o$  and  $p$ , (3) the meteoroid mass distribution index  $\sigma$  for the meteoroids to be encountered, and (4) the exponent of mass in the penetration equation  $\alpha$ . The first two have been determined experimentally and are discussed in the following section. The last two items were estimated from previous data on the meteoroid environment and on hypervelocity impact.

## EXPERIMENTS

### Determination of the Size of Near-Threshold

#### Penetration Holes in Stainless Steel

Hypervelocity impact tests were conducted to determine whether the simplifying assumption made in the analysis was valid. Measurements were made of the size of the holes that were produced when projectiles made near-threshold penetrations in stainless-steel plates.

The projectile mass, velocity, density, impact angle, and shape were varied in the tests. Impact velocities greater than 5 km/s and projectile densities less than 3 g/cm<sup>3</sup> were used in all the tests because it was believed that the simplifying assumption would not be valid for either low impact velocities or projectile densities near the density of stainless steel. Meteoroids are expected to have densities less than 3 g/cm<sup>3</sup> and to strike a spacecraft at velocities greater than 5 km/s (see refs. VIII-1 and VIII-8).

For the three impact conditions tested, a single function of  $P_\infty$ ,  $t$ , and  $d$  was found to fit the data well and supported the simplifying assumption made in the analysis. The data from these hypervelocity impact tests are plotted in figure VIII-1. The equation for the hole size in stainless steel was found to be

$$d = 13 P_\infty - 6.5t$$

so that  $P_\infty$  and hence the function  $f_3(d,t)$  is

$$f_3 = 0.077d + 0.5t \tag{19}$$

### Determination of the Upper and Lower Threshold

#### Pressures of the Transducer

Tests were conducted at Research Triangle Institute, under contract NAS 1-9420 to establish the Paschen curves for the transducers with a gas mixture of 75 percent argon

and 25 percent nitrogen at two temperatures. These Paschen curves, presented in figure VIII-2, show the mutual conditions of voltage across the terminals and gas pressure in the cell which will cause the transducer to conduct. The conditions under which conduction will occur lie above the curve. To provide an example, consider the case where the applied voltage for the switch is 525 volts and the initial pressure in the meteoroid detector cell is greater than 130 torr (1 torr = 133.3 N/m<sup>2</sup>). When a meteoroid penetration occurs, the gas pressure decreases while the applied voltage remains constant so that at 77 K,  $p/p_0 = 0.0667$  and at 295 K,  $p/p_0 = 0.0154$ .

#### CALCULATION OF THE PROBABLE DURATION OF THE TRANSDUCER CONDUCTION PERIOD

When the equation for the hole size in stainless steel (eq. (19)) is substituted into the general probability equation for the leak-down time of a pressurized cell (eqs. (17) or (18)), the result is

$$Q_T = \left[ \frac{\left( \frac{-b}{2} + \sqrt{\frac{b^2}{4} + \frac{a^3}{27}} \right)^{1/3} + \left( \frac{-b}{2} - \sqrt{\frac{b^2}{4} + \frac{a^3}{27}} \right)^{1/3} + \frac{t}{2}}{13} \right]^{-\sigma/\alpha} \quad \left( \frac{b^2}{4} + \frac{a^3}{27} \geq 0 \right) \quad (20)$$

$$Q_T = \left[ \frac{\left( -\frac{2a}{3} \right) \cos \left[ \frac{\cos^{-1} \left( \frac{-b/2}{\sqrt{-a^3/27}} \right)}{3} \right] + \frac{t}{2}}{13} \right]^{-\sigma/\alpha} \quad \left( \frac{b^2}{4} + \frac{a^3}{27} < 0 \right) \quad (21)$$

where a and b are

$$a = \left[ \frac{4V \log_e \frac{p}{p_0}}{\pi \tau \left( \frac{N_A kT}{2\pi M} \right)^{1/2}} \right]$$

$$b = \frac{3t}{4} \left[ \frac{4V \log_e \frac{p}{p_0}}{\pi \tau \left( \frac{N_A kT}{2\pi M} \right)^{1/2}} \right]$$

The probability that a hole produced in a Pioneer 10 or Pioneer 11 meteoroid detector would result in a transducer conduction period of  $\tau$  or shorter was calculated by using equations (20) and (21). The Pioneer cells have a volume of 2.5 cm<sup>3</sup> and are pressurized with a gas mixture which is 75 percent argon and 25 percent nitrogen. A molecular weight of 37 was used in the calculations in this paper. The value of  $\alpha$  found experimentally (ref. VIII-9) to be 0.352 was used in this paper.

Calculations were made for both detector thicknesses used for the Pioneer experiments, the 25.4- $\mu$ m-thick detector results are shown in figures VIII-3 and VIII-4, and the 50.8- $\mu$ m-thick detector results are shown in figures VIII-5 and VIII-6. The meteoroid mass distribution index for meteoroids near the earth has been calculated to be in the 0.2 to 1.2 range (ref. VIII-1) depending on the size of the meteoroids, and has been estimated to be 0.84 in the asteroid belt (ref. VIII-8). Values of 0.67, 1.0, and 1.34 were used for the meteoroid mass distribution index in this paper and the effect of this parameter is shown in figures VIII-3 and VIII-5. Calculations were made for temperatures of 77 K and 295 K and the effect of the detector temperature is shown in figures VIII-4 and VIII-6.

#### CONCLUDING REMARKS

The leak-down times calculated were used in electronic system design trade-off studies and an inhibit time of 85 minutes selected. The calculations indicate there is only a 0.09 to 0.18 probability that a 25- $\mu$ m cell and a 0.06 to 0.12 probability that a 50- $\mu$ m cell will take longer than 85 minutes to leak down, depending on the cell temperature and the mass distribution of the meteoroids. The inhibit time selected is sufficiently short that the probability of a legitimate penetration occurring during the 85-minute period is small.

## REFERENCES

- VIII-1. Anon.: Meteoroid Environment Model - 1969 Near-Earth to Lunar Surface .  
NASA Space Vehicle Design Criteria (Environment). NASA SP-8013, 1969.
- VIII-2. Maiden, C. J.; Gehring, J. W.; and McMillan, A. R.: Investigation of Fundamental  
Mechanism of Damage to Thin Targets by Hypervelocity Projectiles. TR 63-225  
(Contract No. Nonr-3891(00)(X)), General Motors Corp., Sept. 1963.
- VIII-3. Anon.: Meteoroid Damage Assessment. NASA Space Vehicle Design Criteria  
(Structures). NASA SP-8042, 1970.
- VIII-4. Humes Donald H.: Calculation of the Penetration Flux for a Multiwall Structure  
on the Lunar Orbiter Spacecraft. NASA TN D-5455, 1969.
- VIII-5. Naumann, Robert J.: The Near-Earth Meteoroid Environment. NASA TN D-3717,  
1966.
- VIII-6. Dolnanyi, J. S.: Collisional Model of Meteoroids. TR-67-340-3 (Con-  
tract NASw-412), Bellcomm, Inc., July 1967. (Available as NASA CR-88864.)
- VIII-7. Santeler, Donald J.; Holkeboer, David H.; Jones, Donald W.; and Pagano, Frank:  
Vacuum Technology and Space Simulation. NASA SP-105, 1966.
- VIII-8. Anon.: Meteoroid Environment Model - 1970 Interplanetary and Planetary .  
NASA Space Vehicle Design Criteria (Environment). NASA SP-8038, 1970.
- VIII-9. Denardo, B. Pat; Summers, James L.; and Nysmith, C. Robert: Projectile Size  
Effects on Hypervelocity Impact Craters in Aluminum. NASA TN D-4067, 1967.

	Projectile	Impact velocity	Impact angle	Target temperature
○	1.59-mm glass sphere	6.2 km/sec	45°	298 K
▲	1.59-mm glass sphere	6.3 km/sec	30°	110 K
□	5.60-mm Lexan cylinder	7.3 km/sec	0° (normal)	298 K

Solid symbols denote no penetration hole created.

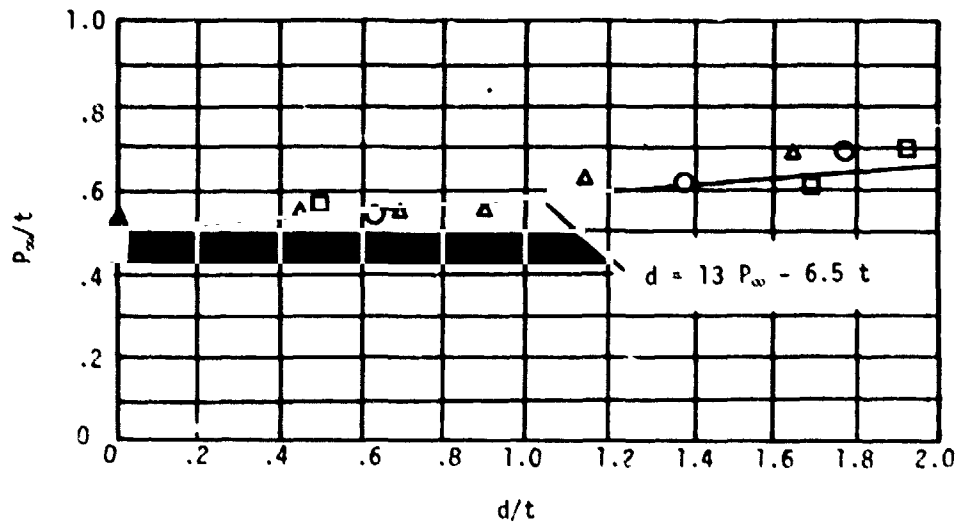


Figure VIII-1.- Size of threshold penetration hole as a function of the penetration the projectile could have produced in an infinitely thick target of the same material. Targets: stainless steel 507.

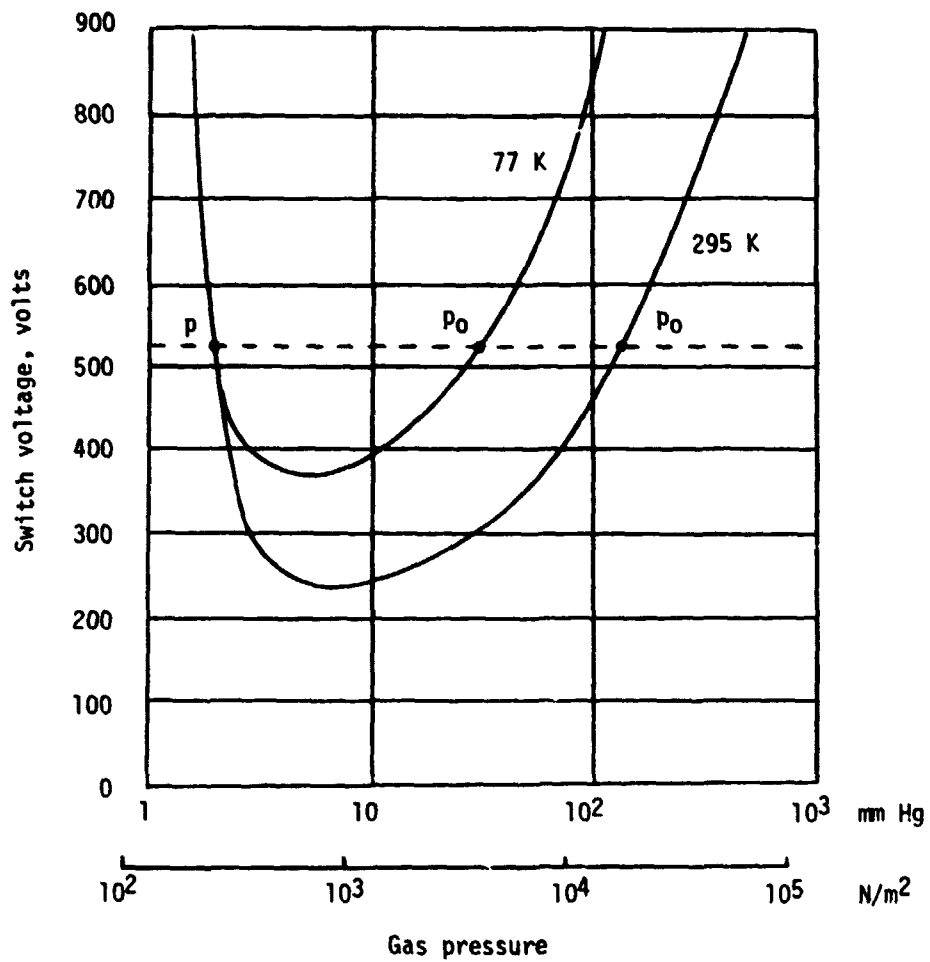


Figure VIII-2.- Paschen curves with a gas mixture of 75 percent argon and 25 percent nitrogen for transducers coated with Ni<sup>63</sup>.

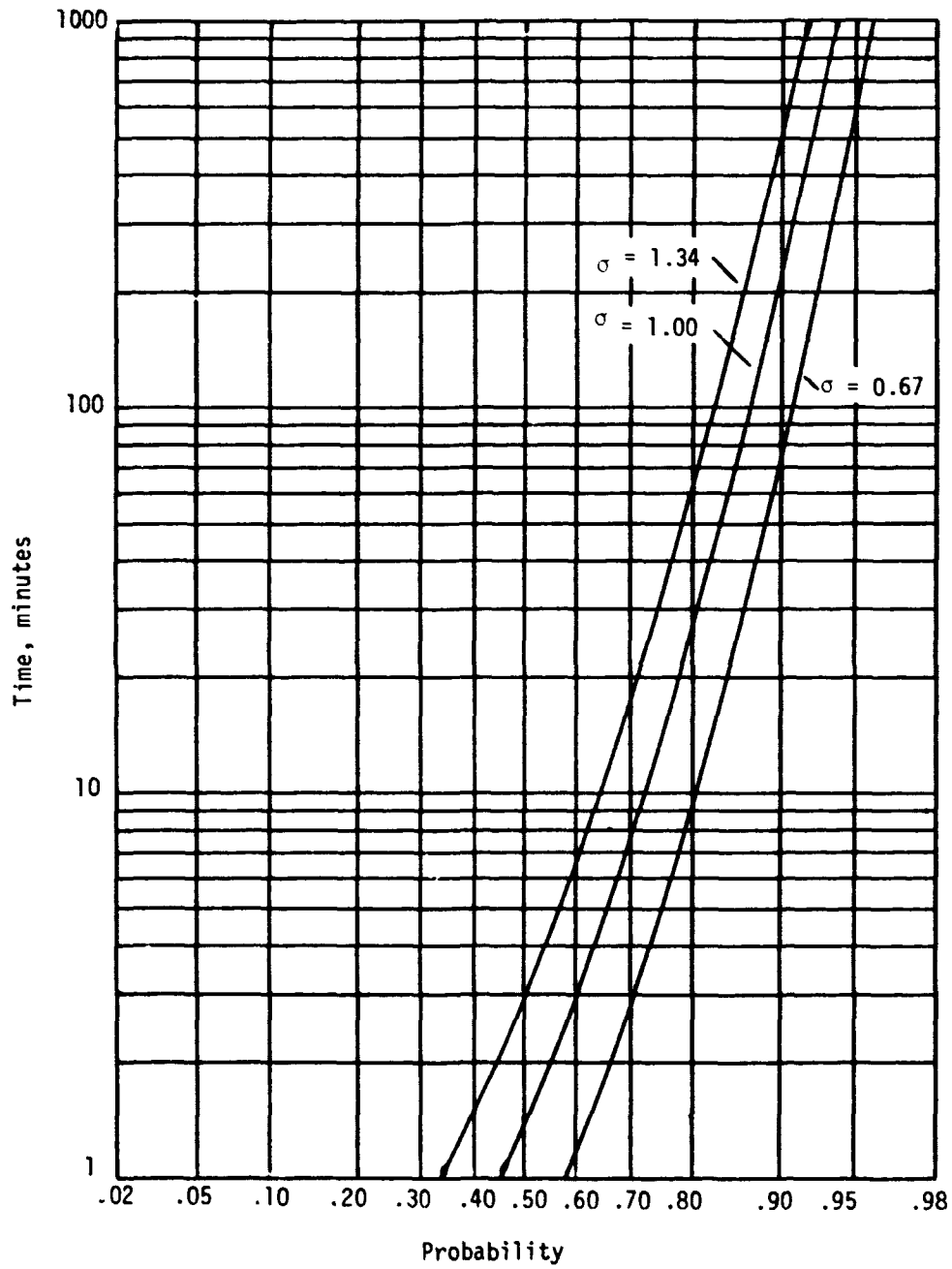


Figure VIII-3.- Probability of transducer conduction period being less than a given time, showing effect of meteoroid mass distribution index. 25- $\mu$ m-thick detector; detector temperature, 295 K; transducer potential, 525 volts.

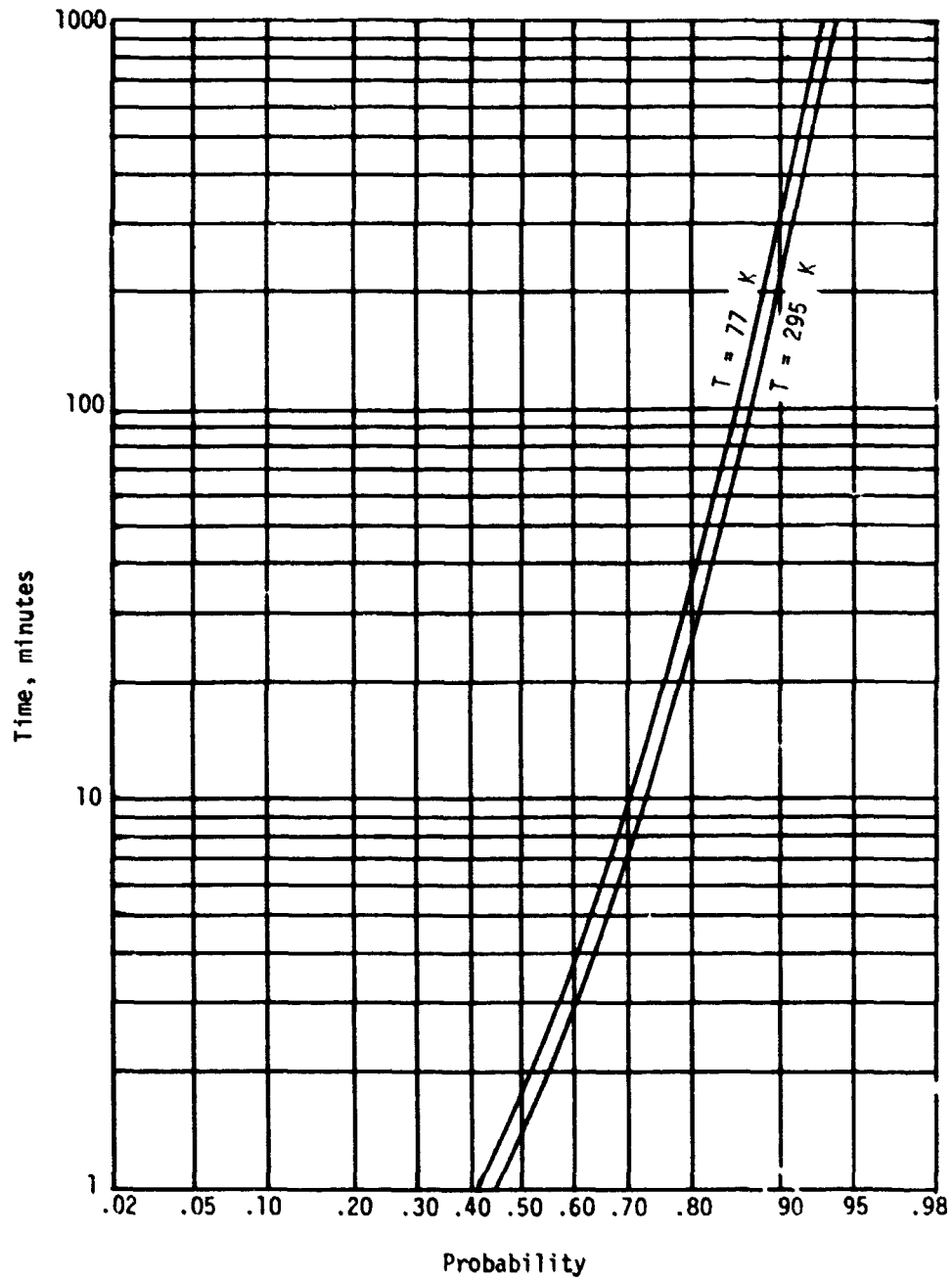


Figure VIII-4.- Probability of transducer conduction period being less than a given time, showing effect of detector temperature. 25- $\mu$ m-thick detector; transducer potential, 525 volts; meteoroid mass distribution index, 1.0.

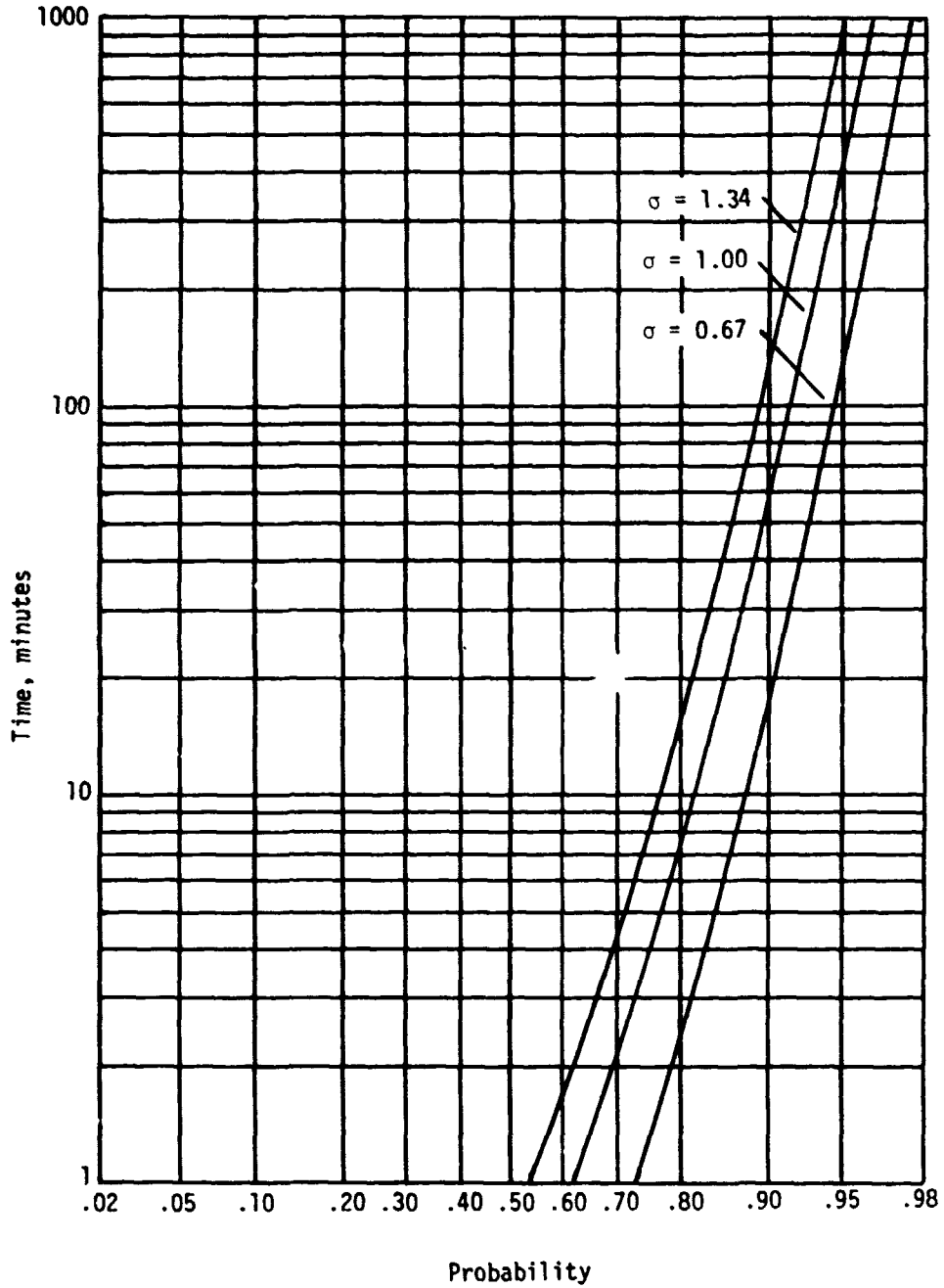


Figure VIII-5.- Probability of transducer conduction period being less than a given time, showing effect of meteoroid mass distribution index. 50.8- $\mu\text{m}$ -thick detector; detector temperature, 295 K; transducer potential, 525 volts.

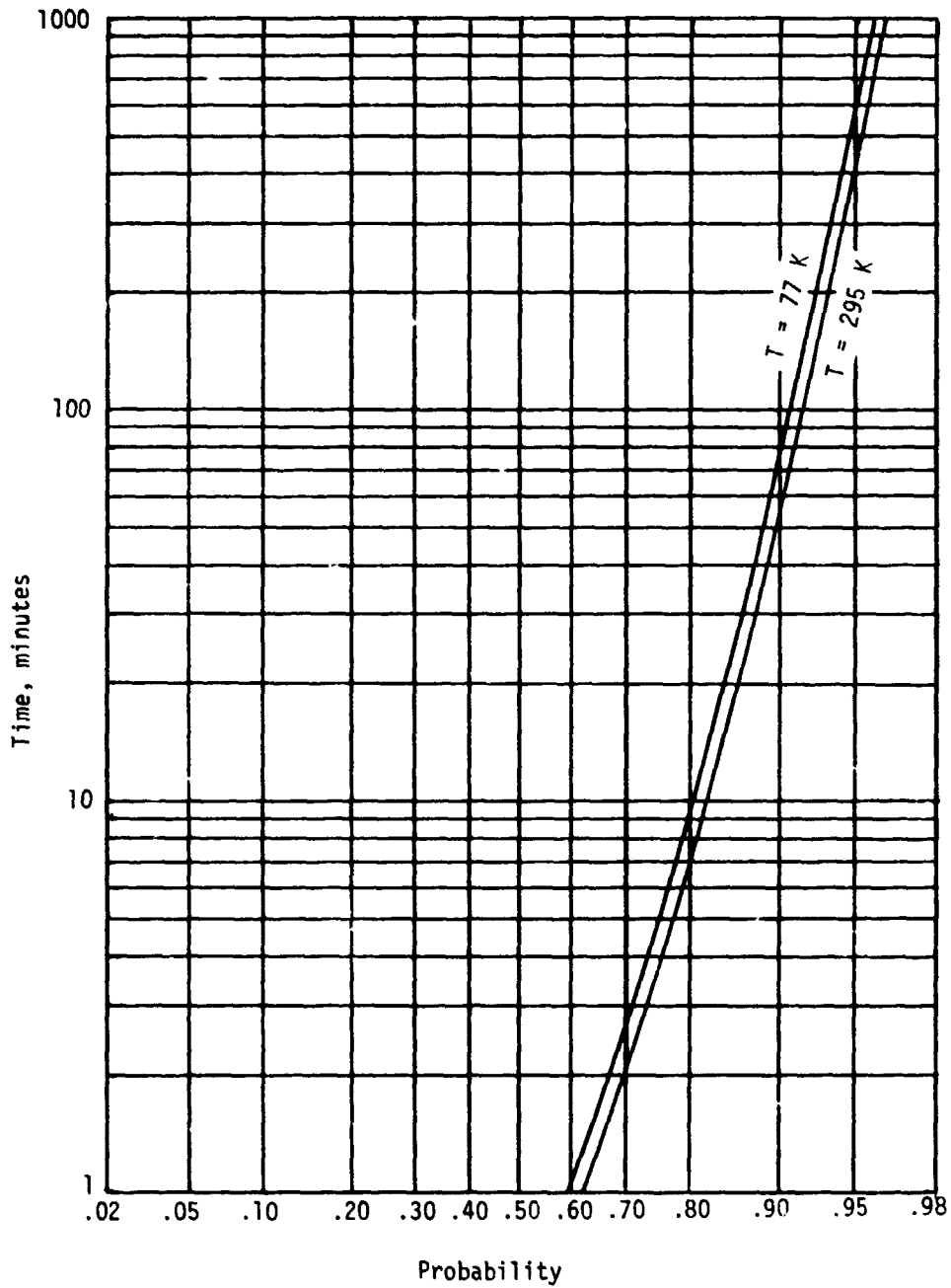


Figure VIII-6.- Probability of transducer conduction period being less than a given time, showing effect of detector temperature. 50.8- $\mu\text{m}$ -thick detector; transducer potential, 525 volts; meteoroid mass distribution index, 1.0.



## IX. CONCLUDING REMARKS

By Robert L. O'Neal  
Langley Research Center

The instrument system described in this report is a part of the instrument complement on the Pioneer 10 and the Pioneer 11 spacecraft launched in 1972 and 1973 on Jupiter flyby missions. Early in December of 1973, the Pioneer 10 spacecraft passed near the planet Jupiter and thus completed the primary phase of that mission. The Pioneer 11 spacecraft is on a trajectory to pass near Jupiter early in December of 1974.

One anomaly has occurred in the Meteoroid Detection Experiment instrument during the Pioneer 10 mission. Approximately 4 months after launch, spurious signals began causing the event counter for one of the two redundant channels to advance periodically. Since the instrument contained no diagnostic measurements, the source of the spurious signals activating the counter could not be determined. This occurrence has not detracted from meeting the experiment objectives since the data rate from the second channel is adequate for the definition of the meteoroid environment level.

With the exception of the one anomaly, the performance of the instruments on both spacecraft has been normal. Both instruments continue to provide data on the interplanetary meteoroid environment, and the objectives of both experiments are being successfully achieved.

Langley Research Center,  
National Aeronautics and Space Administration,  
Hampton, Va., June 3, 1974.

PRECEDING PAGE BLANK NOT FILMED